NOVEL OLEFIN POLYMERIZATION PRE-CATALYST BEARING AN INVERSELY-POLARIZED PHOSPHAALKENE ETHENOLATE MONOANIONIC BIDENTATE LIGAND AND ITS POLYMERIZATION STUDIES.

Juan Enrique Rodriguez Villanueva

A thesis submitted to the faculty graduate studies in partial fulfillment of the requirements for the degree of Master of Science

Graduate program in Chemistry
York University
Toronto, Ontario

September 2019

Abstract

The synthesis and structure elucidation of the first monoanionic bidentate ligand bearing an inversely-polarized phosphaalkene, its precursors and the first titanium complex bearing such ligand are herein reported. Single-crystal X-ray studies of the titanium complex confirmed the coordination of the bidentate ligand using the phosphaalkene phosphorus and ethenolate oxygen atoms with a strong evidence that there is charge delocalization through the metallocycle and the imidazole ring. The thermal stability of the phosphaalkene–ethenolate ligand and the titanium complex at high temperature is reported. The new titanium complex displayed an activity for ethylene polymerization up to 9.2 kg PE mol cat^{-1} h^{-1}. The polyethylene produced was linear with a low degree of branching, an average molecular weight of ~ 6000 g mol^{-1} and a T_m of 130.0 °C.

Dedication

Esta tesis es dedicada con mucho cariño a mi familia, pero en especial a mi mamá por todo el amor y apoyo que me ha brindado durante todos mis estudios. – Por eso y más

Muchas Gracias.

Acknowledgements

I would like to thank Professor Gino G. Lavoie for the guidance, patience and support throughout my MSc. degree. I would like to thank Professors Pierre Potvin, Arturo Orellana, and Bridget Stutchbury for being part of my supervisory and/ or examination committee. I wish to thank the Orellana group; Nour, Minhao, Faizan, Andrei, and Anmol for all the discussions and suggestions that helped me with the progress of my research project. My thanks are also extended to Dr. Alan Lough from the University of Toronto for his help with X-ray analysis and helpful discussions. I would like to also thank Dr. Howard Hunter for his help with several NMR experiments and his unending disposition to discuss interesting data that was observed. I wish to thank the past student Faidh Hana and present students Brandon Khan and Matthew Wiebe of the Lavoie group for their help and support throughout my degree. Faidh Hanna for teaching / showing me how to use several instrumentation and techniques in the lab. Matthew for his unending help proofreading several of my documents and his constructive criticism that was always welcomed. Brandon for all those conversations and discussions we had to get a better and clearer understanding of the chemistry I was dealing with at the moment.

Finally, I wish to thank my family, and specially my parents Guillermo Rodriguez and M. Guadalupe Villanueva for the immense love and support provided throughout my degree.

Table of Content

List of Tables

List of Figures

List of Schemes

List of Acronyms

b	Broad
BCF	Tris(pentafluorophenyl)borane
COD	1,4-Cyclooctadiene
COSY	Correlation Spectroscopy
Cp	Cyclopentadienyl
d	Doublet
DCM	Dichloromethane
DFT	Density Functional Theory
Dipp	2,6-diisopropylphenyl
DME	Dimethoxyethane
DSC	Differential Scanning Calorimetry
e.a.	Elemental Analysis
FI	Phenoxy-Imine
FLP	Frustrated Lewis pair
h	hour
HDPE	High Density Polyethylene
HMBC	Heteronuclear Multiple-bond correlation spectroscopy
HOMO	Highest Occupied Molecular Orbital
HSQC	Heteronuclear Single-Quantum Correlation Spectroscopy
IPP	Inversely-polarized Phosphaalkene
IR	Infrared Spectroscopy
L	Ligand
LDPE	Low Density Polyethylene
LUMO	Lowest Unoccupied Molecular Orbital
m	Multiplet
MAO	Methylaluminoxane
MMAO	Modified methylaluminoxane
Mes	2,4,6-trimethylphenyl

min	minute
MO	Molecular Orbital
NaHMDS	Sodium hexamethyldisilazide
NHC	N-Heterocyclic Carbene
NMR	Nuclear Magnetic Resonance
NOESY	Nuclear Overhauser Effect Spectroscopy
OCP	phosphaethynolate
OTf	Triflate
PE	Polyethylene
s	Singlet
sept	Septet
SHOP	Shell Higher Olefin Process
t	Triplet
TBDMSCl	*tert*-butyldimethylsilyl chloride
T_c	Crystallization Temperature
T_g	Glass Temperature
THF	Tetrahydrofuran
T_m	Melting Temperature
TMEDA	Tetramethylenediamine
TMS	Trimethylsilyl
TMSCl	Trimethylsilyl chloride
TOF	Turn over frequency
TON	Turn over number

1. Introduction

Transition metal-based catalysts have had an immense impact in the advancement of synthetic chemistry. Catalysts are an essential part in industrial and bench-top scale reactions to decrease the activation energy barrier of reactions, and to increase the efficiency and the selectivity to the targeted final product. Many catalysts are prepared using first row earth-abundant d-block metals that are decorated with spectator ligands. The ligands around the metal centre can impart selectivity to the catalyst, thus the physical and chemical properties of the final product can be tailored. Some common organic transformations that rely on the use of catalysts include hydrogenation of double bonds, olefin metathesis and polymerization of alkenes.

To meet the growing demands of the chemical industry, the production of polyethylene has relied on the implementation of various inorganic catalysts such as the Ziegler-Natta catalyst.[1] However, Ziegler-Natta catalysts do not polymerize polar monomers, limiting their scope and their ability to build tailored materials containing functional groups, such as ethers, esters and amides. Therefore, the synthesis, isolation and characterization of catalysts for olefin polymerization and oligomerization of olefins and polar monomers is of great interest.

As less expensive metals, nickel and group 4 metals are ideal for the design of new olefin polymerization catalysts. Several research groups have shown that catalysts based on group 4 and group 10 can polymerize olefins and incorporate polar monomers with minimal deactivation of the catalyst.[2–5]

1.1 Polymerization

Molecules that are constituted of a large number of repeating units, called monomers, sequentially linked together by covalent bonds are called polymers. The prefix “mono” and “poly” comes from Greek and respectively means “single” and “many”, while the suffix “mono” means “single”.[6] For example, the polymerization of ethylene olefin produces polyethylene where the double bond present in the monomer is transformed into new single bonds in the presence of a catalyst. (**Figure 1**)

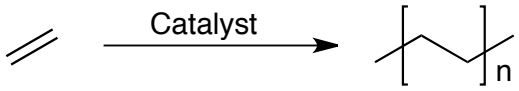

Figure 1. Polymerization of ethylene.

Theoretically, there is no limit for the number of repeating units present in a polymer.[6] The polymers can have distinctive characteristics based on the features, such as chemical structure of the repeating unit, the linkage type between repeating units, such as ester and amide bonds in polyesters and polyamides, the architecture of the main chain (branched or linear) and the composition of the chemical main chain (copolymerization).

Types of polymerization

The types of polymerization are classified into two different groups based on how the polymeric chains are built and the kinetics of the polymerization: step-growth and chain-growth.

Step-Growth Polymerization:

Step-growth polymerization requires either a monomer that has two different functional groups that can react with each other or more than one monomer that each has different functional groups that can be used to form a new single bond. Polyamides are examples of polymers normally made by step-growth polymerization (eq. 1)[6]. The polymerization starts from reactions between two monomers to form dimers. This formed dimer can continue reacting with a monomer, dimer, trimer, or short oligomers present in solution to extend the polymeric/oligomeric chains.[7]

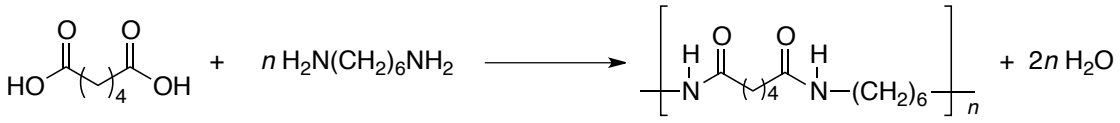

(1)

In order to obtain high molecular weight polymers, the stoichiometric ratios of the functional groups must be tightly controlled and conversion greater than 99% must be achieved. As a result, another requirement for the preparation of high molecular weight polymers is the purity of the monomeric starting materials. In addition to leading to an excess of one of the reactants, the presence of impurities in the reaction can lead to the formation of undesired products. Similarly, the reaction between two different functional groups must be selective to avoid the formation of side products.[7]

Chain-Growth:

Chain-growth polymerization has three steps: initiation, propagation, and termination. This type of polymerization requires an initiator to form the active species. This initiator can either be a free-radical source (radical polymerization), a Brønsted, or

Lewis acids (cationic polymerization), a nucleophile, or electron transfer reagents (anionic polymerization).[6] (**Scheme 1**). The subsequent step in the polymerization process is the propagation of the polymeric chain. The active species reacts with one equivalent of monomer, thereby regenerating a new active species that is one monomeric unit longer (**propagation**). This process continues until all monomer units are consumed. The propagation can be stopped (**termination**) by "quenching" the reaction (i.e. adding a reagent that will react with the propagating species and give an unreactive chain end) to give the targeted polymer. Alternatively, termination can result from a hydride transfer forming a polymer chain with a terminal alkene.[6]

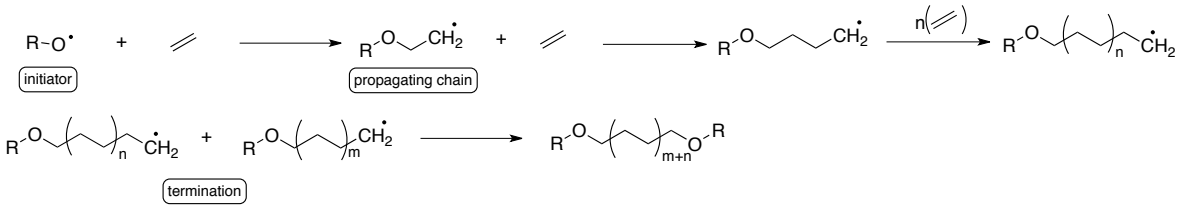

Scheme 1. Chain-growth polymerization of ethylene *via* radical initiation.

Alternatively, metal-based complexes have been widely used as initiators in chain-growth polymerizations because this polymerization process does not require harsh conditions as in radical polymerizations (temperature above 300°C, and high pressures ≈ 2000 bar) and is not limited to certain monomers that require functional groups able to stabilize the propagating species as in ionic polymerization.[6]

These metal complexes however often require activation by a co-catalyst such as methyl aluminoxane (MAO), to generate the actual active species (**I***) needed to enter the catalytic cycle (**Figure 2**). However, the activation of late transition metal complexes often can be achieved by the dissociation of a ligand followed by the coordination of a

monomer. The coordination of the monomer to the metal center activates the C=C bond. This is then followed by the insertion of an anionic fragment forming a M–C single bond, generating an empty coordination site that can be used for the coordination of another monomer and the propagating species (**M***). The polymerization cycle keeps on repeating itself until the termination step occurs. Instead of the insertion of a growing chain into the coordinated ethylene monomer to propagate chain growth, β–hydrogen elimination occurs. In this case, the long polymeric propagating chain is released from the metal center, as an alkene-terminated polymer, generating a free coordination site and the active species, which can undergo the polymeric cycle again.[6]

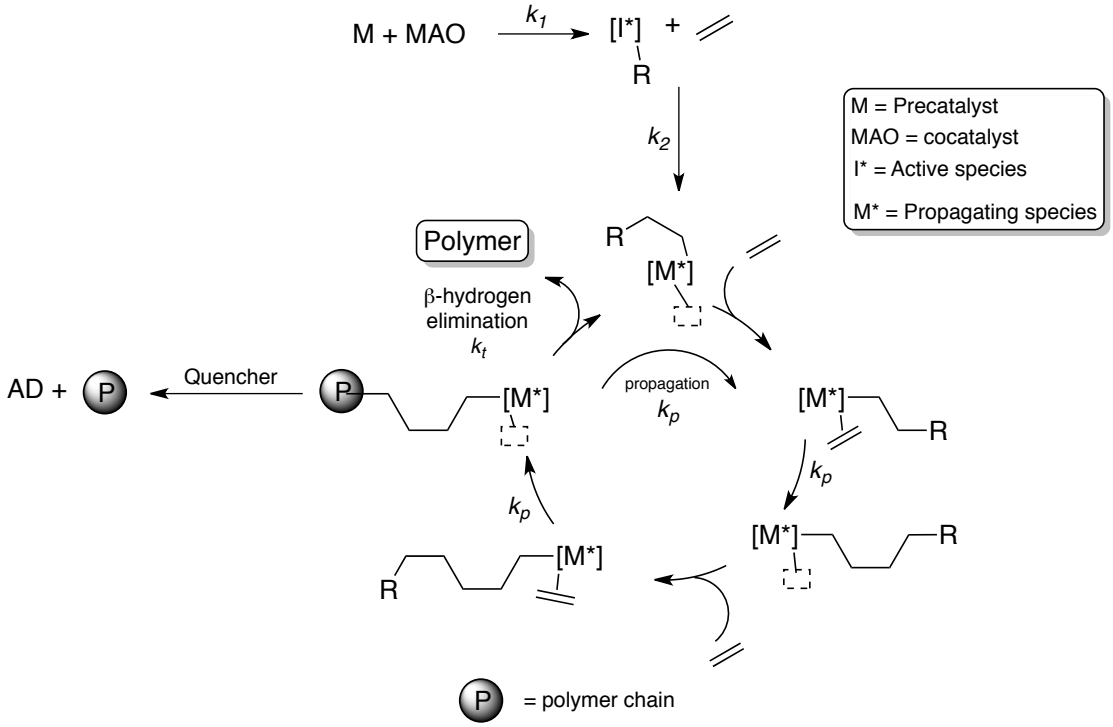

Figure 2. Metal-based mediated polymerization of ethylene.

Kinetics of Polymerization in Chain-Growth Polymerization

The following kinetics section is specific to zirconocene and any other metallocenes paired with an initiator.[8] The chain-growth polymerization process has three key steps as mentioned earlier: initiation, propagation and termination. During initiation, the precatalyst (**M**) is activated with either a monomer or by a co-catalyst (*e.g.,* MAO) forming an active species (**I***) (eq. 2). The next step is the reaction of the active species (**I***) with a monomer (**m**) to form a propagating species (**M***) (eq. 3).[8]

$$M + MAO \underset{}{\overset{K_1}{\rightleftharpoons}} I^* \qquad (2)$$

$$I^* + m \overset{K_2}{\rightleftharpoons} M^* \qquad (3)$$

In the propagation step, the propagating species reacts with one equivalent of monomer, leading to the incorporation of the monomer unit into the polymer chain and generating a new active species (**M*$_{+\,m}$**) (eq. 4).[8]

$$M^* + m \xrightarrow{k_p} M^*_{+\,m} \qquad (4)$$

The rate law of reaction for this step can then be denoted as $R_3 = k_p\,[m][M^*]$. The polymerization process is therefore directly affected by the concentration of both the monomer (**m**) and the active species (**I***) present in the solution mixture. If the active species is consumed by side-reactions or impurities in solution, then the concentration of the active species or propagating chain will decrease affecting the propagation of the polymer chain and thus the amount of polymer being produced.

The termination step results in either the quenching of the active species present in solution by the addition of a quencher or via β-hydrogen elimination. In the case of β-

hydrogen elimination, the released polymer chain has a terminal olefin, which can be easily detected by Nuclear Magnetic Resonance (NMR) spectroscopy and at the same time another active species is generated which can continue the catalytic cycle. In the case of the addition of a quencher to a polymerization reaction, the polymer is released, and an inactive species is formed (AD) (eq. 5).

$$\text{M}^* + \text{Quencher} \xrightarrow{k_t} \text{Polymer} + \text{AD} \qquad \textbf{(5)}$$

When the reaction in eq. 3 occurs rapidly and irreversibly the polymerization rate is defined in eq. 6. However, if the reaction is slow and reversible then the polymerization rate is shown in eq. 7.[8]

$$R_p = K_1\, k_p\, [\text{M}]\, [\text{MAO}]\, [\text{m}] \qquad \textbf{(6)}$$

$$R_p = K_1 K_2\, k_p\, [\text{M}]\, [\text{MAO}]\, [\text{m}]^2 \qquad \textbf{(7)}$$

In the polymerization process, the rate of propagation (k_p) should be higher than the rate of termination (k_t) in order to form a high molecular weight polymer. On the other hand, a rate of termination higher than a rate of propagation would lead to the formation of oligomers (including dimers and trimers).

The kinetics of this polymerization process are still not very clearly established as several research groups have carried on polymerization studies using a variety of metallocenes and co-catalysts which have shown a range of a first to second order dependence of R_p on the type of monomer being used.[8]

1.1.1. Group 4 Based Catalysts

Ziegler's Catalyst

Transition metal-based catalysts have found use in numerous chemical transformations over the years, specially olefin polymerization.[9–12] Ziegler had worked on ethylene polymerization with lithium alkyls in the 1940's and in his experiments showed that these reacted with ethylene to produce oligomeric α-olefins.[13] However, the complete isolation of the final product posed several difficulties. Lithium aluminum hydride ($LiAlH_4$) was thus used in lieu of alkyllithium compounds to ease the isolation of the formed products. The use of $LiAlH_4$ demonstrated that several ethylene units were inserted into the Al–H bonds. After several experiments, the Ziegler group found that Et_2AlH and Et_3Al could also insert ethylene at 100 °C to give ethylene oligomers (eq. 8). The formed oligomer chains could be used in further transformations to form long-chain alcohols that are used extensively in soaps and detergents.[13]

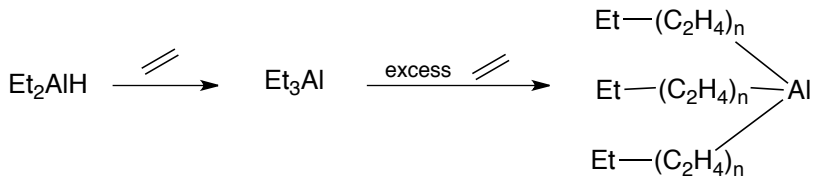

(8)

As the Ziegler group continued their research on triethylaluminum for the formation of long alkyl chains, an interesting observation was made. Instead of forming a mixture of long alkyl chains, the 1-butene dimer was in fact sometimes formed. After further investigation as to why the results had changed, they found that the glassware used during those experiments contained residual amounts of nickel salts. This finding intrigued Ziegler and he decided to investigate the effect of incorporating metal salts on

the oligomerization of ethylene. The addition of titanium salts to aluminum alkyls generated high molecular weight polyethylene instead of oligomers.[13]

The discovery of the Ziegler's catalyst $TiCl_4/Et_2AlCl$ for olefin polymerization was of great impact in the industry since it required lower temperature and pressures compared to the common methods used at the time, which required high temperature (up to 200 °C), high pressure (2000 atm) and radical initiators.

Natta's Catalyst

The outstanding discovery by Ziegler led several research groups into the application and development of catalytic systems for the polymerization of olefins. Natta investigated and discovered that a modified Ziegler's catalyst ($TiCl_3/AlClR_2$) could also polymerize α-olefins, such as propylene.[14] The polymerization of propylene using the modified catalyst produced atactic polymeric chains that were soluble in the solvent medium. Further modification of Ziegler's catalytic system led to the control of the stereoregularity of the polymers (**Figure 3**). The polymerization of prochiral monomers, such as styrene and propylene, leads to polymer chains with chiral centers on every other carbon in the polymer chain leading to the three possible tacticities: atactic, syndiotactic, and isotactic.[15] In the atactic configuration, the polymer chain has the R groups off of the main chain pointing at random space orientation which leads to a relative configuration of the stereogenic centers to be random (e.g. RSSRRSSRSR). In the syndiotactic case, the R groups have an alternating space orientation leading to an alternate configuration of the stereogenic centers to be RSRSRSRS. In the isotactic case the R groups have the same relative orientation of the substituent leading to a configuration of the stereogenic

centers to be either RRRRR or SSSSS. The formation of a specific conformation can be controlled by the structure of catalyst used for the polymerization process.[6]

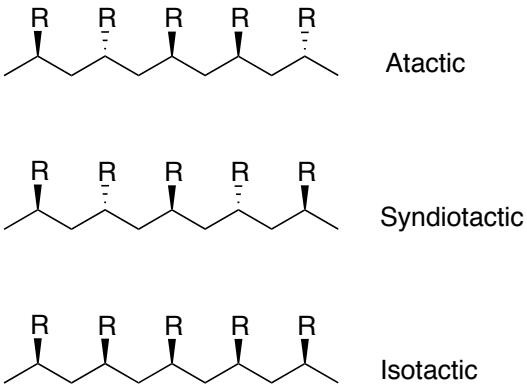

Figure 3. Different tacticities of a substituted polymer.

Natta's group was able for the first time to isolate crystalline products from the polymerization of propylene, styrene and α-butylene.[16] The physical properties of the crystalline products were compared to those of the related amorphous polymers. It was determined that the crystalline product had a higher melting point, were denser and these compounds had limited solubility in organic solvents. In the case of polypropylene, X-ray experiments shed light into the chemical structure of the main chain as well as the configuration of the methyl groups and it was determined that the methyl groups have the *R* or S configuration at the stereogenic centers (isotactic).[16]

Metallocenes.

The use of Ziegler-Natta catalysts ($TiCl_4$ supported on $MgCl_2$ with triethylaluminium) is limited due to the difficulty to influence the polymer structure. The first metallocene (ferrocene) was reported by Fischer and Wilkinson in 1952 (**Figure 4**).[17] These compounds have a π-bonded metal atom "sandwiched" between two aromatic rings systems. After the discovery of metallocenes, several analogs were prepared using metal precursors from group 4 and 5.[18] As such, zirconocene dichloride can polymerize up to 100 tons of ethylene per gram of zirconium in the presence of MAO (**Figure 5**).[19]

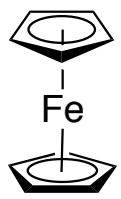

Figure 4. Ferrocene, the first metallocene synthesized

The implementation of metallocenes as olefin polymerization catalysts has increased due to their better solubility in hydrocarbons, the formation of only one active species, the catalyst tuneability, and the higher catalytic activity (10 – 100 times) than that of the common Ziegler-Natta systems.[19] These advantages over those of the Ziegler-Natta systems allowed to predict and control the stereochemistry and thus the properties of the formed polymer. The facile structure tunability of metallocenes allowed the synthesis of chiral version, such as the bridged metallocene reported in 1982 by Brintzinger *et al.* that produces partially isotactic polypropylene (**Figure 6**).[20]

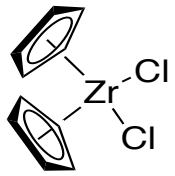

Figure 5. Bis-cyclopentadienyl zirconium dichloride

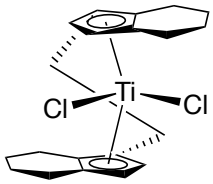

Figure 6. Chiral metallocene reported by Brintzinger.

Following the synthesis of metallocenes and their higher catalytic activity for olefin polymerization than the common Ziegler-Natta systems, several analogs were reported to impart higher stereoregularity on the polymer chain (**Figure 7**). The addition of substituents off the aromatic rings increase the stereoselectivity for syndiotactic polymer than its parent structure. These catalytic systems showed a catalytic activity up to 7 000 kg polymer mol^{-1} Zr h^{-1} at 60 °C in the presence of MAO as cocatalyst.[4,21–23]

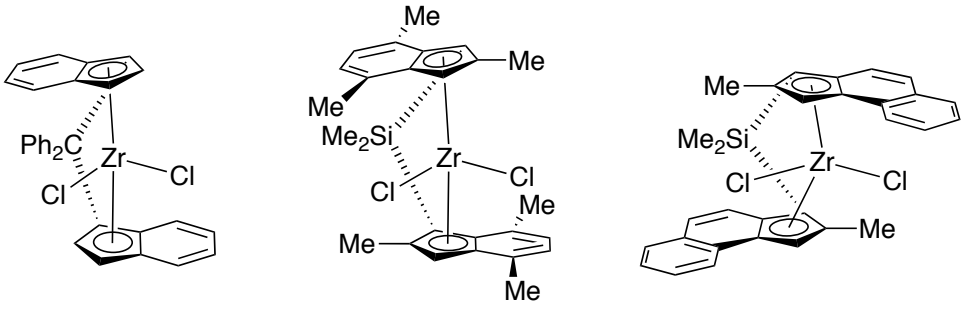

Figure 7. Example of metallocenes analogs from the work by Brintzinger.

Fujita and FI Catalyst.

A separate family of olefin polymerization catalysts, based on the Schiff base phenoxy-imine, commonly known as FI catalysts, have been developed by Fujita.[23] The FI pre-catalysts have an octahedral geometry where two bidentate phenoxy-imine ligands and two X type ligands coordinate to the metal centre, generating up to five isomers with different catalytic activity (**Figure 8**).[24]

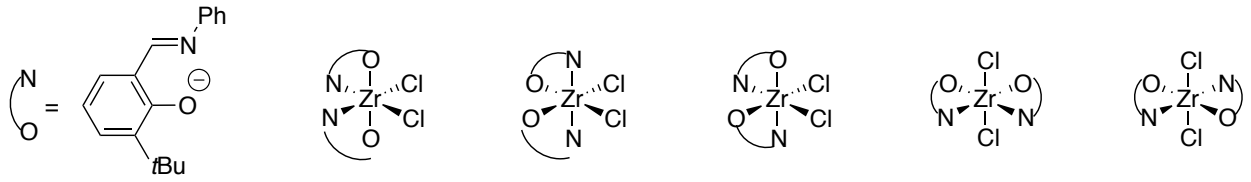

Figure 8. Possible isomers observed from the coordination of the FI ligand onto Zr (with only one of the two enantiomers shown, if applicable).

These catalysts benefit from high catalytic activities in olefin polymerization under mild conditions. A common phenoxy-imine (FI) complex **1** (**Figure 9**) has shown an activity of 519 kg PE $mmol^{-1}$ Zr h^{-1}, which is a notable increase from that of the Cp_2ZrCl_2/MAO catalyst system (27 kg PE $mmol^{-1}$ Zr h^{-1}).[23] These catalytic systems are capable of producing ultrahigh molecular weight linear polyethylene and block polymers.[25]

The highly oxophilic nature of group 4 transition metals normally prevents their use in either homo- or copolymerization of polar monomers, such as acrylates. However, these complexes are already composed of heteroatom ligands (**Figure 9**), which can donate additional electron density to the metal center making it less oxophilic. Therefore, the tendency to be deactivated by a polar monomer is less, resulting in catalysts with a higher tolerance of variety of polar monomers. This feature has enabled these catalysts to copolymerization of ethylene with polar vinylic monomers such as acrylates, vinyl acetate, and acrylonitrile.[26]

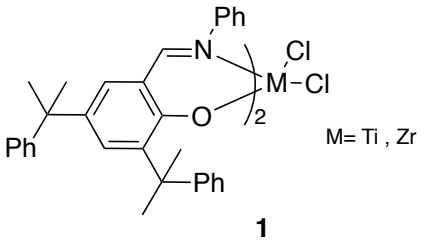

1

Figure 9. FI catalyst.

The copolymerization of ethylene and polar vinylic monomers was achieved in the presence of a large excess of MAO (250 equiv. with respect to ethylene). The authors used MAO as a cocatalyst and as a “protecting group” to mask the heteroatom of the

polar vinylic monomer to impede the formation of the σ-complex between the heteroatom and the metal center and prevent catalyst deactivation. Another interesting fact is that the polar vinylic monomer (5-hexene-1-yl acetate) was chosen to work in this polymerization, which has four CH_2 spacers between the double bond and the polar group. This large spacer between these groups and a large excess of the Lewis acidic aluminum with respect to the functional group leaves the double bond as the only moiety that can be coordinated and thus activated by a Ti-based complex. These reactions are however not viable for any large-scale commercial processes. Therefore, there is still a need to develop better group 4-based catalysts that can copolymerize ethylene and a wide variety of polar vinylic monomers under common conditions.

Imidazol-2-imine Ethenolate Complexes

The Lavoie group was inspired by the work on the salicylaldiminate system for the preparation of the first monoanionic bidentate ligand imidazol-2-imine ethenolate, because of the versatility to modify the electronic and steric characteristics of the building blocks. This ligand can access two canonical forms as depicted in **Figure 10**. The ligand scaffold consists of an imidazol-2-imine fragment and an enolate as the anionic fragment.[27]

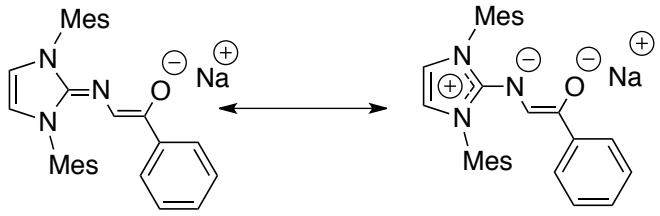

Figure 10. Canonical forms that the imidazol-2-imine ethenolate ligand can access.

The bidentate ligand was coordinated to group 4 metal centers and the activity of the metal complexes were assessed for ethylene polymerization in the presence of MAO

as cocatalyst (**Scheme 2**). The zirconium complexes only gave traces of polyethylene, while the titanium complexes demonstrated a catalytic activity up to 170 Kg PE mol cat^{-1} h^{-1}.The most active catalyst bore an electron-withdrawing chlorine atom at the *para* position of the phenyl ring. It was thus demonstrated that electronic modifications of the bidentate ligand had a drastic impact on the activity of the resulting catalysts.

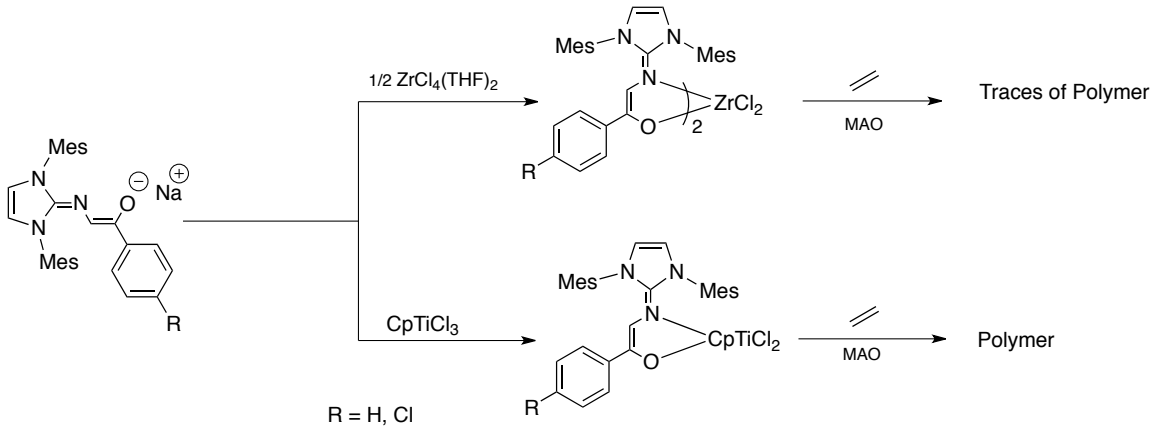

Scheme 2. Synthetic route to access group 4 metal complexes bearing the novel bidentate anionic ligand.

1.1.2. Group 10 Based Catalysts

Complexes based on early transition metals have been used extensively in the polymerization of ethylene and propylene as discussed in the previous sections. However, these highly oxophilic complexes faced several issues when polar vinylic monomer were used. In contrast, late transition metal-based complexes are less oxophilic and therefore their implementation in copolymerization of ethylene and polar vinylic monomers have drawn significant interest to address the shortcomings of early transition metals. Several research groups have investigated the use of these less oxophilic complexes in copolymerization.

Nickel-based catalysts

Shell Higher Olefin Process Catalyst (SHOP)

The Shell Higher Olefin Process (SHOP) catalyst, developed by Keim e*t al*. in 1979, is a nickel(II)-based complex that produces oligomers of ethylene.[28] The preparation of compound **2** can be achieved via oxidative addition of a keto-stabilized phosphorus ylide which in turn can be transformed into the active nickel hydride complex **3** (**Scheme 3**). The activation can be accomplished when reacting compound **2** with ethylene.[29,30]

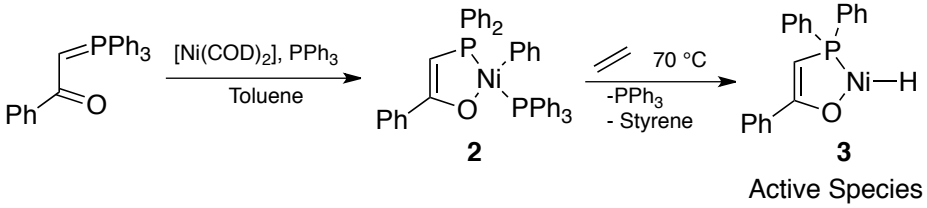

Scheme 3. Synthesis and activation of a SHOP-type pre-catalyst.

The spectator ligands used in the nickel complex impart a square planar geometry and provide a free coordination site for the incoming olefin to coordinate to the metal in the catalytic cycle.[3] The selectivity for dimers and oligomers and activity of the catalyst can be enhanced by varying the P^O^{-} chelating ring size, and by changing the electronic and steric features of the phosphinoenolate bidentate ligand. For example, as the chelating ring size and the rigidity of the ligand increases, the catalytic activity decreases with very little to no activity observed with metallacycle ring sizes larger than seven.[30] The incorporation of electron-withdrawing groups on the bidentate ligand motif was also found to increase the catalytic activity of the catalyst. For example, when a sulfonato group is incorporated at the $C_{\alpha\text{-}P}$ atom of **3** has shown an almost 90-fold in catalytic activity.[30,29]

The deactivation of SHOP catalysts can occur by the coordination of two phosphinoenolate ligands to form the bis-chelated complex **4** (**Scheme 4**), resulting in a catalytically-inactive compound.[31] However, the isolated bis-chelated complex can be activated by the addition of trimethylaluminum forming a new species (**Scheme 4a**). The resulting complex dissociates the complex composed of Al, O, and P by the addition of a neutral ligand to give the known pre-catalyst as shown below (**Scheme 4b**) and an inactive aluminum complex (**Scheme 4c**).[31]

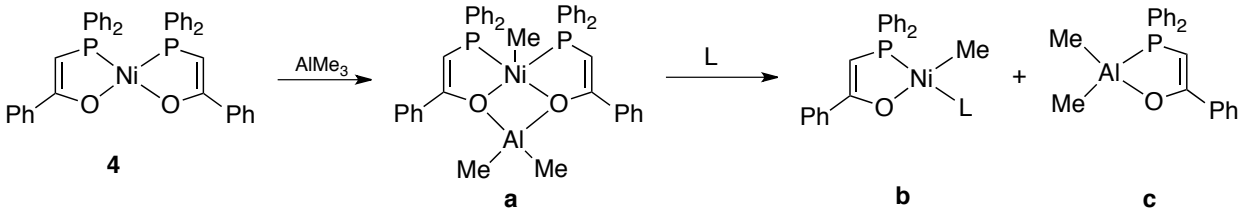

Scheme 4. Reactivation of the bis-chelated nickel complex to the active catalyst.

Modification of the SHOP-type Catalyst

Grubbs replaced the phosphorus-oxygen (P^O$^-$) ligand with the phenoxy-imine (FI, as described above) N^O$^-$ ligand. The corresponding nickel catalysts (**5**) were active in olefin polymerization and copolymerization of ethylene with heteronuclear vinylic monomers such as acrylates albeit with relatively poor rates (eq. 9).[32] One deactivation pathway was mitigated by increasing the overall steric bulk of the ligand, thereby minimizing the propensity of a second ligand to coordinate and generate an analog inactive species as in the case of compound **4** .[29]

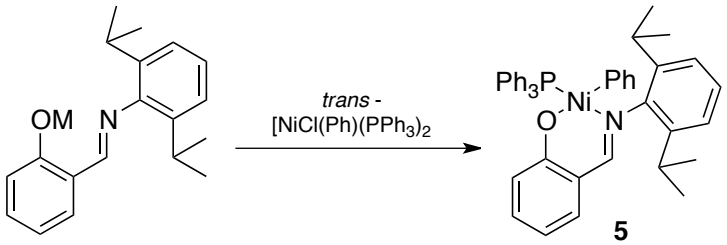

(9)

Brookhart-type catalyst

Copolymerization of ethylene and functionalized vinyl monomers has historically been achieved by radical polymerization and often requires high pressure.[33] In 1996, Brookhart *et al.* reported new catalytic systems (**Scheme 5**) based on late transition metals (Pd and Ni) to facilitate the copolymerization of ethylene and polar monomers, such as alkyl acrylates. [34]

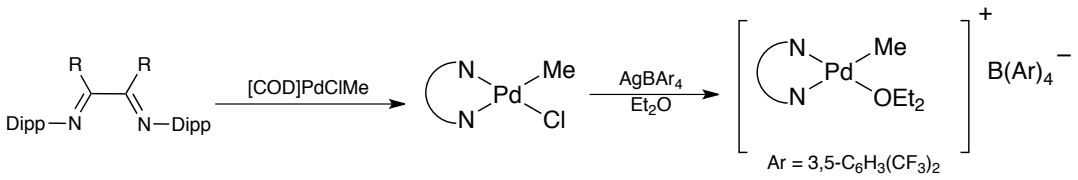

Scheme 5. Synthesis and activation of a Brookhart-type complex for olefin polymerization.

Employing the cationic catalytic system, olefin copolymerization of ethylene and acrylates was accessed giving copolymers with high molecular mass.[34] However these systems faced several problems, including catalyst deactivation due to the interaction of the polar monomer and the two possible insertion pathways of the growing polymer chain into the polar vinylic monomer as displayed in **Scheme 6**.

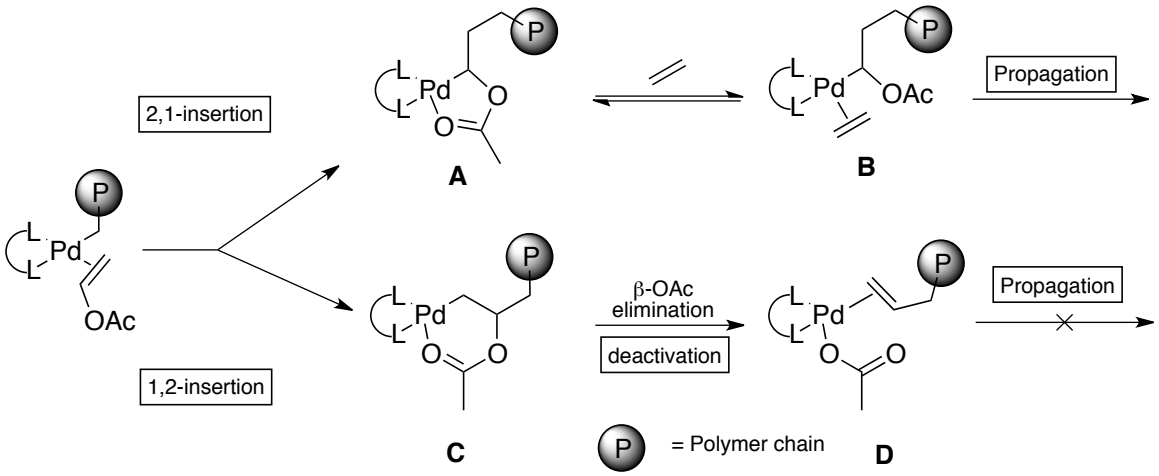

Scheme 6. Chain termination (via 1,2-insertion) and chain propagation (via 2,1-insertion) for the polymerization of vinyl acetate.

Insertion of the monomer preferably proceeds via a 2,1-insertion pathway (**Scheme 6 top**), which leads to the formation of a weak five-membered chelated complex (**A)**. The oxygen donor atom dissociates to generate a free coordination site used for another equivalent of monomer to occupy (**B**). On the other hand, the 1,2-insertion leads to the deactivation of the active species by generating the palladium acetate complex **D** from the intermediate **C** through the irreversibly β-acetate elimination.

The Brookhart catalytic system gives highly branched copolymers of ethylene and propylene. This catalytic system also shows great activity for copolymerization of olefins (ethylene or propylene) with alkyl acrylates giving copolymers with high molecular weight. However, the functional group was not included in the main polymer chain but rather at the end of the branches (eq. 10). Interestingly, the change of the substituents off of diimine backbone did not affect the percentage of alkyl acrylate incorporated in the main polymer chain.[34]

(10)

Drent-type catalyst

To build on the previous work reported by Keim, Grubbs, and Brookhart, Drent reported a new palladium-based catalyst in 2002.[35] This has been of great interest because it requires milder conditions compared to earlier copolymerization systems of ethylene and polar vinyl monomers. Moreover, new types of polymers were generated, such as random linear poly(ethylene-*co*-carbon monoxide) and alternate poly(polar vinyl monomer-*alt*-carbon monoxide).[36] Another property that was improved was the percentage of polar monomer in the main polymer chain in contrast to what was observed when the Brookhart catalyst was used. The utilization of Drent-type catalysts has increased due to the ease to form stereo-regular copolymers of vinyl monomers containing polar groups. With different polar groups present in the main chain of the polymer, the physical properties of the polymer and scope of applications broaden and allow for enhanced printability, dyeability and adhesion over that of simple polyethylene or polypropylene.[36]

The catalyst was accessed by the reaction of a neutral palladium precursor $Pd(OAc)_2$ with di(2-methoxyphenyl)phosphinobenzene-2 sulfonic acid) (eq. 11). The first copolymerization reported by Drent was with alkyl acrylate and ethylene.[35]

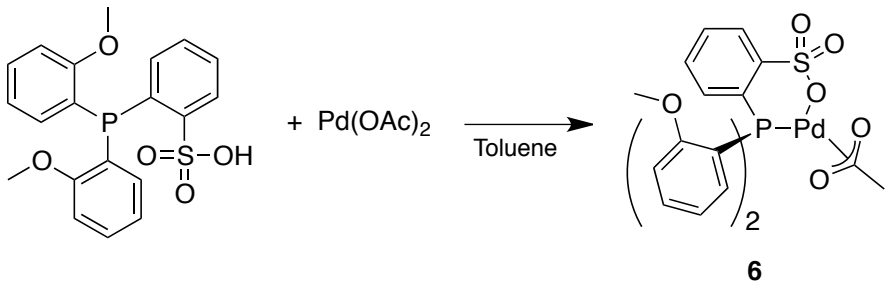

(11)

Copolymerization of ethylene and acrylates was carried on using complex **6**. The resulting polymer incorporated approximately 10% of polar monomer units in the linear polyethylene backbone chain (eq. 12). In order to increase the incorporation of methyl acrylate, an increase in its concentration was required, which was detrimental to the activity of the catalyst.

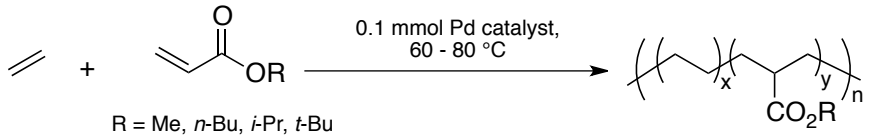

(12)

Several analogues (**Figure 11**) of the original Drent catalyst, where the electronic and steric characteristics of the phosphine donors have been modified, have been reported by Claverie[37] and Nozaki.[36,38] These systems showed great catalytic activity for ethylene polymerization and formed high-molecular weight polymer that had not being possible using group 10 metal centers. Furthermore, the use of these complexes aided with the formation of new polymers, for example, linear copolymers of polar monomers and ethylene, and copolymers of polar monomers and carbon dioxide that had not been observed before.

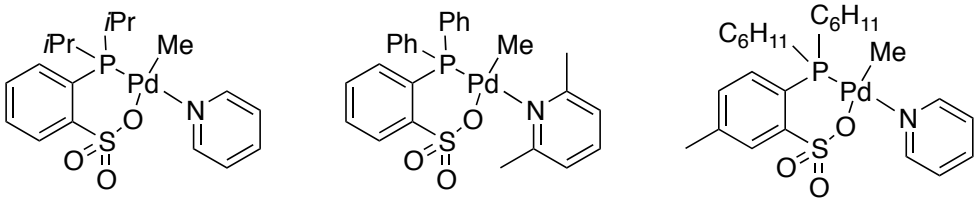

Figure 11. Examples of the Drent-type complex.

1.2 Frustrated Lewis Pairs

Lewis acids and Lewis bases normally form adducts. As an example, borane (BH_3) has an empty *p*-orbital that can be populated by an electron pair, making it a Lewis acid. In contrast, tetrahydrofuran (THF), a Lewis base, has two lone pairs that can be donated. When these two compounds react, they form a Lewis pair. Frustrated Lewis pairs are Lewis acids and bases that cannot form an adduct due to the steric hindrance impeding the interaction between the lone pair of the Lewis base and the empty orbital of the Lewis acid.

The hydrogenation of functional groups, such as alkenes and alkynes, requires the presence of a metal catalyst, such as nickel and palladium. In heterogenous catalytic systems, hydrogen is adsorbed on the metal surface, resulting in the activation of the H–H bond leading to the breakage of the bond and the formation of relatively weak Pd–H bonds. The substrate to be hydrogenated also adsorbs on to the metal surface weakening the double bond. A hydrogen atom is then transferred from the metal surface to one of the carbon atoms from the double bond. Subsequently, another hydrogen atom is transferred from the catalyst bed to the substrate forming the saturated molecule that in turn desorbs from the metal surface for a new catalytic cycle to begin.

A breakthrough in the hydrogenation of substrates containing a double or triple bond such as imines, enamines, while alkene and alkynes can also be hydrogenated under high H_2 pressure, was reported by Stephan *et al.* in 2006.[39] Stephan and his group pioneered the use of frustrated Lewis pairs as a transition metal-free hydrogenating agents.[40] In their early work, bulky secondary phosphine, such as bis(2,4,6-trimethylphenyl)phosphine, was reacted with tris(pentafluorophenyl)borane (BCF), resulting in an aromatic substitution at the *para* position of BCF, displacing a fluorine atom and making a new P–C bond (**Scheme 7**). The fluorine atom, in turn, makes a bond with the boron atom. Treatment of the zwitterion compound with chlorodimethylsilane led to the replacement of the fluorine atom on boron with hydrogen, resulting in a molecule that formally contains both a proton and a hydride.[40] When the zwitterionic compound is heated to 100 °C, hydrogen gas is released. The activation and release of hydrogen gas was shown to reversible. However, the catalytic activity of this system for hydrogenation for olefins and alkynes (under normal condition) is still far behind from the activity that metal-based catalysts showed.[41]

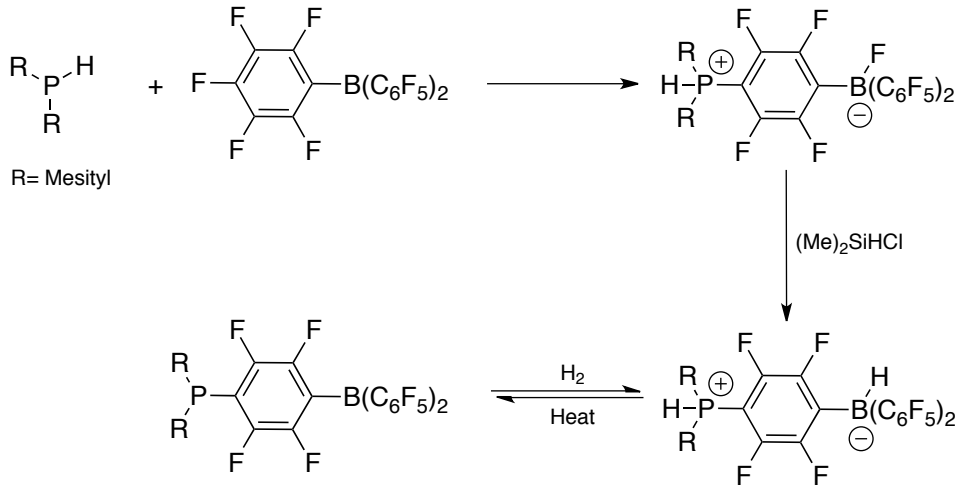

Scheme 7. Reaction scheme for the formation of a H_2 activating compound from frustrated Lewis pairs.

1.3 Inversely-Polarized Phosphaalkenes

A phosphaalkene refers to both a phosphorus–carbon double bond and to a molecule containing such functional group. Under most circumstances, P–C bonds are polarized with a partial negative charge on the carbon atom and a partial positive charge on phosphorus, as predicted from the Pauling electronegativity values. In this case, the phosphorus atom behaves as an electrophile. However, when electron-donating atoms are attached to the carbon in the C–P bond, the polarity of the double bond is reversed, resulting in a partially negatively-charged and nucleophilic phosphorus atom (**Figure 12**).

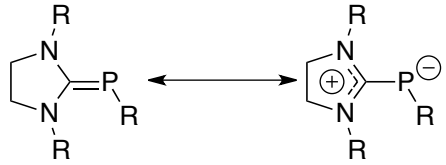

Figure 12. Canonical resonance forms of an inversely-polarized phosphaalkene.

The first inversely-polarized phosphaalkene (IPP) **7** was reported by Schmidpeter *et al.* in 1980.[42] The IPP was obtained by reacting the dicyanophosphide anion with benzimidazolone followed by the addition of sodium diethylphosphite forming the desired cyanophosphinidene (**Scheme 8**).

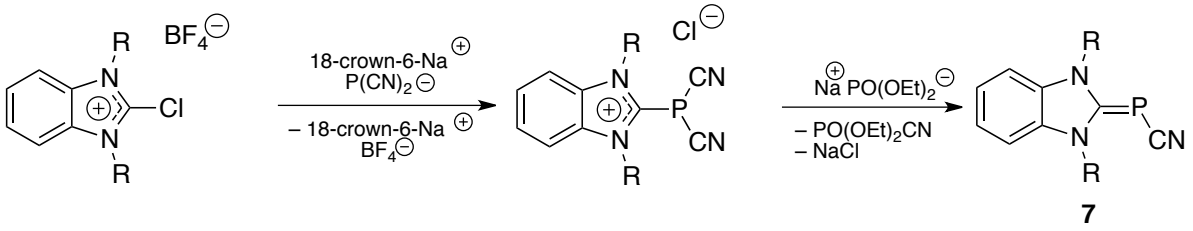

Scheme 8. Synthesis of the first inversely-polarized phosphaalkene reported by Schmidpeter.

The infrared (IR) and nuclear magnetic resonance (NMR) spectroscopies of **7** are consistent with a partial negative charge on the PCN fragment and a partial positive

charge on the benzimidazole group, as shown in its resonance forms (**Figure 13**), as supported by infrared (IR) and nuclear magnetic resonance (NMR) spectroscopies. The IR stretching frequency for the CN group in compound **7** was reported to be 2105 cm^{-1}, close to that reported for the $P(CN)_2^-$ anion (2120 cm^{-1}). This supports the hypothesis that the PCN moiety bears a partial negative charge as shown in its resonance form.[42]

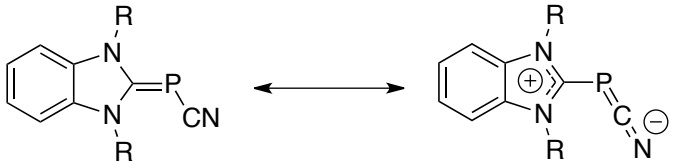

Figure 13. Resonance forms of the first IPP compound.

To further support the hypothesis that a negative charge is delocalized over the PCN moiety, three previously synthesized compounds were used to rationalize the electronic environment around the phosphorus atom: the free counterion $P(CN)_2^-$ (^{31}P NMR: δ –193.0 ppm)[43], compound **8** and compound **9** (**Figure 14**)[43]. Compound **7** resonates at –133.0 ppm that resides within the chemical shift range of the counter ion $P(CN)_2^-$ and **9**.

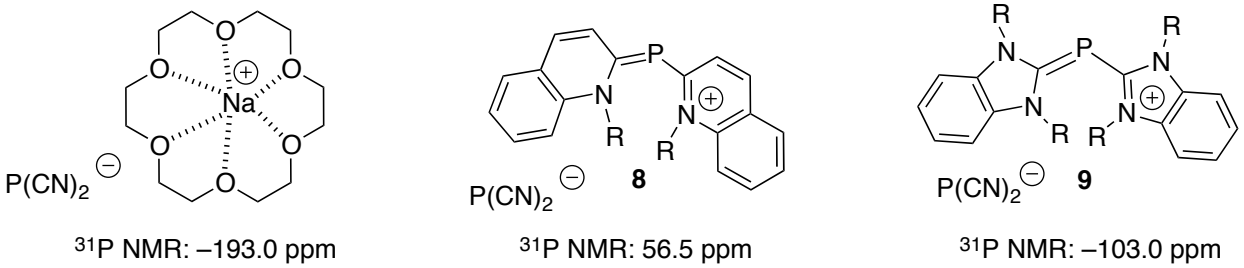

^{31}P NMR: –193.0 ppm ^{31}P NMR: 56.5 ppm ^{31}P NMR: –103.0 ppm

Figure 14. Molecules used to determine the chemical shift of the new synthesized IPP (**7**).

In 1989, Regitz *et al.* demonstrated the synthesis a phosphaalkene with inverse electron density in a modified synthetic route to that of Schmidpeter.[44] This modified approach utilized cyclopropenone and lithium phosphide followed by the addition of TMSCl to form the desired phosphaalkene (eq. 13).

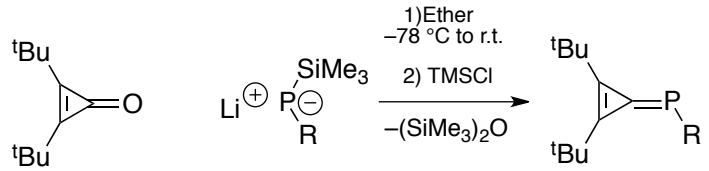

(13)

^{31}P NMR: – 74.1 ppm

This species demonstrated resonance structures in which the phosphorus atom has a partial negative charge and the carbon bears a partial positive charge (**Figure 15**). This compound was the very first one to have an inversed electron density distribution where the substituents attached to the carbon atom in the C=P bond are only alkyl substituents.[44]

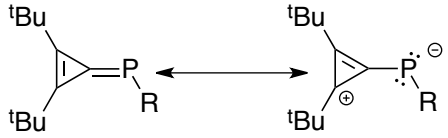

Figure 15. Resonance forms of the IPP synthesized by Regitz.

Regitz *et al.* also demonstrated *via* chemical reactions that the phosphorus atom had in fact a partial negative charge (**Scheme 9**). Methyl lithium was added to the phosphaalkene giving as product the cyclopropenyl phosphide (**Scheme 9b**)**.** This compound was subsequently treated with trimethylsilyl chloride (TMSCl) to give the neutral phosphane (**Scheme 9c**).[44] The nucleophilic attack of the methyl group on the carbon bearing the *t*-butyl occurs because the p orbital on the carbon in the C–P bond is partially populated by the electron density from the phosphorus atom. The atoms where

the nucleophile can attack is either carbon bearing the *t*-butyl groups, which is the case for the formation of **b**.

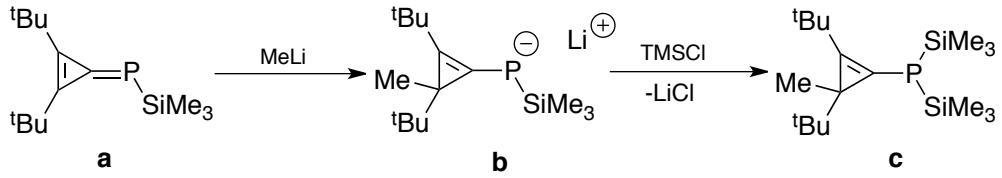

Scheme 9. Nucleophilic attack on an inversely polarized phosphaalkene displaying only alkyl groups.

Inspired by the reaction of N-heterocyclic carbene (NHC) building blocks and elemental sulfur to give imidazol-2-thiones, Arduengo *et al*. reported the first synthesis of an inversely-polarized phosphaalkene utilizing an isolated NHC free carbene and a cyclic phosphinidene (eq. 14).[45] The free carbene was reacted with pentaphenylcyclopentaphosphorane in a 5:1 ratio to attain the desired compound. The resulting compound showed a resonance in the ^{31}P NMR spectrum at –53.6 ppm, indicative of an inversely polarized phosphaalkene.

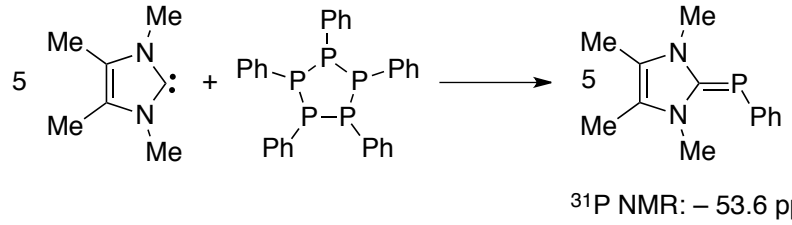

(14)

^{31}P NMR: – 53.6 ppm

Since then, several research groups have synthesized inversely polarized phosphaalkenes based on the synthetic route developed by Arduengo.[45] For example, Bertrand reported a two-step synthesis with moderate yields (eq. 15). The first step in this one-pot synthesis involved the reaction between an NHC and dichlorophenylphosphine

generating the chloroimidazolphenylphosphonium chloride, which was immediately reduced to access the phenylphosphaalkene.[46]

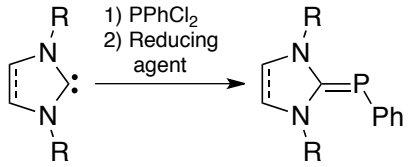

(15)

These phosphaalkenes were used by Bertrand *et al.* to qualitative assess the π-acidity of several NHC by ^{31}P NMR spectroscopy. Several IPPs were synthesized following the procedure shown previously and using the synthetic route described by Arduengo. [47,48] When highly π-acidic carbene motifs are used, the "phosphinidene" can donate more electron density into the *p*-orbital on the carbenoid carbon. As a result, the C–P bond has a greater double character and the resonance in the ^{31}P NMR spectrum appears downfield (**Figure 16**).

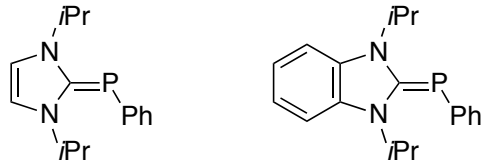

^{31}P NMR = –61.2 ppm –34.6 ppm

Figure 16. Electronic effect of the π-acidity of the imidazole-2-ylidene (**left**; more π-acidic) and of the benzimidazole-2-ylidene (**right**; less π-acidic) carbene building block on the ^{31}P NMR chemical shift of the resulting phosphaalkene.

Hudnall reported a one-pot synthesis for phosphaalkenes based on highly π-acidic NHCs, decorated with carbonyl groups. Reaction of these NHCs with dichlorophenylphosphine followed by addition of TMSOTf formed the desired phosphaalkene in moderate yields (30–60%) (eq. 16)[49]. Hudnall *et al*. explored the effect of electron-withdrawing groups decorating the backbone of the NHC carbene on the

donation of electron density to the phosphorus atom. The presence of a π-acidic carbene motif led to a significant increase in the ^{31}P NMR chemical shift to values that are not characteristic of inversely-polarized phosphaalkenes. For example, the 4,5-dicarbonyl-1,3-dimesityl-(phenylphosphinylidene) imidazolidine resonated at 78.6 ppm indicating that the phosphorus atom was electron poor and therefore a very weaker nucleophile than the parent 1,3-dimesityl-(phenylphosphinylidene) imidazolidine (^{31}P NMR *∂* –10.5 ppm).[49]

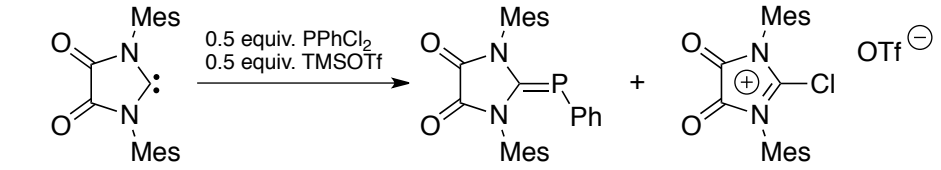

Mes= 2,4,6-trimethylphenyl

(16)

The steric and electronic characteristics of the phosphorus atom in IPPs can be further tuned by changing the substituent on phosphorus. By replacing the phenyl group with a hydrogen atom, the phosphorus atom becomes a stronger nucleophile (**Figure 17**). It furthermore opens new synthetic strategies for ligand design. Evidence of the strong nucleophilicity of this phosphorus atom is supported by the ^{31}P NMR chemical shift of –132 ppm.[50,51] The hydrido IPP can thus be used to undergo classic S_N2 reactions to prepare derivatives to be used as bidentate ligands.

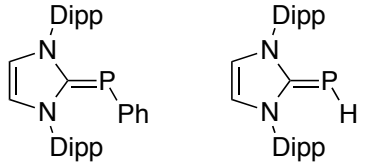

Dipp= 2,6-diisopropylphenyl

^{31}P NMR: –18.3 ppm –132.0 ppm

Figure 17. The effect of the phosphorus substituent on the ^{31}P NMR chemical shift.

There are several synthetic routes to access the NHC-based hydrido phosphaalkenes depicted in **Scheme 10.** Grützmacher demonstrated the utility of sodium phosphaethynolate Na(OCP) as an alternate method to synthesize inversely-polarized phosphaalkenes.[50] Na(OCP) was reacted with one equivalent of imidazolium salt to give the corresponding phosphaalkene with a hydrogen atom bonded to phosphorus (**Scheme 10a**). However, the synthetic routes to access M(OCP) are quite difficult and dangerous; in some cases M_3P_7 (M= Na, K) is used in the presence of carbon monoxide (CO) at high temperatures.[50]

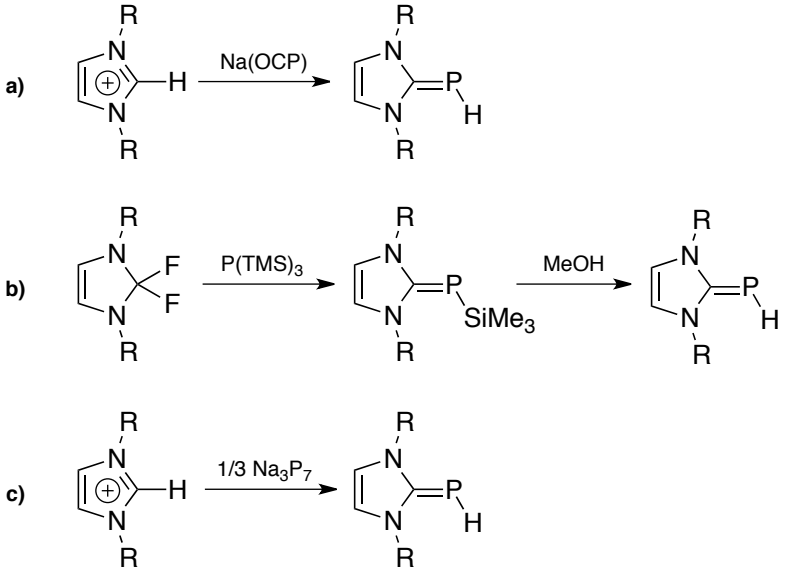

Scheme 10. Synthetic routes to access the hydrido phosphaalkene.

Tamm *et al*. also prepared an IPP (**Scheme 10b**) which contained a hydrogen atom instead of a phenyl group bonded to the phosphorus atom. The IPP was access through the reaction of N,N'-1,3-bis(2,6-diisopropylphenyl)-2,2-difluoroimidazole and tris(trimethylsilyl)phosphine ($P(TMS)_3$). This reaction yielded a phosphaalkene with a TMS group attached to phosphorus in good yields (83%).[52] In turn, this phosphaalkene was treated with methanol to replace the TMS group for a hydrogen atom.

The preparation of hydrido-IPPs has been also reported by Cicač-Hudi, using Na_3P_7 (**Scheme 10c**).[51] The phosphorus source (Na_3P_7) reacts with either imidazolinium and imidazolium salts to generate the corresponding inversely-polarized phosphaalkenes, NHC=PH in great yields.[51] Similar results were observed when tris(trimethylsilyl) heptaphosphide ($P_7(TMS)_3$) was used as a phosphorus source to access the corresponding IPP. The synthesis of M_3P_7 also have dangerous steps such as the reflux step of a solution of tetrahydrofuran (THF) and dimethoxyethane (DME) containing red phosphorus and the corresponding metal. However, the temperature is not as high as that required for the synthesis of M(OCP) and the use of CO is not needed. In the case of $P_7(TMS)_3$, its synthesis is done at colder temperature (–78 °C) in toluene and to isolate the product a filtration step is required.

1.3.1 Inversely-Polarized Phosphaalkenes employed as ligands.

Since the synthesis and isolation of the first inversely-polarized phosphaalkene by Schmidpeter in 1980,[42] a few research groups have investigated these as spectator ligands in coordination chemistry. In 1993, the first transition metal complex bearing an IPP was reported by Weber *et al*.[53] Compound **10** was reacted with Fe and Ru metal precursors to form the corresponding complexes (eq. 17).[53]

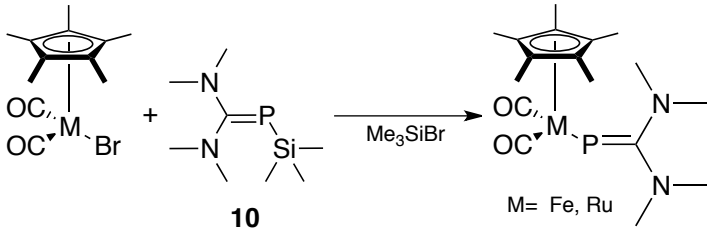

10

(17)

Mézailles *et al*. demonstrated the flexibility of the coordination modes of inversely-polarized phosphaalkenes (**Scheme 11**) as monodentate (**top**), bridging (**middle**), and bidentate ligands (**bottom**) utilizing metal centers from group 10.[54]

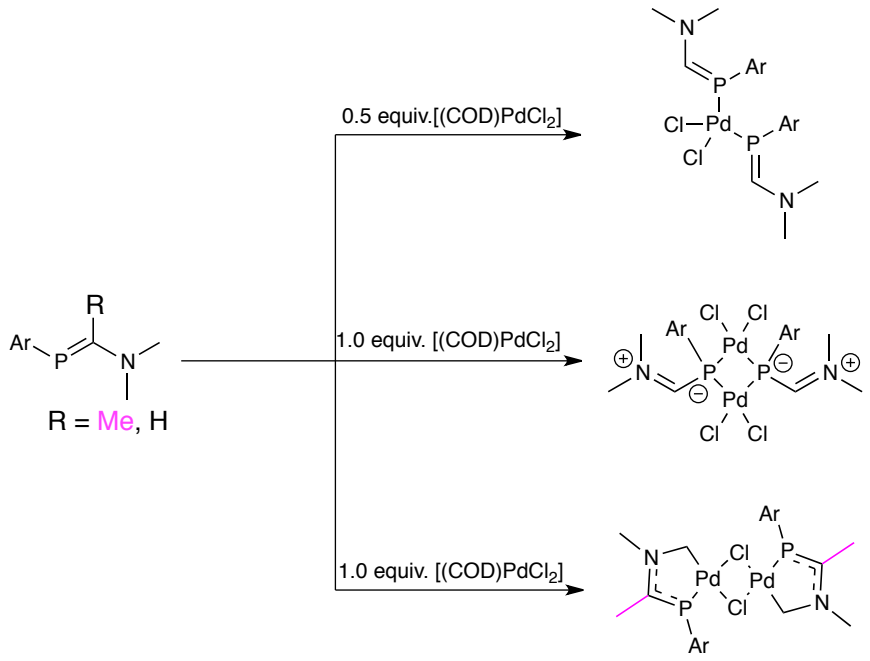

Scheme 11. Monodentate (**top**), bridging (**middle**) and bidentate (**bottom**) coordination modes reported for inversely-polarized phosphaalkene can access.

Bertrand *et al.* demonstrated the coordination of inversely-polarized phosphaalkenes as a bridging ligand in the presence of Lewis acids, such as BH_3, and of coinage metals (copper, silver and gold) (**Scheme 12**). The IPP employed in these examples displayed more contribution of the canonical form in which the phosphaalkene has two lone pairs are on the phosphorus atom that can coordinate to two molecules.[55]

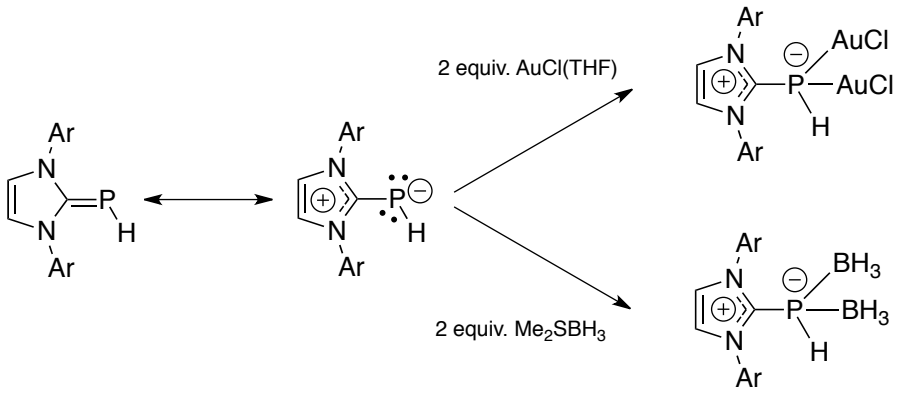

Scheme 12. Coordination of IPP to two equivalents of boron (**bottom**) and gold (**top**)

Tamm *et al.* have also utilized IPP's as monodentate anionic ligands to coordinate on to transition metal centers such as ruthenium and rhodium.[52] 1,3-bis(2,6-diisopropylphenyl)-2-((trimethylsilyl)phosphinylidene)-2,3-dihydro-1H-imidazole was reacted with $[(\eta^5\text{-}C_5Me_5)RhCl_2]_2$ and $[(\eta^6\text{-}$ *p*-cymene$)RuCl_2]_2$ to yield the corresponding complex bearing an IPP as a monodentate monoanionic ligand. (**Scheme 13**)[52]

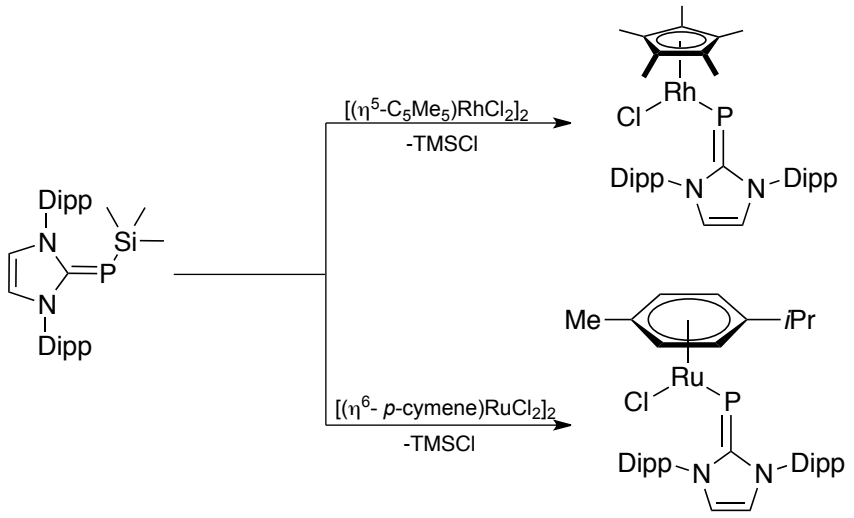

Scheme 13. Coordination of IPP's on to metal precursors as a monoanionic ligand.

The Lavoie group has also investigated these inversely-polarized phosphaalkenes as neutral monodentate ligands. IMes=PPh was reacted with Grubbs first-generation ruthenium benzylidene complexes $RuCl_2L_2(CHPh)$ (L= PPh_3 or PCy_3). The phosphaalkene reactivity varied depending on the nature of the metal precursor. In the case of $RuCl_2(PPh_3)_2(CHPh)$, the phosphaalkene displaced one of the PPh_3 groups leading to compound **11** (**Scheme 14**). If a solution of **11** is left for a long period of time, compound **11** undergoes additional reactions to give **12**. On the other hand, the reaction of the phosphaalkene and $RuCl_2(PCy_3)_2(CHPh)$ did not form the expected compound analog to **11** but rather the unexpected compound **13b**. A proposed mechanism for the

formation of **13b** is that the targeted adduct was formed (**13a**) and was subsequently followed by a nucleophilic attack of the electron-rich phosphaalkene on the benzylidene group forming a zwitterionic metal complex where the positive charge is delocalized in the azole ring while the negative charge is on ruthenium. Followed by two C–H activations of a mesityl ring with the release of HCl generates compound **13b.** Compound **11** was tested for ring-closing metathesis of diallyl sulfide at room temperature, however it was found to be inactive. Interestingly, when the reaction using compound **11** and diallyl sulfide is done at higher temperature, compound **11** decomposed into **12** which is an analog of **13b**.

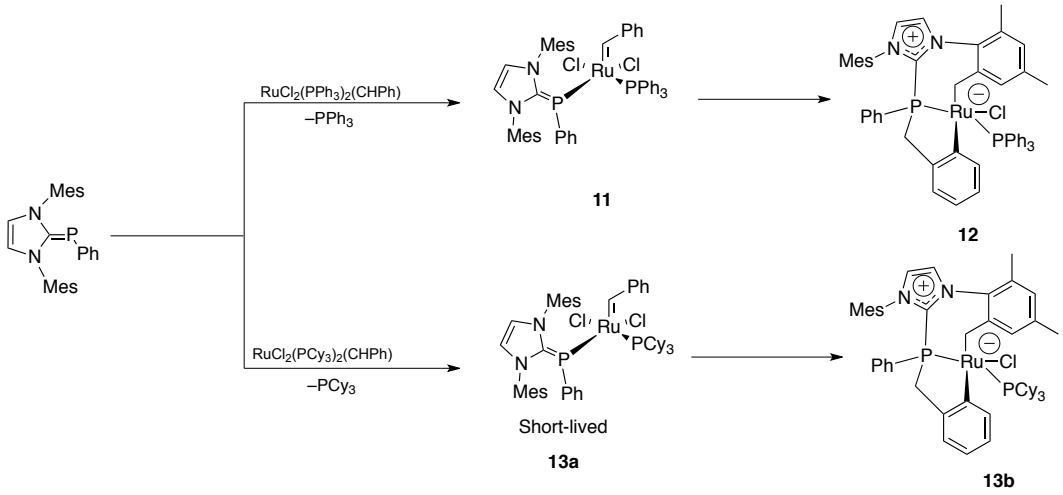

Scheme 14. Coordination of an IPP on ruthenium and its C-H activation product**.**

In addition, the coordination chemistry of IPP's has been well investigated using transitions metal from group 6 to 12 by several other research groups (**Figure 18**).[52,56,57] However, there is no report of any bidentate monoanionic ligand that incorporates an IPP moiety in their scaffold.

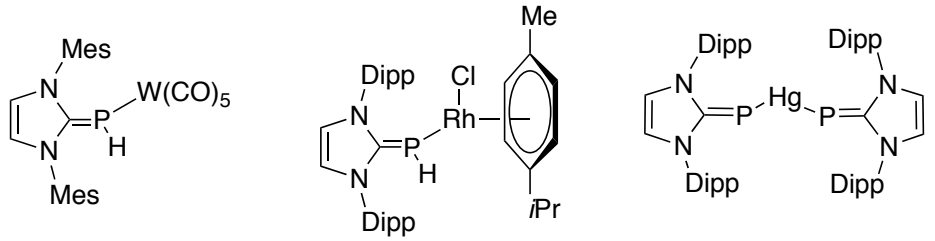

Figure 18. Example of transition metal complexes bearing an IPP as a ligand.

1.4 Proposed Work

Given the ability to tune the electronic and steric characteristics of the phosphaalkene through both building blocks, namely the N-heterocyclic carbene (NHC) motif and the phosphinidene, further exploring their use as spectator ligand and expand the toolbox available to coordination chemists is warranted.

The Lavoie group has shown great interest in incorporating inversely-polarized phosphaalkenes (IPPs) in bidentate anionic ligands for the coordination to metal centres, expanding on the earlier work on the related guanidine/imidazole-2-imine derivatives. The structural and electronic nature of these complexes make them suitable for use in polymerization and copolymerization of olefins, including those with polar functional groups **(Figure 19**).[5,25,35]

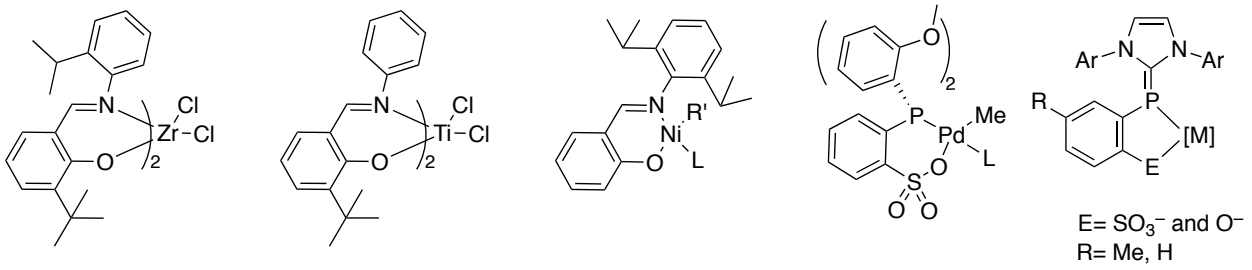

Figure 19. Transition metal-based complexes use to copolymerize ethylene and polar vinylic monomers and the proposed metal complex bearing an IPP (**rightmost structure**).

The research presented herein looks into the utilization of inversely-polarized phosphaalkenes as spectator ligands as they pertain to olefin polymerization and to frustrated Lewis pair chemistry (**Figure 20**).

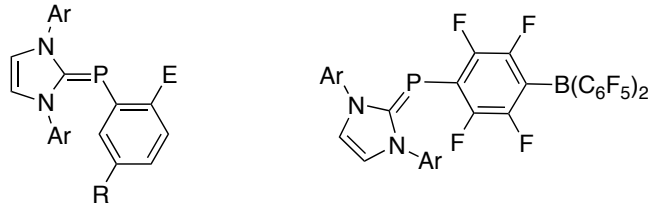

14 E= SO_3H, R= Me
15 E= OH, R= H

16
Frustrated Lewis pair

Figure 20. Target ligands for olefin polymerization (**14** and **15**) and frustrated Lewis pair system for activation of small molecules (**16**)

The objectives of the present research are: (1) the synthesis of the target ligands **14** and **15**. (2) The coordination of the corresponding salt of **14** and **15** to metal precursors from group 4 and 10. (3) The evaluation of the polymerization activity of the resulting complexes to address issues related to the SHOP- Drent- and FI-catalysts. (4) The synthesis of a Frustrated Lewis pair system bearing an IPP in its scaffold for small molecule activation. The preparation of the phosphaalkene bidentate ligands systems are to explore the ligand scaffold for potential use in copolymerization of ethylene and polar vinylic monomers. The incorporation of an IPP will yield a widely tunable ligand in terms of steric and electronics properties. The electronic properties of the phosphorus atom can be modified to tune the electron density that is donated to the metal center which can disrupt the deactivation of the metal complex in the presence of polar monomers. The tunable structure of the inversely polarized phosphaalkene may yield a desirable frustrated Lewis pair such as **16** which may give unprecedented reactivity in main group catalysis.

2. Results and Discussion

2.1 Synthesis of targeted ligands.

The synthesis of the inversely-polarized phosphaalkene-sulfonate **14** was attempted, toluene sulfonic acid was treated with 2 equiv. of *n*BuLi and the dianion species **17** was quenched with 1 equiv. of PCl_3 yielding **18**.[36]After the addition of a free carbene led to the formation of an intermediate salt which was then reduced to give compound **14** (**Scheme 15**). However, after the reduction step of the intermediate formed during the reaction of **18** and a free carbene using KC_8, Mg (granules), or Zinc (dust), multiple signals were observed in the ^{31}P NMR spectrum, complicating the determination of the phosphorus species corresponding to **14**. As a result, a signal for compound **14** could not be determined. The solvent was removed under vacuum and the solids were washed with toluene, DCM, and pentane to try to separate the several phosphorus species based on their solubility in these solvents. However, these phosphorus species had a similar solubility making the separation challenging. A solution of the isolated solids was prepared in toluene and then concentrated under reduced vacuum. Pentane was added to precipitate an isolable species from the reaction mixture; however, that step was also unsuccessful.

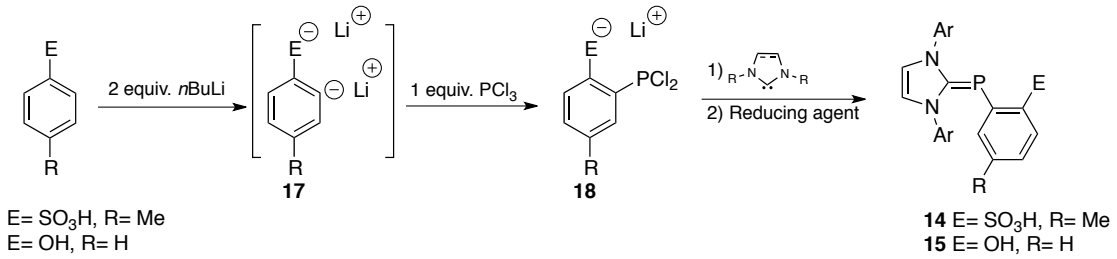

Scheme 15. Synthetic route to access the target ligands **14** and **15**

By analogy on a similar synthetic route reported by Geisler,[58] upon the addition of TMSCl and Li^0 to a solution of **18a**, compound **19** could be formed. Compound **19** would react with 1,3-bis(2,6-diisopropylphenyl)-2,2-difluoroimidazole giving the targeted compound **14**, with the production of trimethylsilyl fluoride as the driving force (**Scheme 16**). The reaction was carried on and an orange/yellow precipitate was observed after the addition of TMSCl and the reaction mixture was subsequently stirred for an additional hour at –78 °C. The ^{31}P NMR spectrum of the isolated solids showed seven phosphorus species and ranging from 39.7 to –6.59 ppm. A prominent species was observed at –5.36 ppm and its isolation was attempted. The solvent was removed under reduced pressured to give yellow solids, and these were washed with pentane to attempt to remove the pentane soluble fraction. The ^{31}P NMR spectrum of the pentane non-soluble solids (90 mass%) displayed ten signals except the predominant signal at –5.06ppm. This observation suggests that the presumed compound **19** either was not formed or it was consumed to form the additional unknown species.

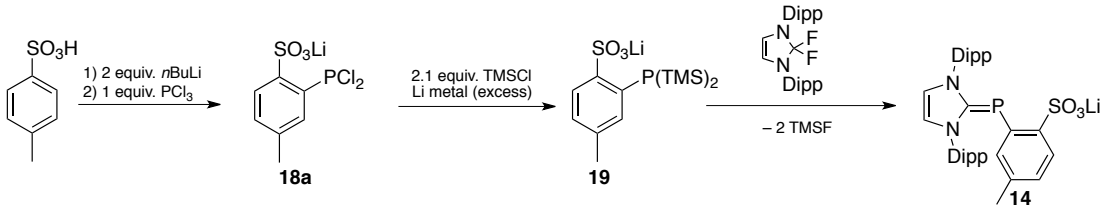

Scheme 16. Alternative synthetic route to access ligand **14**.

To further study the viability of the proposed synthetic route, isolation of compound **18a** was attempted, rather than simply producing it *in situ*. The first attempt to isolate **18a** was using the same procedure showed in **Scheme 15** and the reaction was stopped before the addition of the free carbene. The isolated white solids were analyzed using ^{31}P NMR spectroscopy and several resonances were observed. Thus, it was hypothesized

that compound **18a** was not stable and could decompose through an intramolecular or intermolecular pathway (**Scheme 17**). In the proposed intramolecular route (**A**), the weakly nucleophilic oxygen atom of the sulfonate group attacks the electrophilic phosphorus atom forming a stable five-membered ring. Another nucleophile could attack the phosphorus atom because it still has a good leaving group leading to addition of another molecule of **18a** and the formation of another LiCl equivalent. In the intermolecular route (**B**), the oxygen atom attacks the PCl_2 group of a second equivalent of **18a**. This decomposition pathway forms a molecule that contains both a nucleophilic sulfonate group and an electrophilic PCl_2 group allowing subsequent cyclization and polymerization/oligomerization reactions. To disfavor this pathway, attempts to protect the oxygen atom using TMSCl and *tert*-butyldimethylsilyl chloride (TBDMSCl) were investigated. The experiments were performed following the reaction conditions in **Scheme 15** with addition of 1.05 equiv. of the silyl chloride to the dianion species **18** at –40 °C. However, using the protecting groups did not aid in the isolation of silylated analog of **18a** evident by multiple observed species in the ^{31}P NMR spectrum of the isolated solids.

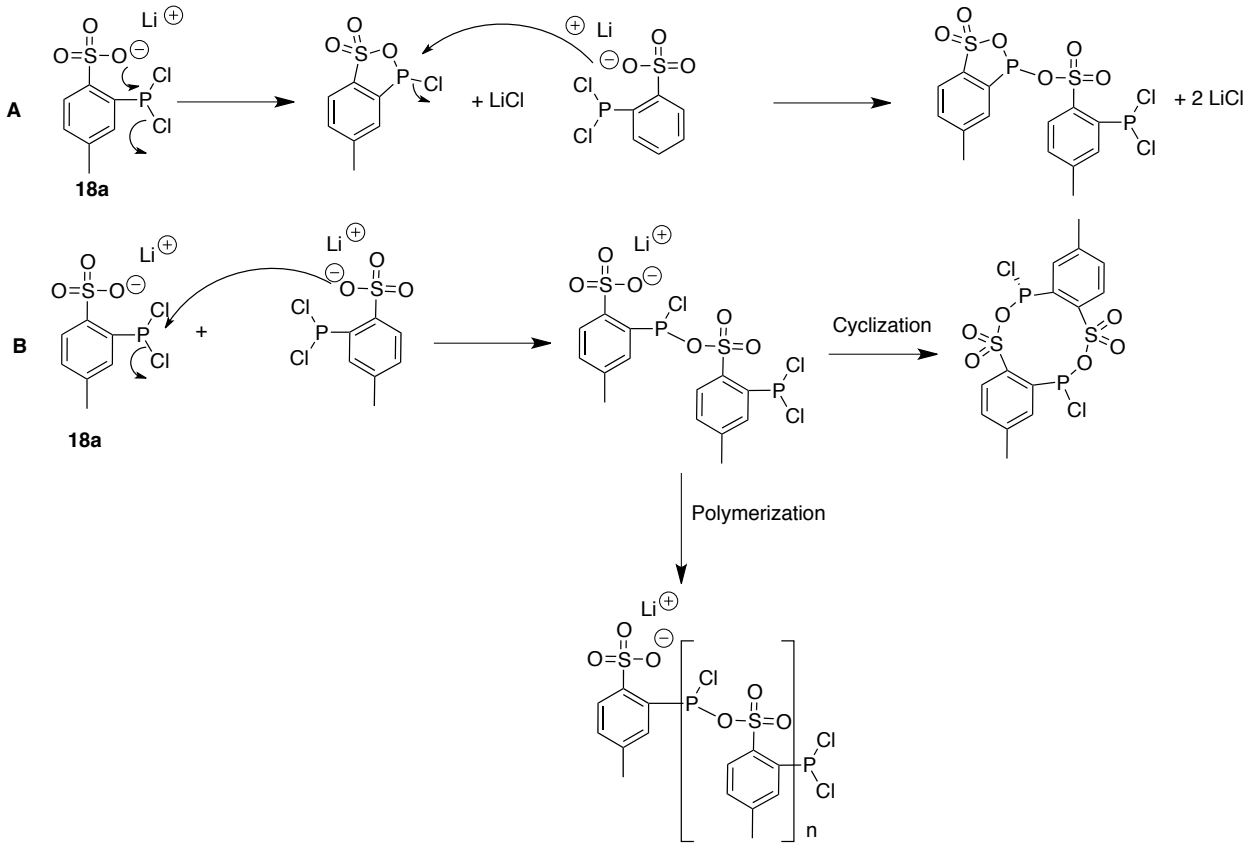

Scheme 17. Proposed decomposition pathways of **18a** (**A**) intramolecular attack and **(B)** intermolecular attack.

The nucleophilicity of the toluenesulfonate moiety can be observed in the preparation of the Drent-type complexes in which a phosphino toluenesulfonate ligand coordinates to palladium through the anionic oxygen atom and the neutral phosphorus atom (eq. 11).[35] Several Drent-type catalysts have been prepared and isolated displaying the same coordination mode (**Figure 11**)[36–38]. The sulfonate is nucleophilic enough to coordinate to a relatively electron rich palladium center. In comparison, the sulfonate group present in compound **18a** is in the proximity of an electron deficient phosphorus atom which bares two good leaving groups. The nucleophilic attack of the sulfonate to the $RPCl_2$ moiety can also be driven by the formation of a stable five-membered ring, the formation of a new P–O bond and LiCl as a product.

In the case of the inversely-polarized phosphaalkene-phenol, compound **15,** the same isolation strategy of the intermediate **18b (Scheme 18)** was attempted without success, possibly due to similar decomposition pathways as postulated for **18a**. The intramolecular decomposition pathway is not likely to occur because it would form a highly strained 4-member ring product (**A**). However, the intermolecular decomposition pathway is still sensible for this product (**B**)

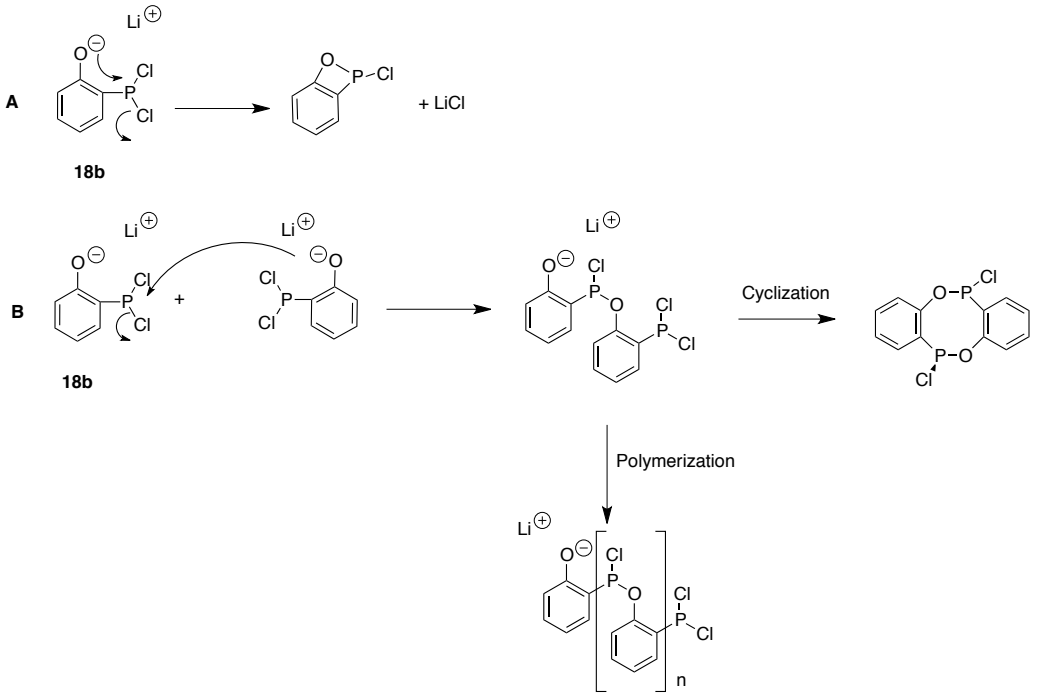

Scheme 18. Proposed decomposition pathways of **18b** (**A**) intramolecular attack and **(B)** intermolecular attack.

An alternate synthetic pathway to access the targeted compound was developed using the hydrido-phosphaalkene **20**, which is prepared through several synthetic routes reported in the literature (**Scheme 19**).[50–52,55]

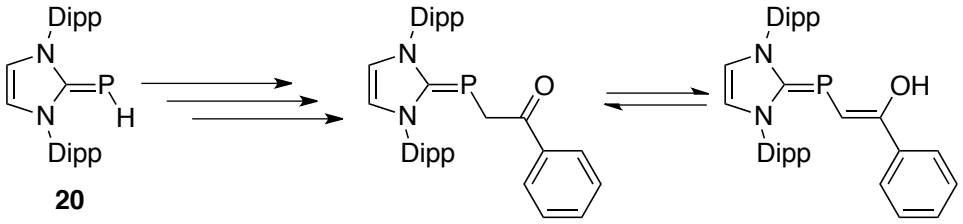

Scheme 19. Alternate synthetic route for the targeted ligand.

In the procedure described by Cicač-Hudi,[51] Na_3P_7, reacts with an imidazolium salt bearing aryl groups on the nitrogen centres. The reaction takes place in THF overnight at room temperature giving **20** in isolated yields in excess of 60%. However, following the reported procedure, the synthesis of **20** was not as successful as reported in the literature, yielding only ~20% of **20** along with the corresponding free carbene as a by-product (eq. 18). A control experiment was then set up and monitored over time *via* colour change. The reaction took roughly four weeks to attain the colour reported in the literature. When the reaction was worked-up, compound **20** was isolated in decent yield (~50%). It was determined the reaction mixture had to be stirred for longer than what was reported in literature.

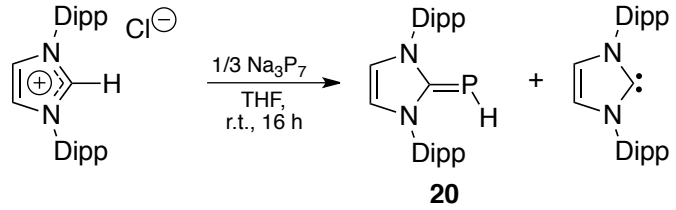

(**18**)

The synthetic procedure was thus modified. Addition of tetramethylethylenediamine (TMEDA) was performed to chelate the sodium cation and form a more reactive heptaphosphide species. This approach was successful as the use of TMEDA decreased the reaction time to 9–11 days, as indicated by ^{1}H and ^{31}P NMR analyses. However, the use of TMEDA introduced a new challenge as it was difficult to

remove it completely due to its high boiling point and similar solubility to compound **20** in toluene, ether, and pentane. Therefore, making it impractical for use in future reactions.

Cicač-Hudi reported that alkyl substituted imidazolium salts were refluxed overnight to synthesize the corresponding hydrido-phosphaalkene.[51] Therefore, the reaction mixture of Na_3P_7 and the corresponding imidazolium salt was heated at different temperatures (from 40 to 60 °C). After several attempts, optimal reaction conditions of 60°C for 24 hours and a subsequent 16 hr at room temperature were established as the most effective reaction conditions (eq. 19). The isolated yield was not affected by these conditions, as 50 – 60% yields of the IPP were consistently obtained in multiple attempts. In some cases, a very small amount of free carbene is also generated and could not be removed due to the similar solubility to **20**. Nonetheless, the IPP was used for subsequent reactions, at a purity of 95%.

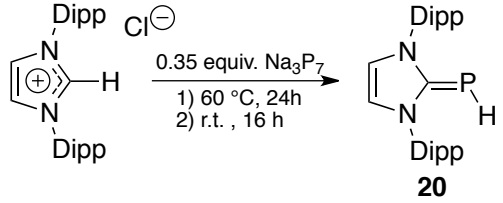

20 **(19)**

The attempted synthesis of bidentate ligand **15** using the hydrido-phosphaalkene **20** was based on a procedure reported by our group, reacting a related guanidine derivative with 2-bromoacetophenone to give the desired guanidinium salt after reflux for several hours (75–89%) (eq. 20).[27]

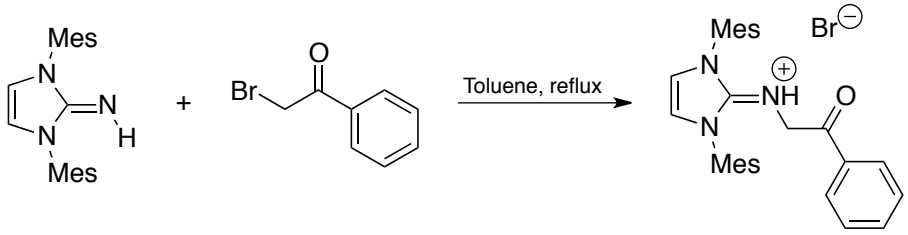

(20)

The analogous reaction using **20** as the nucleophile was thus attempted to access the desired phosphonium salt **21 (Scheme 20)**. When the reaction was performed at reflux in toluene, the corresponding imidazolium salt was obtained in 90% yield. Repeating the reaction at room temperature yields a product that is consistent with the phosphonium salt **21** based on ^{31}P and ^{1}H NMR spectroscopy; however, the corresponding imidazolium salt was also observed in a 1:1 molar ratio. Alternatively, when the reaction is performed at –40 °C for 16 h, **21** is obtained as the major product in 90% yield, with only small amounts of imidazolium salt present when the corresponding free carbene is present along **20** as an impurity.

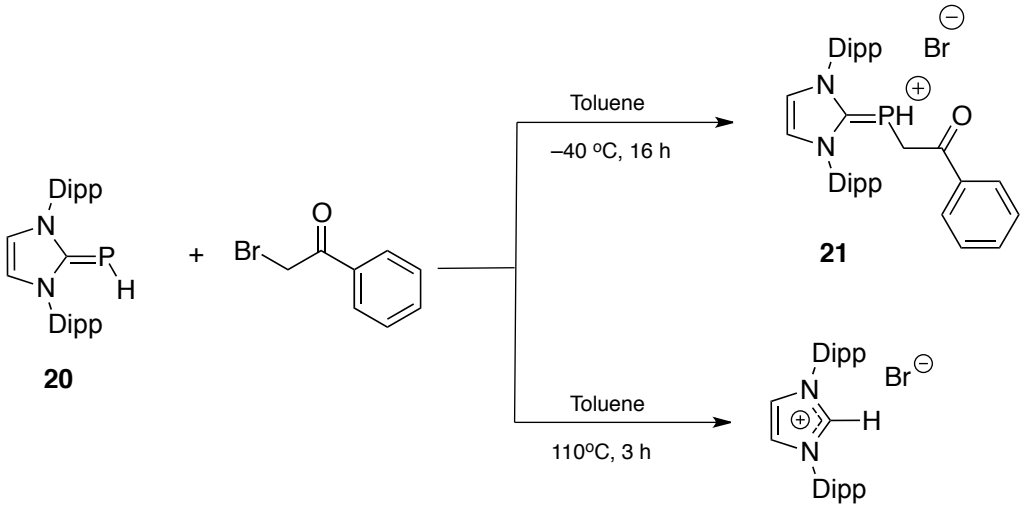

Scheme 20. Modified synthetic procedure to access compound **21**.

NMR spectroscopic analysis performed on **21** reveals the ^{31}P NMR (**Figure A3**) resonance at –102.8 ppm as a doublet of doublets with $^{1}J_{PH}$ = 241.2Hz and $^{2}J_{PH}$ = 7.8 In

the ^{1}H NMR spectrum (**Figure A1**), the proton bound to phosphorus is observed at 4.19 ppm as a doublet of triplets with $^{1}J_{HP}$ = 241.3 Hz and $^{3}J_{HH}$ =7.8 Hz. The carbenoid carbon of **21** resonates at 150.0 ppm in the ^{13}C NMR spectrum (**Figure A2**) as a doublet ($^{1}J_{CP}$ = 49.0 Hz) while the methylene carbon resonance appears as a doublet at 29.0 ppm ($^{1}J_{CP}$ = 13.0 Hz). Additional resonances were observed in the ^{1}H NMR and ^{13}C {^{1}H} NMR spectra indicating that the aryl substituents on nitrogen are different, resulting from the increase of double bond character of the $C_{imidazole}$–P bond and the restricted rotation of the imidazole–phosphorus bond. In the ^{1}H NMR spectrum, the *meta* protons from the Dipp groups are inequivalent and appeared as two overlapping doublets of triplets. The proper splitting pattern for the *para* proton is difficult to determine because of overlap with other resonances belonging to the *meta* and *para* protons of the phenyl ring. The benzylic protons appeared as two slightly overlapping doublets of septets resonating from 2.52 to 2.37 ppm. The methyl protons are also inequivalent and appeared as four set of doublets. In the ^{13}C{^{1}H} NMR spectrum, there are four different resonances assigned to the $meta_{(Dipp)}$ and $ortho_{(Dipp)}$ carbon and 2 set of 3 resonances corresponding to one benzylic and two methyl carbon nuclei.

The ATR-IR spectrum of **20** was obtained to assist in the interpretation of the IR spectrum of **21**. Compound **20** is known to have more C–P single bond character based on the bond lengths obtained from solved X-ray structures.[52] It has been reported that the C–P single bond has a stretching band in the range of 1450–1250 cm^{-1}.[59] The IR spectrum of compound **20** displayed a strong stretching band at 1346 cm^{-1} that was assigned to the $C_{imidazole}$–P bond. The stretching band of the $C_{imidazole}$–P bond of **21** is observed at 1446 cm^{-1}, thus, the $C_{imidazole}$–P bond of **21** has more double bond character

than **20**. The increase in bond order in **21** is likely due to the electron donation from the electron-rich phosphinidene to the p-orbital of the carbenoid carbon and the donation of electron density from the alkyl group to the phosphorus atom. The P–H bond of **20** is observed a moderate band stretching at 2309 cm^{-1} while the P–H bond of **21** is not observed due to the lack of a strong dipole moment between these atoms. Furthermore, the C=O bond of **21** is observed as a strong sharp band at 1670 cm^{-1}, which is characteristic of C=O bonds.

The neutral derivative **22** is easily accessed through the addition of one equivalent of sodium hexamethyldisilazide (NaHMDS) to **21** (**Scheme 21**). Deprotonation of the related guanidinium salt previously reported by our group yields the enol tautomer as a major product over the keto tautomer in a 3:1 ratio.[27] This is not the case in the deprotonation of **21**, where only the ketone **22** is isolated from the reaction.

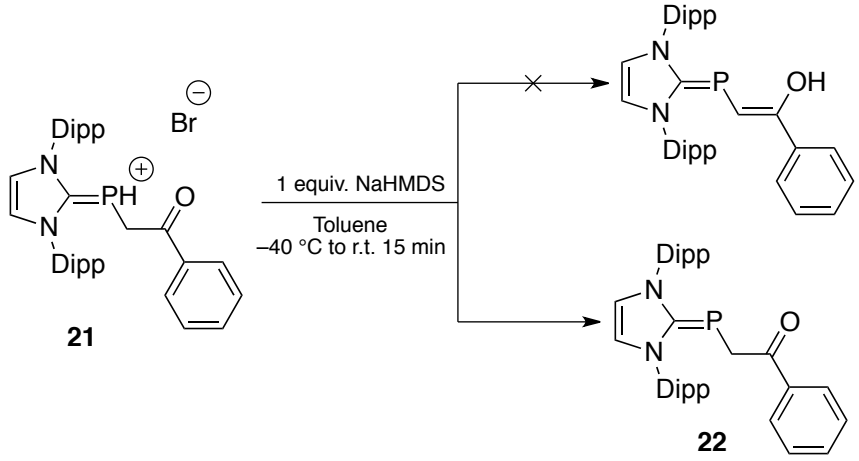

Scheme 21. Deprotonation of **21** to give the neutral ligand precursor **22**.

The red-orange solids of **22** were analyzed through ^{1}H, ^{13}C, and ^{31}P NMR spectroscopy as well as ATR-IR spectroscopy. In the ^{1}H NMR spectrum (**Figure A4**), the methylene protons resonate at 3.02 ppm coupling to phosphorus, as confirmed by 2D ^{1}H–

^{31}P HMBC NMR experiments. However, the coupling constant is too small to be observed in the ^{1}H NMR spectrum. In the ^{13}C{^{1}H} NMR spectrum (**Figure A5**), the methylene spacer carbon is observed as a doublet at 30.1 ppm ($^{1}J_{CP}$ = 16.0 Hz) and the carbenoid carbon from the imidazole ring appears at 173.8 ppm as a doublet ($^{1}J_{CP}$ = 109.0 Hz). The chemical shift of the carbenoid carbon increased from 150.0 ppm in **21** to 173.8 ppm in **22** indicating that the carbon atom is more electron deficient in **22**. This suggests delocalization of a positive charge in the imidazole ring favoring a higher contribution of the canonical form in which there is a negative charge on phosphorus **(Figure 21)**. The ^{31}P NMR spectrum (**Figure A6**) displays a singlet at –45.1 ppm with not visible coupling to the methylene protons to actually give a doublet, which is also consistent with the lack of a doublet corresponding to CH_2 protons of in the ^{1}H NMR spectrum. In the ATR–IR spectrum for **22**, the stretching band for $C_{imidazole}$–P bond is observed at 1323 cm^{-1}, which is consistent with a C–P single bond.[59] While the stretching band for C=O was found at 1655 cm^{-1}.

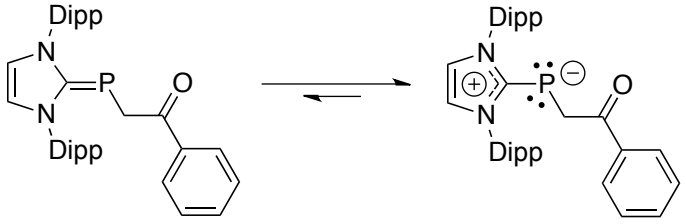

Figure 21. Compound **22** displays more of a $C_{imidazole}$–P single bond character.

For the analogous guanidine systems reported previously by our group, keto-enol tautomerism was observed yielding the enol tautomer as the major product.[27] As this is not the case with **22**, DFT studies were performed to explain this observation at the B3LYP/6-31G(d) level of theory. The computations performed revealed that the keto-

tautomer of **22** is –18 kcal mol^{-1} more stable than the enol-tautomer. The tautomer ratio can thus be calculated when solving for K using the Gibbs free energy formula: $\Delta G = RT\ln K$, where R is the gas constant (1.987 x 10^{-3} kcal mol^{-1} K^{-1}) and T is temperature (Kelvin). The large difference in energy values for the phosphaalkene-ethanone and the tautomer ratio giving the keto tautomer as the only product explains the lack of tautomerization observed experimentally.

$K = e^{-\Delta G/(RT)}$

$K = e^{-(-18/(0.001987)(298)}$

$K = 1.593 \times 10^{13}$

tautomer percentage = $\frac{K}{K+1} * 100\%$

%keto = 100%

DFT calculations in the gas phase and solvated (THF and $CHCl_3$) using the B3LYP functional with the 6-31G(d) basis set on the guanidine analog predicted the exclusive formation of the keto tautomer. This is in disagreement with previously reported data showing the isolation of the enol and keto tautomers in a 3:1 ratio.[27] The level of theory used in the DFT calculations was thus likely inappropriate, leading to errors in calculated energy levels. However, the relative position of the molecular orbitals is believed to still be accurate, including the actual nature of the HOMO and HOMO-1 (**Figure 22**).

To further support the presence of electron density being distributed mainly on phosphorus and thus a $C_{imidazole}$–P single bond for **22**, the molecular orbitals (MOs) were calculated from an optimized structure of **22** using the B3LYP functional with the 6-31G(d) basis set (**Figure 22**).

HOMO **HOMO-1**

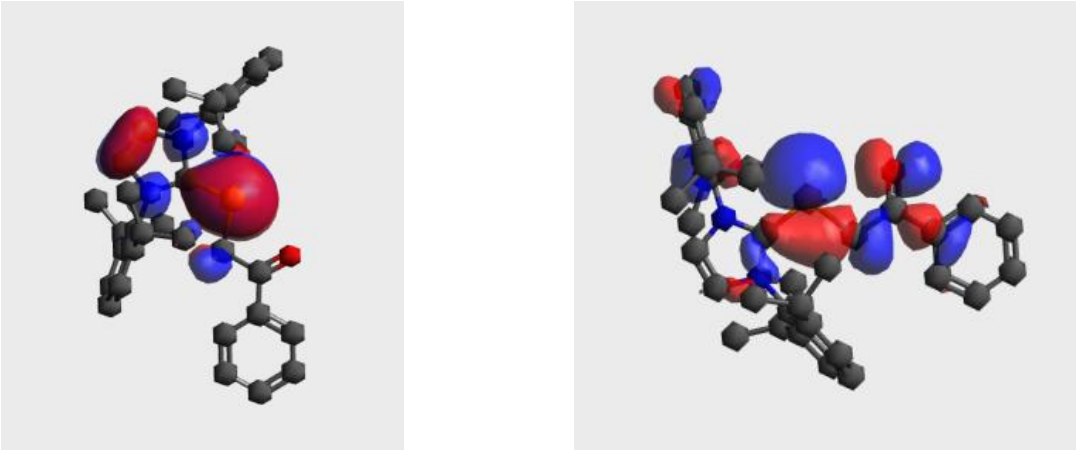

Figure 22. HOMO and HOMO–1 for compound **22.** (hydrogen atoms are omitted for clarity)

The HOMO shows a double bond character between phosphorus and carbon. However, **22** can be described as an adduct in which the carbenoid carbon has a partial populated p-orbital while the phosphorus has a lone pair in the p-orbital. These p-orbitals have the same symmetry; thus, they can overlap to give the appearance of a double bond. The teardrop shape of this interaction is due to the difference in size of the orbitals leaving the majority of the orbital interaction on phosphorus. This hypothesis is corroborated by NMR and IR-ATR spectroscopic data in which the $C_{imidazole}$–P bond has more of a single bond character. The electron density distribution can also be seen in the HOMO–1 which is largely located on the phosphorus atom. Thus, the data collected so far suggest **22** favours a higher contribution of the canonical form **B** in which there is more of a $C_{imidazole}$–P single bond.

In an attempt to prepare phosphaalkene-ethenolate **23**, compound **22** was reacted with one equivalent of NaHMDS (**Scheme 22**).

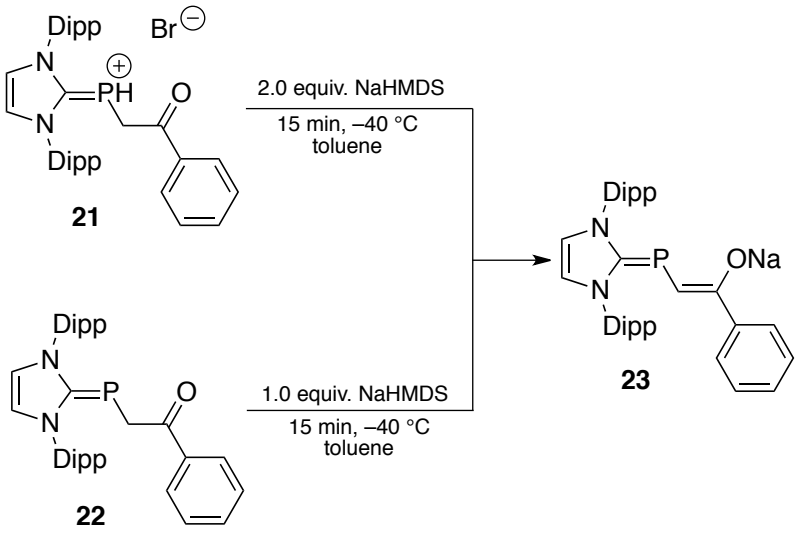

Scheme 22. Synthetic routes to access compound **23** for further coordination reactions.

After 10 min, three major phosphorus resonances were observed in the ^{31}P NMR spectrum (**Figure 23 top**). The solution was allowed to stir for an hour to observe if some of the phosphorus species present would transform into **23**. However, after 1 h additional new species were observed (**Figure 23 bottom**), thus suggesting **23** is either not produced or is generated but rapidly decomposes to give multiple unidentifiable phosphorus-containing species.

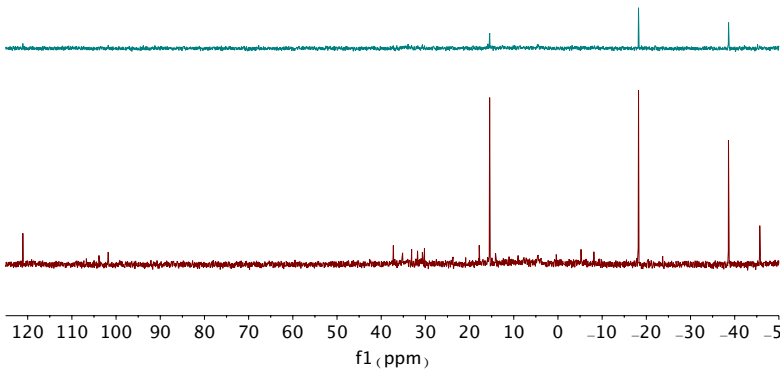

Figure 23. ^{31}P NMR spectra of an attempt to synthesize compound **23** for further reactions. (**Top**) reaction time: 10 min. (**Bottom**) reaction time 1h. (121 MHz, THF/C_6D_6)

In order to confirm that the enolate was in fact formed, the synthesis of the more stable silyl-vinyl ether was attempted (**Scheme 23**). Compound **21** was suspended in toluene cooled down to –40 °C and two equivalents of NaHMDS were added to the suspension, yielding a red solution after 15 minutes. Excess TMSCl was added producing a yellow solution with a white precipitate after stirring for 30 minutes at room temperature. Removal of volatiles *in vacuo*, subsequent extraction with toluene, filtration through Celite and removal of the volatiles yields **24** as yellow solids in good yields, thereby confirming formation of the enolate upon addition of base.

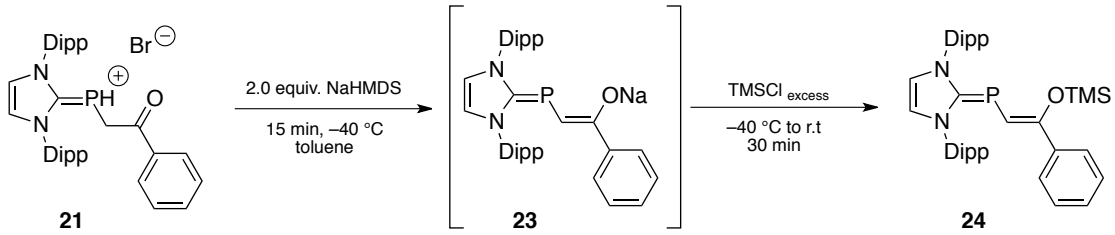

Scheme 23. Synthetic route to access compound **24** for further reactions.

The ^{1}H NMR spectrum of compound **24** (**Figure A7**) shows the characteristic vinylic resonance at 6.19 ppm as a doublet ($^{2}J_{HP}$ = 7.2 Hz). The other characteristic resonance that indicated the successful silylation of the enolate is that of the trimethyl silyl group (TMS) which appeared at 0.23 ppm as a singlet. In the ^{13}C{^{1}H} NMR spectrum (**Figure A8**), the characteristic vinylic carbon resonates at 110.7 ppm as a doublet ($^{2}J_{CP}$ = 37.5 Hz) while the central imidazole ring carbon appears at 171.1 ppm as a doublet ($^{1}J_{CP}$ = 91.5 Hz). The chemical shift of the carbenoid carbon did not have a significant change from that of compound **22** (173.8 ppm) which still indicates that the imidazole ring has a partial positive charged delocalized within the ring. In the ^{31}P NMR spectrum (**Figure A9**), a doublet with a coupling constant of 7.3 Hz was observed at –37.7 ppm.

The infrared spectroscopy analysis of **24** showed a similar stretching band at 1328 cm^{-1} to that of compound **22**. The spectroscopic data indicates that compound **24** also displays more of a single bond character in the $C_{imidazole}$–P bond. The change in bond order from a double bond to a single bond between the carbon and oxygen atoms caused the shift of that band to a lower frequency (1249 cm^{-1}).

A 2D NOESY experiment was used to determine the configuration of compound **24**. In the spectrum (**Figure A10**), the vinylic proton showed correlation to the *ortho*-protons of the phenyl group. Another correlation observed was between the TMS group to the *ortho*-protons from the phenyl group. These correlations indicate a *cis*-configuration (P and O atoms reside on the same side of the double bond) compound **24 (Figure 24)**.

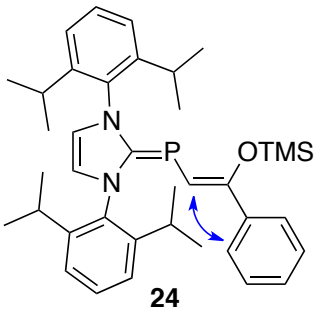

24

Figure 24. Selected NOESY correlations of compound **24**.

The thermal stability of compound **24** was assessed at 60 °C in benzene-d_6. With 72 hours at 60 °C, compound **24** did not show signs of decomposition. NMR and IR data collected during the characterization of **24** showed evidence that this compound displays more of a single bond character in $C_{imidazole}$–P leading to a major contribution of the canonical form **B**. The stability of **24** can be attributed to the delocalization of the partial negative charge in phosphorus throughout the π-system (**Figure 25**) and to the strong

O–Si bond present (191.1 kcal mol^{-1}).[60] As a result, compound **24** could be used at higher temperature during coordination to metal centers to give a target complex if required.

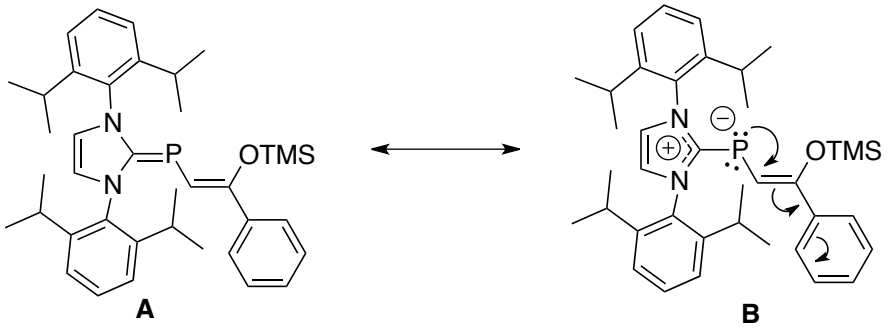

Figure 25. Canonical forms **A** and **B** compound **24** can access. The partial negative charge in the canonical form **B** can be delocalized throughout the π-system (**right**).

2.2 Coordination Chemistry

The attempted coordination of **21**, **23**, and **24** to several metal precursors from group 4 and 10 was performed (**Figure 26**). Group 10 metal precursors were employed to access complexes similar to the SHOP– (Ni) and Pd-based catalysts which would then be used for olefin polymerization and copolymerization of polar monomers (**Figure 26 A-D**). However, after several attempts the coordination of **23** or **24** on to group 10 metal center was unsuccessful leading to the consumption of the ligand and metal precursor forming several unknown species.

Group 4 metal centers were also employed because these metals are more Lewis acidic and oxophilic than those from group 10, which could facilitate the coordination of the inversely-polarized phosphaalkene-enolate ligand (**Figure 26 E-H**). Furthermore, previous work in the Lavoie group using imine–ethenolate ligands gave successful coordination and isolation of the corresponding complexes. However, several of the attempted reactions between ligand precursors and group 4 metals did not yield an

isolable complex bearing the intact ligand. The successful coordination and isolation of a complex was accomplished when compound **24** was reacted with $CpTiCl_3$ (**Figure 26 I**)

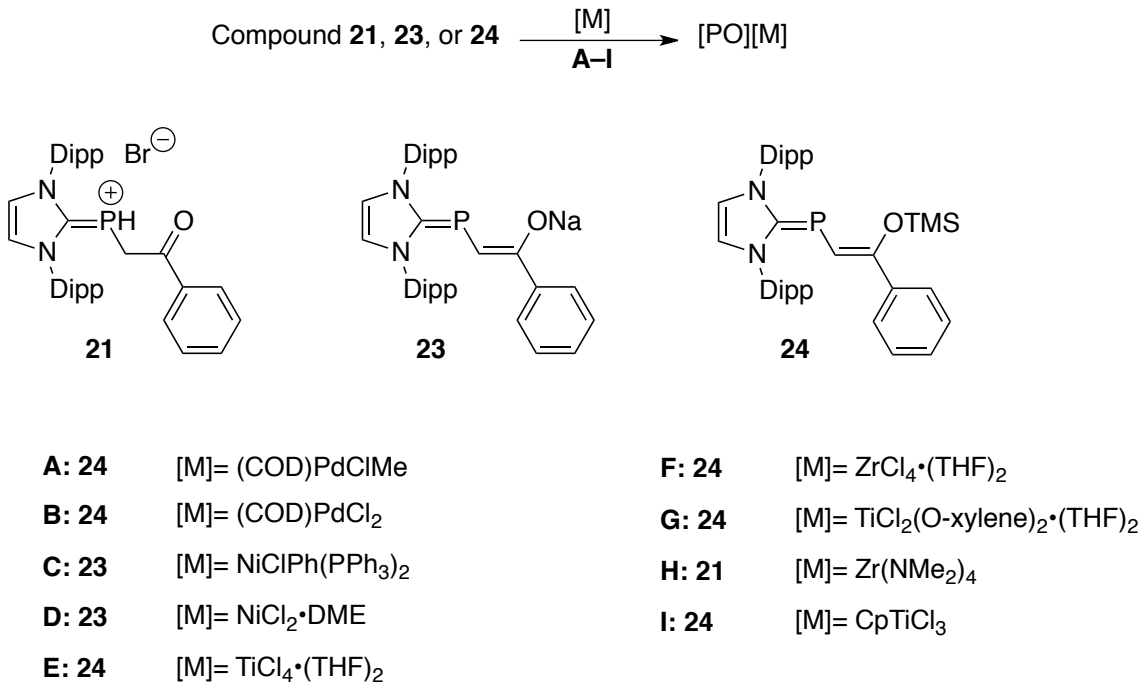

A: 24	[M]= (COD)PdClMe	**F: 24**	[M]= $ZrCl_4$•$(THF)_2$
B: 24	[M]= (COD)$PdCl_2$	**G: 24**	[M]= $TiCl_2$(O-xylene)$_2$•$(THF)_2$
C: 23	[M]= NiClPh$(PPh_3)_2$	**H: 21**	[M]= Zr$(NMe_2)_4$
D: 23	[M]= $NiCl_2$•DME	**I: 24**	[M]= $CpTiCl_3$
E: 24	[M]= $TiCl_4$•$(THF)_2$		

Figure 26. Metal precursors employed in the coordination of **21**, **23**, or **24**.

The cyclopentadienyl (phosphaalkene ethenolate) complex (**25**) was prepared by adding compound **24** to a solution of $CpTiCl_3$ resulting in an immediate colour change of the toluene solution form yellow to dark green (eq. 21). The colour change is indicative of ligand to metal charge transfer, with the formation of compound **25** in a 92% yield. The ^{1}H NMR spectrum (**Figure A11**) showed an identical pattern for the resonances of the ligand as in compound **24**, with two sets of inequivalent methyl groups. The cyclopentadienyl (Cp) protons resonate at δ 6.36 ppm. In the $^{13}C\{^1H\}$ NMR spectrum (**Figure A12**) the central carbon of the imidazole ring resonates at 168.8 ppm as a doublet ($^1J_{CP}$ = 93.6 Hz), while the vinylic carbon appears at 118.2 ppm also as a doublet ($^1J_{CP}$ = 43.8 Hz). The phosphorus resonance (**Figure A13**) of the ligand scaffold, observed as a

doublet ($^2J_{PH}$ = 6.5 Hz) shifted downfield from δ –37.6 to –27.1 ppm, a clear indication of the coordination of the phosphorus atom to the metal center.

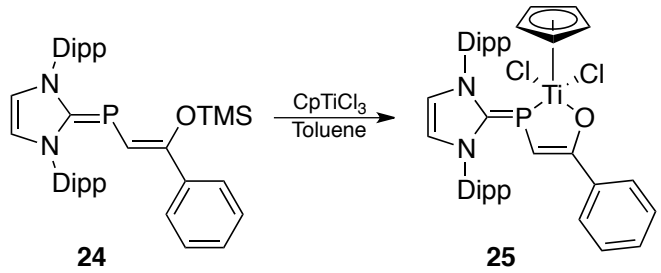

24 **25** **(21)**

Crystals of the titanium complex suitable for X-rays diffraction studies were grown at –40 °C under a nitrogen atmosphere by liquid diffusion of pentane into a saturated toluene solution of **25**.

Table 1. Selected Bond Lengths and Bond Angles for compound **25**.

Selected Bond Lengths (Å)		Selected Bond Angles (deg)	
Ti1 – Cl1	2.442(9)	O1 – Ti1 – P1	73.38(8)
Ti1 – Cl2	2.427(9)	O1 – Ti1 – Cl1	92.18(8)
Ti1 – O1	1.955(3)	P1 – Ti1 – Cl1	138.43(4)
Ti1 – P1	2.585(11)	O1 – Ti1 – Cl2	142.22(9)
Ti1 – C36	2.361(4)	P1 – Ti1 – Cl2	82.82(3)
Ti1 – C37	2.387(5)	Cl1 – Ti1 – Cl2	86.48(3)
Ti1 – C38	2.379(5)	Ti1 – P1 – C1	116.77(10)
Ti1 – C39	2.373(5)	Ti1 – P1 – C28	67.35(12)
Ti1 – C40	2.353(4)	Ti1 – O1 – C29	90.43(19)
C1 – N1	1.357(4)	C1 – P1 – C28	102.24(15)
C1 – N2	1.357(4)	P1 – C28 – C29	114.70(3)
C1 – P1	1.827(3)	C28 – C-29 – O1	116.0(3)
P1 – C28	1.790(4)		
C28 – C29	1.368(5)		
C29 – O1	1.344(5)		

Compound **25** crystallizes in the $P4_2/n$ space group. The complex adopts a distorted four-legged piano stool geometry with an expected η^5 hapticity for the Cp ring. The P^O$^-$ ligand coordinates in a bidentate fashion through the phosphorus and the ethenolate oxygen atoms forming a five-membered metallocycle (**Figure 27**).

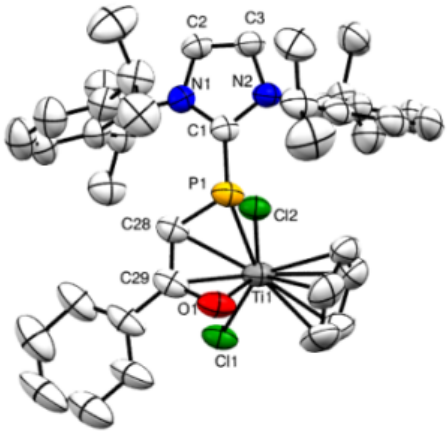

Figure 27. ORTEP plot of (P^O)$TiCl_2Cp$ (**25**) (50% probability level). Hydrogen atoms omitted for clarity

The complex has a P1–Ti1–O1 bite angle of 73.38(8)° (**Table 1**) which is significantly smaller than that of the salicylaldimine complex Cp{2-But-6-(2,4,6-$Me_3C_6H_2NCH)C_6H_3O$}$TiCl_2$ (78.78(11)°).[61] Complex **25** has a smaller bite angle because it formed a five-membered metallocycle whereas the salicylaldimine complex formed a six-membered ring making the metal center less crowded**.** The P1–C1 bond length is 1.827(3) Å, longer than that of the formally P1–C28 single bond (1.790(4) Å), suggesting some single bond character[62] and contribution by the canonical form **B** (**Figure 28**). The P1–C1 bond length is however much shorter than that observed in a related compound that contains a formal phosphorus–carbon single bond (1.883(2) Å).[63] In contrast, it is significantly longer than that for the C–P bond in standard phosphaalkenes (1.646 Å), which do not have electron delocalization over the π-system.[64] The N1–C1–P1–C28 dihedral angle of 37.8° further supports single bond character between P1 and C1.

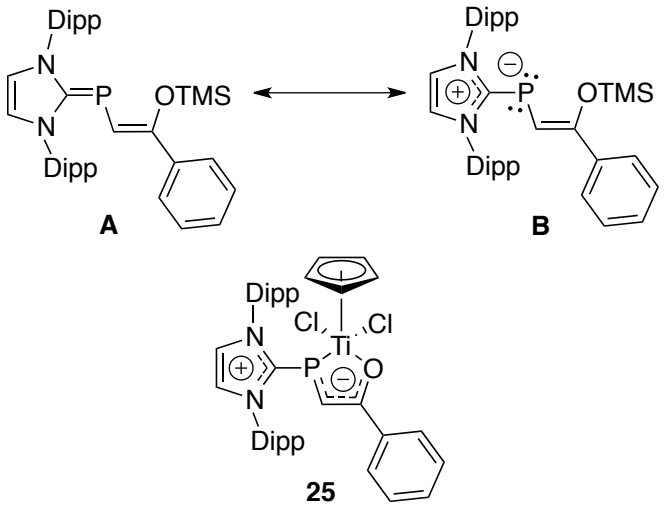

Figure 28. Canonical forms for compound **24** and the more representative resonance form of complex **25**.

Complex **25** shows Ti–C28 (2.511(4) Å) and Ti–C29 (2.377(8) Å) bond lengths that are shorter than calculated titanium–carbon distances in Ti(IV)–ethylene complexes (2.8 Å).[65] These short Ti–C28 and Ti–C29 bonds clearly indicate interactions between the vinylic motif and the titanium metal centre, similar to that observed in the related imidazol-2-imine system.[27] The coordination mode of the ligand resembles that of η^4-1,4-butadiene, with Ti1–P1, Ti1–C28, Ti1–C29 and Ti1–O1 bonds. By analogy, P1–C28 and C29–O1 could be regarded as double bonds, with C28–C29 as a single bond. Interestingly, these bond lengths are intermediate between those of single and double bonds, suggesting significant electron delocalization over the entire ligand system, from the azole ring to the oxygen.

The cyclopentadienyl ring is asymmetrically coordinated to titanium showing Ti–C bond lengths from 2.353(4) to 2.387(5) Å, where the shorter bonds are *anti* to the chloride atoms and the longer bonds are *anti* to the phosphaalkene ethenolate ligand. The angles between the mean planes formed by the imidazole ring and the diisopropylphenyl rings

(C4–C9) measure 71.70° and 88.07°. This contrasts with the related zirconium imidazol-2-imine ethenolate complex, in which an average dihedral angle of 69.8° is observed, which is sp^2-hybridized carbon and nitrogen atoms. Furthermore, the bond between the exocyclic nitrogen and the carbenoid carbon atom is significantly shorter (1.332(4) Å) than that between the nitrogen atom and the vinylic carbon (1.413(4) Å).[27] Thus, the metrical parameters for imidazol-2-imine are consistent with a canonical form related to **A**. In contrast, solid-state data from compound **25** indicate significant contribution of canonical form **B**.

The thermal stability of compound **25** was assessed at 60 °C in benzene-d_6. After 24 hours at 60 °C compound **25** only showed 15% decomposition. The crystal structure of **25** (**Figure 27**) showed evidence that the titanium-bound ligand displays more single bond character between the phosphorus atom and the carbenoid carbon. The lower stability of **25** compared to the free ligand **24** could be due to the increase of steric hindrance around the metal centre once compound **24** is coordinated and the formation of a weaker Ti–O bond (159.3 kcal mol^{-1})[60] than the Si–O bond present in compound **24.** (**Figure 28**)

2.3 Polymerization Studies

Polymerization experiments were performed using compound **25** (0.5 mmol) and $CpTiCl_3$ as a benchmark in 20 mL of toluene under one atmosphere of ethylene with 220 equiv. MMAO (5 mL of 7% wt. toluene solution) as co-catalyst (**Table 2**), unless otherwise stated.

Table 2. Ethylene polymerization activity for compound **25** and $CpTiCl_3$ in the presence of MMAO.[a]

Pre-catalyst	Quantity (10^{-5} mol)	Time (h)	Polyethylene (g)[b]	TON mol C_2H_4 mol Ti^{-1}	TOF kg PE mol cat^{-1} h^{-1}
Compound 25	5.18	0.50	0.240	165	9.24
	5.32	1.0	0.398	270	7.56
	5.18	2.0	0.262	250	3.50
	5.02	3.0	0.575	410	3.83
	5.16	5.0	0.760	530	2.97
$CpTiCl_3$	5.15	0.25	0.50	160	38.8
	5.11	0.50	0.649	520	25.4
	5.01	1.0	1.10	520	21.9
	5.01	2.0	1.95	1390	19.5
	5.20	3.0	2.17	1490	13.9
	2.69	5.0	0.935	1240[c]	6.94

[a] 220 equiv. MMAO were used. [b] Average of multiple runs. [c] 440 equiv. MMAO

Compound **25** displayed a catalytic activity up to 9.24 kg PE mol cat^{-1} h^{-1}. The activity for olefin polymerization process slowly decreased when compound **25** was used over long reaction times (**Figure 29**). In contrast, the activity for olefin polymerization decreased drastically after 15 min when $CpTiCl_3$ is employed. The activity of the active species generated from $CpTiCl_3$ decreased steadily to about 75% of the starting catalytic activity (5.7 kg PE mol cat^{-1} h^{-1}) (**Figure 29 t = 5 h**). This observation suggests that the active species formed from the reaction of **25** and MAO is more stable for longer periods of time than that when $TiCl_3Cp$.

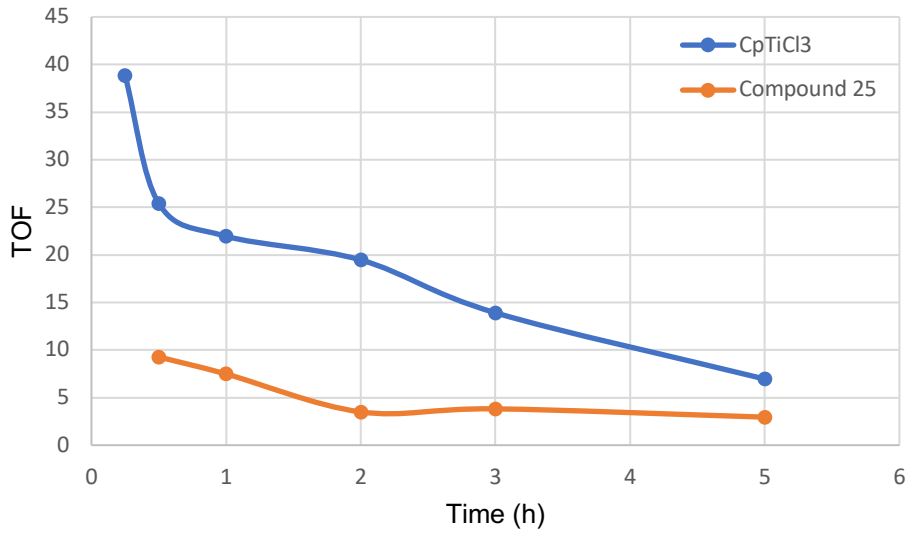

Figure 29. Turnover frequency for ethylene polymerization using $TiCl_3Cp$ and complex **25** in the presence of MMAO as cocatalyst.

When $CpTiCl_3$ was used, stirring problems were observed at t = 2 and 3 h due to the large amount of PE being formed. The turnover number (TON) for these experiments were similar: 1390 and 1490 mol C_2H_4 mol cat^{-1} respectively. It was hypothesized that because of the large amount of PE formed, the active species from the reaction between $CpTiCl_3$ and MMAO could get trapped within the polymer. As a result, ethylene molecules would not coordinate to the active species to promote the propagation of the polymer chain, leading to a lower production of PE which could be the case for the polymerizations with t = 2 and 3 h. To investigate this hypothesis, a polymerization experiment for 5 h was conducted using half the amount of $CpTiCl_3$ (**Table 2**). A larger TON was expected if there was a diffusion issue in the case of $CpTiCl_3$, however the TON (1240 mol C_2H_4 mol cat^{-1}) obtained was within the range of the polymerization at t = 2 and 3 h. The results indicate

that there was not a diffusion problem but rather the lifespan of the active species was decreasing.

The results obtained from the polymerization experiment using **25** can be compared to the related zirconium imidazole-2-imine ethenolate catalyst previously reported by our group that showed to have a moderate rate of 110 kg PE mol cat^{-1} h^{-1}.[27] There is a stronger contribution from the canonical form **A** in the imidazole-2-imine complex where there is more of a double bond character in C=N (**Figure 30**). The solved crystal structure of the zirconium complex showed a $C_{imidazole}$–N bond length of 1.332 Å which is slightly longer than the average C=N (1.27 Å).[27,66] In contrast, the C=P bond (1.827 Å) in complex **25** has more of a single bond character in comparison to the average calculated C=P and C–P bond length of 1.69 Å and 1.86 Å respectively, leading to a bigger contribution of form **B**.[66] In this case, the canonical form **B** can donate more electron density to the metal center compared to **A**, which can slow the rate of coordination of ethylene to the active species leading to a lower catalytic activity. The lower activity observed for this complex compared to that of a similar titanium system (salicylaldiminate)$CpTiCl_2$[61] is likely due to the electron-rich inversely-polarized phosphaalkene moiety and the non-substituted ethenolate moiety as previously mentioned.

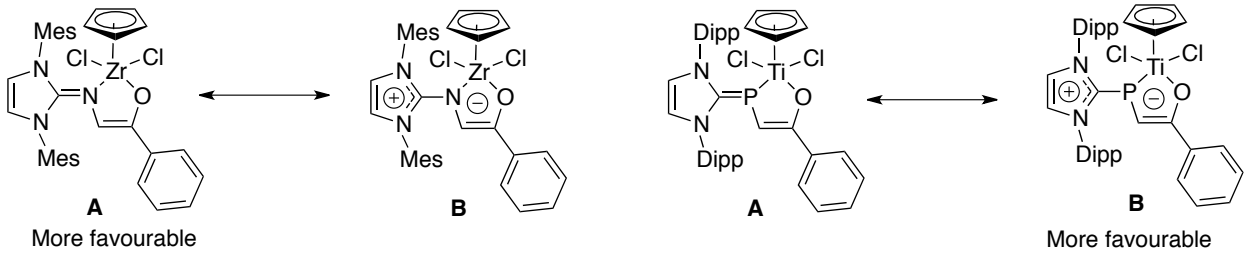

Figure 30. More favorable canonical forms for the guanadine analog(**right**) and compound **25** (**left**)

The isolated material from the polymerization experiments (t= 2h) was analyzed by differential scanning calorimetry (DSC) and the thermogram obtained is shown (**Figure 31**). DSC thermograms show phase transitions that polymers undergo at different temperatures, such as the glass transition (T_g), the melting temperature (T_m), and the crystallization temperature (T_c).[67] In the case of the PE sample analyzed, the T_g transition is not observed as it occurs at around –130 °C for either high density polyethylene (HDPE) or low-density polyethylene (LDPE) and the present instrumentation is not set up to cool down to such low temperatures.

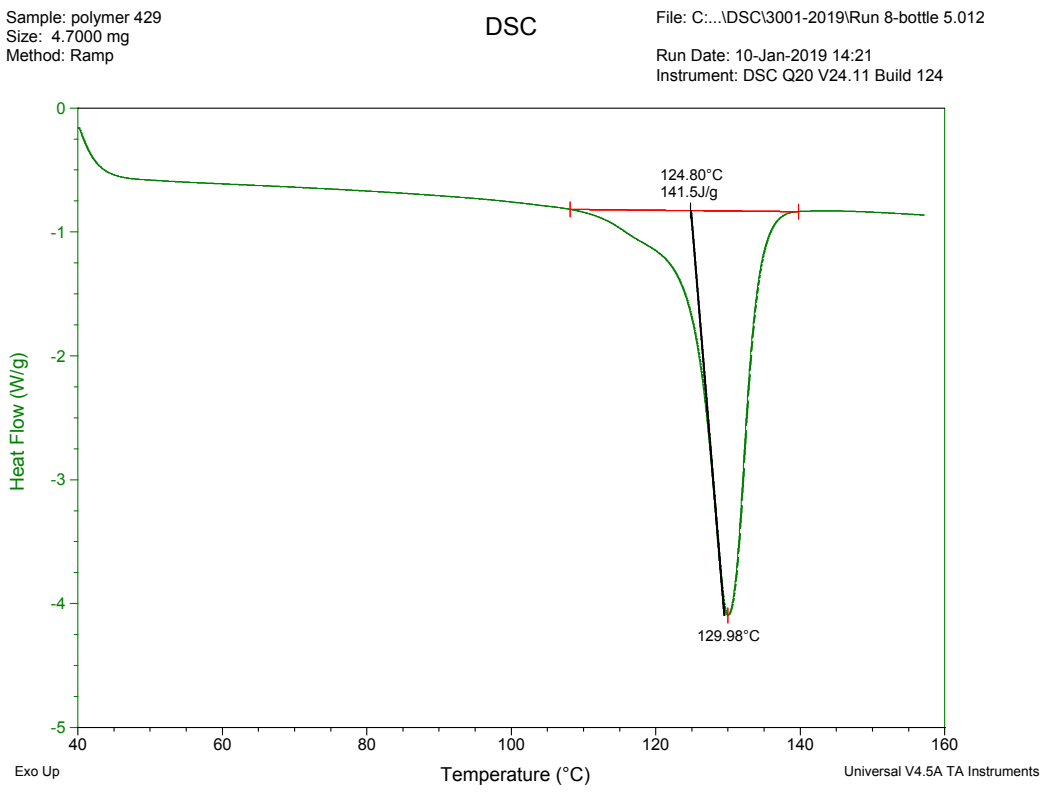

Figure 31. Differential Scanning Calorimetry thermogram for the isolated polymer using compound **25**.

The endothermic transition observed at 130 °C represents melting of the polymer; the polymer melts at this temperature. The T_m value obtained from the thermogram can

help to determine the type of PE produced. The T_m for LDPE is reported as a wide range from 85 ° to 125 °C due to the higher degree of branching that impedes a tight packing of the polymer chains. In contrast, the T_m for HDPE is reported to be in the range of 130 ° to 140 °C while the maximum T_m value for PE is 180 °C.[68] This is due to the lower degree of branching in HDPE leading to more tightly packed polymer chains increasing the intermolecular forces. The observed T_m value for the polymer formed using **25** indicates the formation of HDPE. The area under the curve indicates the amount of heat required for the sample to melt and in this case, it was determined to be 141.5 J/g. This is proportional to the crystallinity percentage present in the polymer. The degree of crystallinity present in the polymer can be calculated using the formula:

$$\% \text{ crystallinity} = (\Delta H_m/\Delta H°_m) \times 100$$

ΔH_m is the value obtained from the thermogram = 141.5 J/g

$\Delta H°_m$ is the value of a 100% crystalline HDPE (293 J/g).[69]

$$\% \text{ crystallinity} = \frac{141.5\ J/g}{293\ J/g} * 100 = 48.7\ \%$$

Thus, the percent crystallinity of the HDPE sample is 48.7% and thus the percent of the amorphous region is 51.3%. The percent crystallinity provides mechanical properties of the polymeric material. The more crystalline a polymer is, more the polymer increases in strength due to the intermolecular forces that are at play between the packed polymeric chains. The crystallization temperature was not determined as the instrument does not have the complete setup.

The polymer obtained during the polymerization experiment using compound **25** was also analyzed by ^{1}H and ^{13}C NMR spectroscopy at 145 °C in deuterated 1,2-dichlorobenzene to determine the molecular weight and the degree of branching present.

The ^{1}H NMR spectrum (**Figure A14**) exclusively showed resonances in the aliphatic region with no olefinic protons in the expected ~ 7.0 to 4.5 ppm range. Instead only terminal CH_3 protons were observed along with the major resonance corresponding to the $–CH_2$-$CH_2–$ repeating unit (**Scheme 24**).

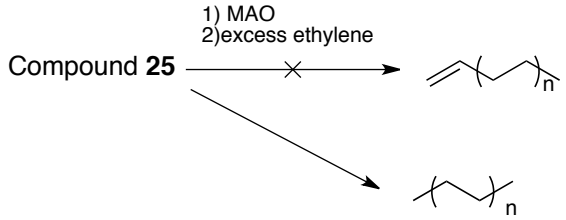

Scheme 24. Polymer formed using compound **25** in the presence of MMAO

The absence of the olefinic protons indicates that the rate of β–hydrogen elimination was slower than the rate of propagation. Ethylene molecules kept adding on to the growing chain until the reaction was quenched, liberating saturated polyethylene. Another possible explanation is that a growing polymer chain was transferred from the metal center to aluminum in MMAO (**Figure 32**). As a result, a free coordination site is reformed after the chain transfer and thus, the coordination and activation of ethylene continues. The polymer chain released from aluminum would not have an olefinic moiety when the polymerization is quenched.

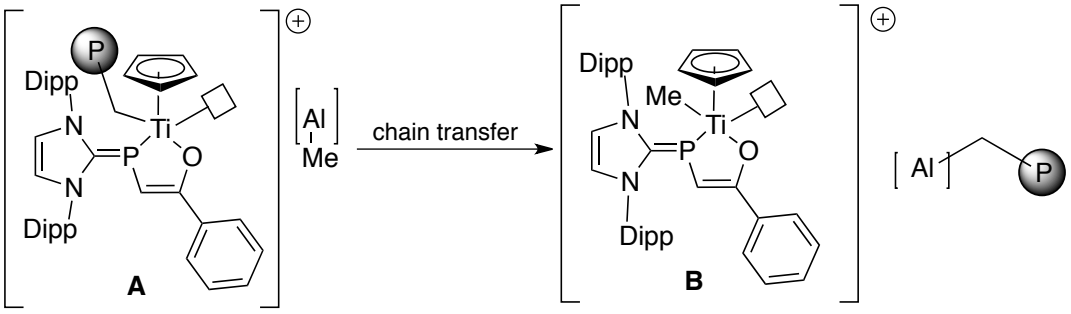

Figure 32. Polymer chain transfer from the catalyst to aluminum (MMAO).

The number average molecular weight (M_n) can be determined using the integration values in the ^{1}H NMR spectrum. The terminal methyl groups account for 6H while the repeating unit integrates to 852 hydrogen atoms allowing to calculate the degree of polymerization (DP) (eq. 22). The degree of polymerization is the number of repeating units present in a polymer.

$$\frac{852\text{H}}{4\text{H (rep. unit)}} = 213 \text{ rep. units} \qquad \textbf{(22)}$$

The M_n of the polymer can be then calculated from the number of repeating units and the terminal CH_3 groups (**Table 3**). The average molecular weight of the polymer was determined be 6005.6 g mol^{-1}.

Table 3. Determination of the number average molecular weight (M_n) for the polymer formed using compound **25** and MMAO as cocatalyst in the presence of a flow of ethylene.

Element	**# Atoms**	**Molecular weight (g•mol^{-1})**	**Total g•mol^{-1}**
H	858	1.008	864.9
C	428	12.011	5140.7
		M_n	6005.6

In the ^{13}C {^{1}H} NMR spectrum (**Figure A15**), only one major signal is observed at 29.9 ppm. The observation of only 1 major signal is an indication of the low degree of branching present in the polymer. Thus, it can be concluded that the polymer formed while using compound **25** is highly linear polyethylene, which supports the DSC data.

2.4 Frustrated Lewis Pair Chemistry

Many phosphorus compounds are known to be Lewis basic due to the lone pair of electrons available for donation and thus are suitable for the formation of adducts with Lewis acids. However, steric hindrance around the phosphorus atom can make the electron pair inaccessible for the interaction with a Lewis acid precluding adduct formation. The Lavoie group is interested in inversely polarized phosphaalkenes due to their tunable Lewis basicity and steric crowding. In addition to the NHC moiety, the organic group bound to phosphorus can be a phenyl ring, *t*-butyl group, or a hydride. To prepare a new FLP system that utilizes an IPP, density functional theory (DFT) calculations using a reported IPP with a phenyl group off of phosphorus and the Lewis acidic tris(pentafluorophenyl)borane (BCF) were performed. The motive of the computational calculations is to determine if the phosphorus atom in the IPP is sufficiently sterically crowded to impede the interaction between phosphorus and boron. Preliminary studies were focused on the compatibility of the adduct formed between the Lewis basic inversely-polarized phosphaalkene **26** and BCF (**Figure 33**).

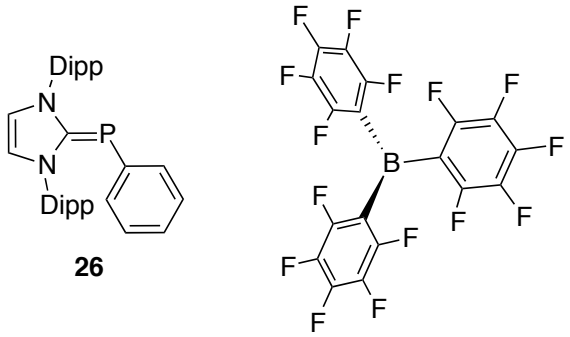

26

Figure 33. Inversely-polarized phosphaalkene and tris(pentafluorophenyl)borane.

Geometry optimization and frequency computations were performed for compound **26** and BCF using density functional theory (DFT) calculations, with B3LYP and 6-31G*

functional and basis set, respectively. For compound **26**, the calculations revealed the highest occupied molecular orbital (HOMO) was localized on the phosphorus atom, in agreement with a basic phosphorus atom (**Figure 34**). The lowest unoccupied molecular orbital (LUMO) is distributed mainly over the aryl groups off of the imidazole ring.

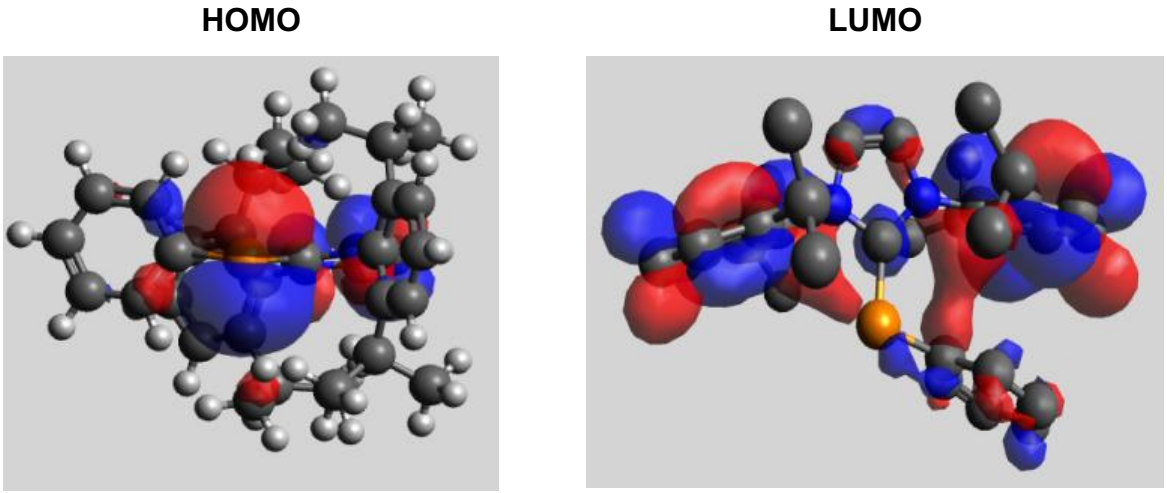

Figure 34. Highest occupied molecular orbital (HOMO) and lowest unoccupied molecular orbital (LUMO) of compound **26** (hydrogen atoms were omitted for clarity)

For BCF, the computations performed showed that the HOMO is distributed over the π-system of the perfluorated phenyl rings, mainly the *ortho* and *meta* positions (**Figure 35**). As expected, the LUMO is located mainly on boron, due to its empty p orbital. The LUMO is also distributed over the *ortho* and *para* position of the perfluorated rings. Therefore, the aromatic rings are good candidates for a nucleophilic aromatic substitution at the *ortho* and *para* positions. The chosen nucleophile will donate electron density in to the p orbital located at the *para* or *meta* positions of a perfluorated phenyl ring. While the formation of the adduct would use the p orbital located on the boron atom.

HOMO **LUMO**

Figure 35. HOMO and LUMO for the Lewis acid BCF.

Further DFT studies were performed in which the optimized structure of BCF and compound **26** were drawn with a distance of 4.47 Å between the phosphorus and boron atom. The resulting optimized structure did not show adduct formation because the distance between the atoms of interest changed to 3.43 Å. As reported in the literature, a common Lewis pair between a phosphine and a borane has a P–B bond length of 1.95 to 2.04 Å.[70,71] Another indication that the adduct did not form was that the boron atom in BCF retained its trigonal planar geometry. If the adduct had formed, the boron atom would gain a tetrahedral conformation. The impediment of adduct formation was due to steric hindrance from the interactions of the bulky perfluorated phenyl rings of BCF with the sterically demanding aryl groups off of the NHC moiety and the phenyl group on phosphorus. These sterically bulky groups impede the formation of the Lewis adduct between the empty p-orbital of boron and the lone pair available on phosphorus, making them good candidates for further studies in frustrated Lewis pair chemistry (FLP) (**Figure 36**).

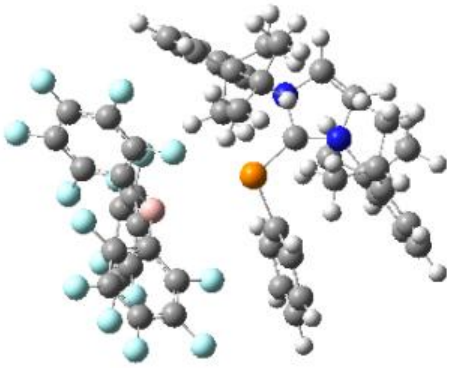

Figure 36. BCF and compound **26** are shown to be sterically hindered to form a Lewis pair.

Initially, these studies focused on the compatibility of **26** with organic substrates containing a carbonyl group as these substrates could be hydrogenated in a metal-free fashion.[39] The chosen substrate and compound **26** were added to an NMR tube in a 1:1 molar ratio and the reaction mixture was monitored by ^{31}P NMR spectroscopy. In the case of acetone and acetophenone, these compounds showed no reactivity with **26** (**Scheme 25**). In the ^{31}P NMR spectrum, the resonance for compound **26** did not change in the presence of the substrate. In contrast, acetyl chloride reacted immediately, evidenced by a new signal observed at 11.6 ppm along with several species in the ^{31}P NMR spectrum and complete/partial disappearance of the resonance attributed to **26**. These reactions exemplified the mild nucleophilicity of the phosphorus atom as a substitution reaction was observed with a good electrophile but was not observed with acetone or acetophenone which have less electrophilic carbon centers.

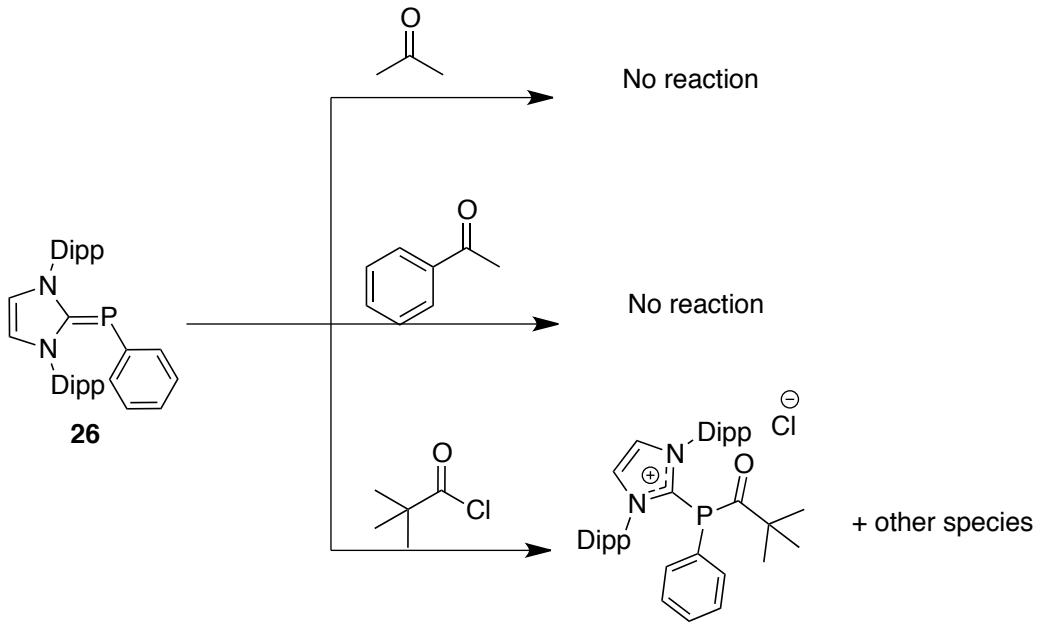

Scheme 25. Results of reactions of compound **26** and substrates containing carbonyl groups.

As **26** was shown to be nucleophilic, it was treated with BCF in toluene and monitored by ^{31}P NMR spectroscopy. No evidence for an adduct formation between **25** and BCF was observed, in agreement with the computational calculations. However, another reaction that can occur with BCF is nucleophilic-aromatic substitution at the *ortho* and *para* position of the perfluorated phenyl groups which is consistent with the DFT study (**Scheme 26**). In the ^{19}F NMR spectrum of the reaction product, there were five new signals ranging from –131.0 ppm to –168.0 ppm, while the starting material was mostly consumed. The ^{19}F–^{19}F COSY NMR spectrum revealed that all five new resonances are correlated to each other. In the ^{11}B NMR spectrum, there are two signals: a sharp peak at –3.48 and a smaller signal at –8.03 ppm. Based on the resonances observed, it can be concluded that there are two magnetically inequivalent boron nuclei present, one of which is starting material and the other is potentially the substitution product.

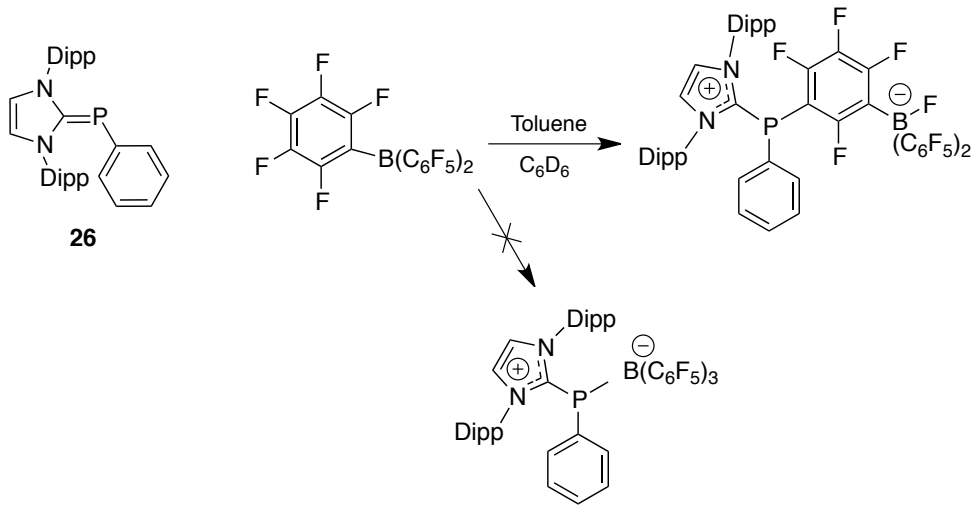

Scheme 26. Reaction scheme between compound **26** and BCF.

Based on the preliminary studies performed using **26** and BCF, the hydride-bearing inversely-polarized phosphaalkene **20** can potentially be used to access a similar FLP system. Compound **20** and BCF were added in equimolar amounts to an NMR tube and dissolved in C_6D_6 (**Scheme 27**).

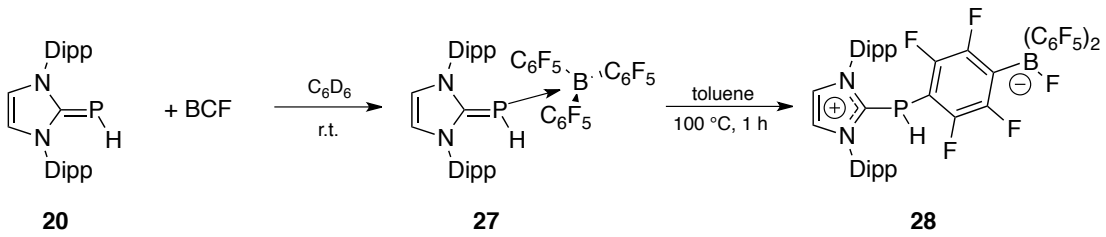

Scheme 27. Synthetic route to access a FLP system bearing an IPP

In the ^{1}H NMR spectrum (**Figure A16**) there are multiple aromatic and aliphatic peaks indicating that there is not a lot of symmetry in the molecule. In addition, several signals are broad, obscuring the multiplicity. The nature of the interaction between compound **20** and BCF can be seen in the ^{31}P NMR spectrum (**Figure A17**), this spectrum shows a doublet of multiplets. The doublet at *∂* 3.86 ppm indicates a 245 Hz coupling to

^{1}H while the multiplet may be caused by the J-coupling to both boron nuclei ^{10}B and ^{11}B. Since the ^{19}F NMR spectrum shown in **Figure A18** indicates very little (if any) coupling, J-coupling to ^{19}F is not expected in the ^{31}P NMR spectrum and the observed multiplets must be caused by boron. The BCF group has a high symmetry about the boron nucleus which tends to reduce the electric field gradient and increase the T_1 relaxation time for both ^{10}B and ^{11}B. These conditions increase the chance of observing coupling to boron as shown in **Figure A17**. The sharpness of the ^{31}P multiplets is a good indication of the strength of the boron-phosphorus bond and helps explain much of the ^{1}H spectrum (**Figure A16**). The formation of the adduct **27** brings the bulky substituents in compound **20** and BCF close to each other. The steric hindrance can impede the free rotation around the $C_{imidazole}$–P bond making the Dipp substituents inequivalent. The presence of two signals for the Dipp methine protons in compound **20** in the ^{1}H NMR spectrum is evidence of the restricted rotation and that the methine protons are in different magnetic environments. Furthermore, the aliphatic and aromatic peaks are also observed as a combination of sharp and broad signals. The unusual appearance of these regions may be caused by the close interaction of the BCF group with only one of the two Dipp groups. The broadness can be attributed to a restricted motion of the Dipp group in the presence of BCF. This interaction leads to the broad appearance caused by the fluxional behaviour observed on the NMR time-scale.

When one Dipp substituent is very close to the BCF group, the other is not and the line shape for both isopropyl groups and aromatic protons is relatively sharp as these protons experience less restricted range of motion. Another interesting observation is that the protons of the imidazole ring have different chemical shift indicating that each proton

is in a unique magnetic environment as a result of the two distinctly different Dipp groups. Altogether, the relatively strong interaction between the phosphorus and born nuclei creates very distinct environments for the NMR active nuclei. Even the BCF ^{19}F peaks in **Figure A18** have noticeably different chemical shift from that of free BCF. This suggests that the nucleophilic aromatic substitution reaction did not occur. Instead, these spectroscopic data suggest that compound **20** and BCF formed the adduct **27**. The adduct **27** cannot be used in the following reaction to access the FLP system because the following step requires the addition of chlorodimethylsilane ($(Me)_2SiHCl$) to replace the fluorine atom on boron for a hydrogen atom, instead compound **28** is required (**Scheme 28**). In order to access the targeted compound **28**, the adduct **27** needs to be heated to promote nucleophilic aromatic substitution. The zwitterionic compound **28** could be formed which potentially could be used to demonstrate the reversible activation of hydrogen gas which could lead to the hydrogenation of ketone substrates. In attempts to access the nucleophilic aromatic substitution product **28**, the reaction was repeated at 100 °C for 1h (**Scheme 27**).

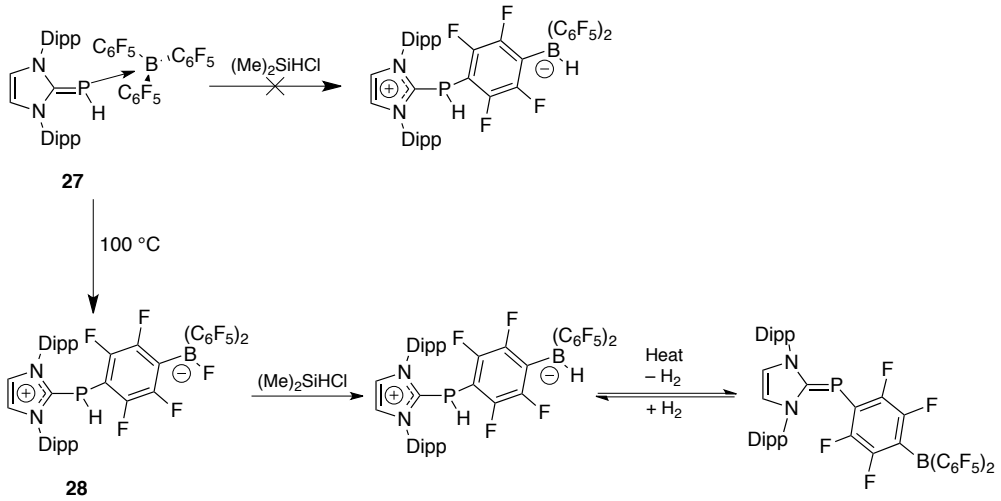

Scheme 28. Synthetic route to access a FLP system bearing an inversely-polarized phosphaalkene.

After heating up a solution of **20** and BCF for 1 h, the solvent was removed *in vacuo*, and the ^{1}H NMR spectrum of the isolated solids revealed signals representative of the corresponding imidazolium salt precursor. To confirm the structure of the product formed during the reaction, X-ray diffraction analysis was performed on a single crystal grown via liquid diffusion at –40 °C under a N_2 atmosphere of pentane into a saturated solution of toluene of the reaction mixture. The chemical structure of the crystals was that of a minor (25 mass%) side-product **29 (Figure 37)**.

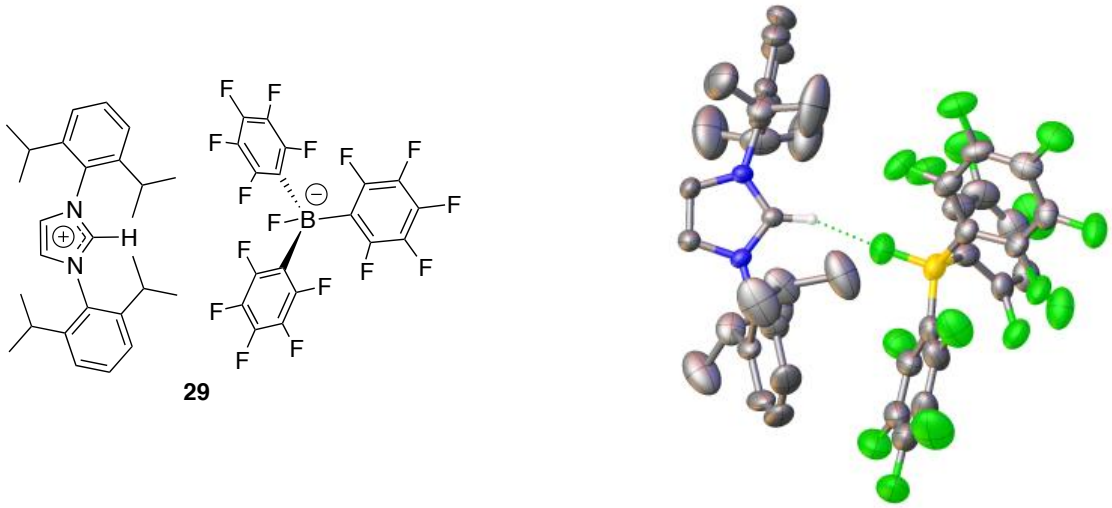

29

Figure 37. ORTEP structure of compound **29** (50% probability). The hydrogen atoms are omitted for clarity (except the hydrogen at C2).

A proposed mechanism (**Scheme 29**) for the formation of **29** starts with the nucleophilic aromatic substitution between **20** and BCF (**A**). The fluorine atom at the *para* position is picked up by another equivalent of BCF forming $[F–BCF]^-$ and compound **B**. The next step would be concerted in which the acidified proton bound to phosphorus in **B** is abstracted using another equivalent of **20** while at the same time delivering a H^- to the carbon in the $C_{imidazole}$–P bond giving the short-lived compound **C**. The restoration of the aromaticity in the central benzene ring leaves a negative charge on the phosphorus

atom giving compound **D**. The highly reactive compound **D** would be quenched via two proton transfers giving compound **E** which now has a good leaving group (RPH_2^+Ar). The lone pair of electrons on one of the nitrogen atoms in the imidazole ring would push the electrons to the *π N–C bond releasing the PH_2^+–(C_6F_4)–BR_2 fragment (**F**) along with the isolated compound **29**. The PH_2^+–(C_6F_4)–BR_2 fragment would then react with other species present in solution forming several unidentified species.

A possible proton source in this reaction is shown at the bottom of the scheme (**Scheme 29**). The formation of the adduct acidifies the hydrogen bound to phosphorus, another equivalent of **20** can act as a base and deprotonate the adduct leading to the formation of a new P–B bond and the protonated analog of **20.**

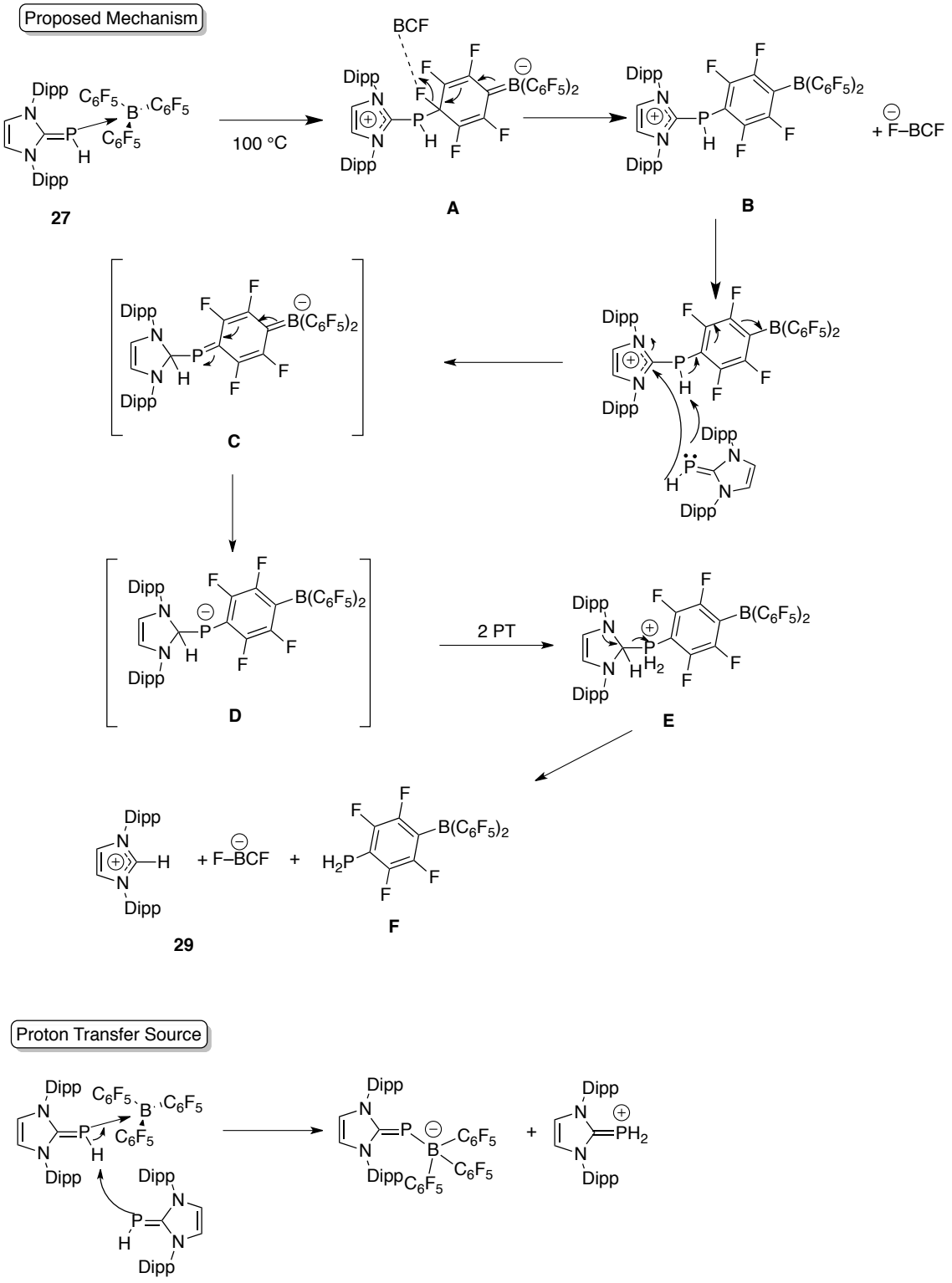

Scheme 29. Proposed mechanism for the formation of **29**.

The solved crystal structure of compound **29** belongs in the space group P2(1)/c. The carbenoid proton was located using the electron density map once all the other atoms had been assigned. There was an observed changed in geometry about the boron atom from a trigonal planar center to a tetrahedral center because of the formation of a new B–F bond. The resulting F–B–C angles are 104.2, 106.4, and 110.6°, which are comparable to those of a tetrahedral (sp^3) carbon atom (109.5°) and distorted tetrahedral boron compounds with angles in the 105.9 to 114.7° range.[72] Intermolecular hydrogen-bonding interactions were observed between the carbenoid proton and the fluorine atom on boron with a distance of 1.96 Å. Even though compound **28** was not the product that was structurally characterized, the formation of compound **29** opened a new area of studies for the reactivity of the C=P bond of inversely-polarized phosphaalkenes.

3. Conclusions

The synthesis of a new bidentate monoanionic ligand bearing an electron-rich inversely-polarized phosphaalkene motif and its precursors was reported for the first time Compound **21** displayed more of a double bond character in the $C_{imidazole}$–P bond than compounds **22, 24, and 25** ,this is supported by the inequivalent methyl and methine protons of the diisopropylphenyl groups off of the NHC moiety and the stretching frequency for the $C_{imidazole}$–P bond, higher than those assigned to **22**, **24**, and **25**. The double bond character is lost when compound **21** is deprotonated to access **22**. Compound **22** displays more of a single bond character based on the stretching band in the IR-ATR spectrum at a lower frequency, leading to conclude that compound **22** showcased more of the canonical form **B**. The keto tautomer of **22** is more stable than its enol tautomer by –18.0 kcal/mol thus only compound **22** was accessed via single deprotonation. Compound **24** had no noticeable changes in the spectroscopic data from compound **22**, except the presence of a characteristic vinylic proton and the TMS protons confirming the successful deprotonation and the protection of the enol synthesized *in situ* using either compound **21** or **22**.

A cyclopentadienyl titanium dichloride complex **25** was prepared successfully and fully characterized. While the IPP motif can exist in two canonical forms, **A** and **B**, the coordination of compound **25** to titanium suggests a stronger contribution from the canonical form **B** which is supported by the stretching band observed in the IR-ATR spectrum in the same area for compound **22** and **24**. The crystal structure of compound **25** showed a four-legged piano stool configuration, confirming the coordination of the bidentate ligand. Thermostability studies of compounds **24**, and **25** showed that

compound **24** displayed great stability at higher temperature with no sign of decomposition after 24 h while compound **25** showed a small amount of decomposition (15%). Polymerization studies using compound **25** demonstrated catalytic activity for ethylene polymerization with an activity up to 9.24 Kg PE mol cat^{-1} h^{-1} in the presence of MMAO as cocatalyst. The active species from the activation of compound **25** showed to be more stable during experimental trials at longer reaction times. The resulting polymer was determined to be linear polyethylene with an average molecular weight of ~ 6000 g • mol^{-1} with a low degree of branching, and a T_m of 130 °C. It is hypothesized that by modifying the electronic characteristics of the bidentate ligand scaffold and thus decreasing the electron density donation from the phosphorus atom to the metal centre, the catalytic activity is likely to increase. The synthesis of a new FLPs system bearing an IPP proved to be unsuccessful and only the adduct formation was observed between compound **20** and BCF. A minor species was characterized and was elucidated to be an imidazolium cation with BCF–F as a counterion (**29**). Although the desired FLPs system was not achieved, it shed light into the stability of the $C_{imidazole}$–P bond present in compound **20**.

4. Experimental Section

General Considerations

Reactions were carried out using oven-dried glassware and performed under an inert atmosphere using either Schlenk techniques or a nitrogen-filled mBraun glovebox. Solvents were dried using an mBraun solvent purification system fitted with alumina columns and stored over molecular sieves and under argon. C_6D_6 and $CDCl_3$ were purchased from Sigma-Aldrich, degassed using three freeze-pump-thaw cycles, vacuum distilled from Na/benzophenone and CaH_2, respectively, and stored under argon. *o*-C_6D_4Cl was purchased from Strem Chemical, degassed using three freeze-pump-thaw cycles and stored under molecular sieves.

NMR data were collected on Bruker AV 400, Bruker AV 300 and Bruker AV 600 spectrometers. The spectra were referenced to the residual protio solvent (^1H) and solvent (^{13}C) resonances. ^{31}P chemical shifts were referenced to 85% phosphoric acid in D_2O.Chemical shifts are reported in ppm (parts per million) and as s (singlet), d (doublet), t (triplet), sept (septet), b (broad), m (multiplet) or a combination of these. Coupling constants are reported in Hertz. Infrared spectra were collected neat on an Agilent Technologies Cary 630 FTIR. Elemental analyses were performed at York University on a Vario EL cube instrument. Differential scanning calorimetry measurement was performed using a DSC Q20 V24.11, aluminum crucibles with lids and compressed air as the purge gas at a flow rate of 50 mL/min. The temperature was raised in increments of 10 °C per minute.

$CpTiCl_3$ was purchased from Strem Chemicals and used as received. Bromoacetophenone, NaHMDS, and deuterated solvents were purchased from Sigma-

Aldrich and used as received. Bromoacetophenone was recrystallized from hot methanol. MAO was purchased from Sigma-Aldrich as a 7% wt. solution in toluene and used as received. Lastly, Na_3P_7 and 1,3-bis(2,6-diisopropylphenyl)-2-phosphinylidene-2,3-dihydro-1H-imidazole (IPr=PH) were prepared as in the literature procedure.[51]

(1,3-Bis(2,6-diisopropylphenyl)-1H-imidazol-2(3H)-ylidene)(2-oxo-2-phenylethyl)phosphonium bromide (21)

A toluene solution (4 mL) of 1,3-bis(2,6-diisopropylphenyl)-2-phosphinylidene-2,3-dihydro-1H-imidazole (IPr=Ph) (841 mg, 1.99 mmol, 1.00 equiv.) was added to a toluene (3 mL) solution of bromoacetophenone (416 mg, 2.09 mmol, 1.05 equiv.) at –40 °C. The solution was stirred at –40 °C for 16 h. The yellow solids that formed were isolated by filtration, washed with cold toluene and pentane, and dried under reduced pressure (1.10 g, 1.78 mmol, 89%). ^{1}H NMR **Figure A1** (400 MHz, $CDCl_3$): δ 8.55 (s, 2H, N–C*H*C*H*–N), 7.68–7.57 (m, 5H, *p*–C*H*$_{(Diip)}$ + *p,m*-C*H*$_{(phenyl)}$), 7.45–7.40 (m, 6H, *m*–C*H*$_{(Dipp)}$ + *o*–C*H*$_{(phenyl)}$), 4.19 (dt, $^1J_{PH}$ = 240.9 Hz and $^3J_{HH}$ = 7.8 Hz, 1H, P*H*), 3.20–3.06 (m, 2H, PCH_2), 2.52–2.37 (m, 4H, CH_3(C*H*)CH_3) and 1.31–1.26 (m, 24H, CH_3(CH)CH_3) ppm. ^{13}C{^{1}H} NMR **Figure A2** (100 MHz, $CDCl_3$): δ 194.9 (d, $^2J_{CP}$ = 4.0 Hz, *C*=O), 150.0 (d, $^1J_{CP}$ = 49.0 Hz, *C*=P), 145.6 (*o*–*C*$_{(Dipp)}$), 145.2 (*o*–*C*$_{(Dipp)}$), 134.8 (*ipso*–*C*$_{(phenyl)}$), 134.8 (*p*–*C*H$_{(phenyl)}$), 132.8 (*p*–*C*H$_{(Dipp)}$), 130.4 (*ipso*–*C*$_{(Dipp)}$), 129.7 (–N*C*H*C*HN–), 129.2 (*m*–*C*H$_{(phenyl)}$), 128.5 (*o*–*C*H$_{(phenyl)}$), 125.6 (*m*–*C*H$_{(Dipp)}$), 125.3 (*m*–*C*H$_{(Dipp)}$), 29.5 (CH_3CHCH_3), 29.4 (CH_3CHCH_3), 29.0 (d, $^1J_{CP}$ = 13.0 Hz, P–*C*H_2), 26.1 (*C*H_3CHCH_3), 25.9 (*C*H_3CHCH_3), 23.0 (CH_3CHCH_3 $_{(Dipp)}$), and 22.9 (CH_3CHCH_3 $_{(Dipp)}$). ^{31}P NMR **Figure A3** (121.5 MHz,

$CDCl_3$): δ –102.8 (dd, $^1J_{P\text{-}H}$ = 241.0 Hz and $^2J_{PH}$ = 7.7 Hz) ppm. **IR (neat)**: 1446 cm^{-1} ($C_{imidazole}$–P) and 1670 cm^{-1} (C=O).

2-((1,3-Bis(2,6-diisopropylphenyl)-1H-imidazol-2(3H)-ylidene)phosphino)-1-phenylethanone (22)

Compound **21** (65.3 mg, 105 μmol, 1.00 equiv.) was suspended in 2 mL of THF. A THF solution (2 mL) of NaHMDS (20.0 mg, 105 μmol, 1.03 equiv.) was added to **21** at –40 °C. The reaction mixture was allowed to warm up to room temperature while stirring over 30 min, resulting in a bright orange/red colour. Volatiles were removed under reduced pressure. The bright red solid was extracted using toluene (6 x 2 mL) and filtered through a bed of Celite. The filtrate was dried in vacuo to give bright red solids (42.8 mg, 79.0 μmol, 75% yield). ^{1}H NMR **Figure A4** (400 MHz, C_6D_6): δ 8.02 (dd, $^3J_{HH}$ = 6.8 Hz and $^4J_{HH}$ = 1.6 Hz, 2H, *o*–C*H*$_{(phenyl)}$), 7.19–7.15 (m, 2H, *p*–C*H*$_{(Dipp)}$), 7.06 (d, $^3J_{HH}$ = 7.6 Hz, 4H, *m*–C*H*$_{(Dipp)}$), 6.98–6.96 (m, 3H, *m*+*p*–C*H*$_{(phenyl)}$), 6.12 (s, 2H, N–C*H*C*H*–N), 3.19 (br 4H, CH_3(C*H)*$CH_{3(Dipp)}$), 3.02 (s, 2H, P–CH_2), 1.47 (d, $^3J_{HH}$ = 6.8 Hz, 12H, CH_3CHC$H_{3(Dipp)}$), 1.14 (d, $^3J_{HH}$ = 6.4 Hz, 12H, CH_3CHC$H_{3(Dipp)}$) ppm. ^{13}C {^{1}H} NMR **Figure A5** (100 MHz, C_6D_6): δ 198.2 (d, $^2J_{CP}$ = 14.0 Hz, *C*=O), 173.8 (d, $^1J_{CP}$ = 109.0 Hz, *C*=P), 147.4 (*o*–*C*$_{(Dipp)}$), 137.9 (*ipso*–*C*$_{(phenyl)}$), 134.5 (*ipso*–*C*$_{(Dipp)}$), 131.8 (*p*–*C*H$_{(Diip)}$), 130.4 (*p*–*C*H$_{(phenyl)}$), 129.2 (*m*–*C*H$_{(Dipp)}$), 127.9 (*m*–*C*H$_{(phenyl)}$), 124.6 (*o*–*C*H$_{(phenyl)}$), 120.2 (–N*C*H*C*HN–), 30.1 (d, $^1J_{CP}$ = 16.0 Hz, P–*C*H_2), 29.1 (CH_3(*C*H)$CH_{3\ (Dipp)}$), 24.9 (*C*H_3(CH)CH_3), 23.4 (CH_3(CH)*C*H_3) ppm. ^{31}P NMR **Figure A6** (162 MHz, C_6D_6): δ –45.3 (s) ppm. **IR (neat):** 1323 cm^{-1} ($C_{imidazole}$–P) and 1655 cm^{-1} (C=O)

1,3-Bis(2,6-diisopropylphenyl)-2-((2-phenyl-2-(trimethylsilyloxy)vinyl)phosphinylidene)-2,3-dihydro-1H-imidazole (24)

NaHMDS (55.7 mg, 0.303 mmol, 2.05 equiv.) was dissolved in 2mL of THF was added to a suspension of compound **21** (90.4 mg, 0.146 mmol, 1.00 equiv.) in 2 mL of THF at –40 °C. TMSCl (37.0 μL, 0.292 mmol, 2.0 equiv.) was added 15 min later. The colour of the solution changed from bright orange to bright yellow, with the formation of solids. The reaction mixture was allowed to warm up to room temperature while stirring for an additional 30 min. The solvent was removed under reduced pressure to give bright yellow solids. The solids were extracted with toluene (6 x 5 mL) and filtered through a bed of Celite. The filtrate was dried under vacuum to give bright brown/yellow solids (62.3 mg, 0.102 mmol, 70%). ^{1}H NMR **Figure A7** (600 MHz, C_6D_6): δ 7.30 (t, $^{3}J_{HH}$ = 7.8 Hz, 2H, *p*–C*H*$_{(Dipp)}$), 7.15 – 7.12 (m, 4H, *m*–C*H*$_{(Diip)}$ + *m*–C*H*$_{(phenyl)}$) 7.01 (d, $^{3}J_{HH}$ = 7.2 Hz, 2H, *o*–C*H*$_{(phenyl)}$), 6.98 (t, $^{3}J_{HH}$ = 7.2 Hz, 1H, *p*–*CH*$_{(phenyl)}$), 6.19 (d, $^{2}J_{PH}$ = 7.2 Hz, 1H, P–C*H*), 6.07 (s, 2H, N–C*H*C*H*–N), 3.12 (sept, $^{3}J_{HH}$ = 6.6 Hz, 4H, (CH_3(C*H*)CH_3), 1.41 (d, $^{3}J_{HH}$ = 7.2 Hz, 12H, (C*H*$_3$(CH)CH_3), 1.14 (d, $^{3}J_{HH}$ = 7.2 Hz, 12H, (CH_3(CH)C*H*$_3$), and 0.23 (s, 9H–*TMS*) ppm. ^{13}C {^{1}H} NMR **Figure A8** (150 MHz, C_6D_6): δ 171.1 (d, $^{1}J_{CP}$= 91.5 Hz, *C*=P), 147.4 (*C*–OTMS), 147.2 (*o*–*C*H$_{(Dipp)}$), 140.0 (d, $^{3}J_{CP}$= 4.5 Hz, *ipso*–*C*$_{(phenyl)}$), 135.0 (*ipso*–*C*$_{(Dipp)}$), 130.3 (*p*–*C*H$_{(Dipp)}$), 128.4 (*m*–*C*H$_{(phenyl)}$), 125.1 (*p*–*C*H$_{(phenyl)}$), 124.8 (*m*–*C*H$_{(Dipp)}$), 124.2 (*o*–*C*H$_{(phenyl)}$), 120.3 (N–*C*H*C*H–N), 110.7 (d, $^{1}J_{CP}$ = 37.5 Hz, P–*C*H), 29.1 (CH_3(*C*H)$CH_{3(Dipp)}$), 24.5 (*C*H$_3$(CH)$CH_{3(Dipp)}$), 23.6 (CH_3(CH)*C*H$_{3(Dipp)}$), 1.39 (d,$^{2}J_{C\text{-}P}$ = 6.0 Hz) ppm. ^{31}P NMR **Figure A9** (243 MHz, C_6D_6): δ –37.7 (d $^{2}J_{PH}$ = 7.2 Hz) ppm. **IR (neat)**: 1328 cm^{-1} ($C_{imidazole}$–P) and 1249 cm^{-1} (C–OTMS).

Cyclopentadienyl 2-((1,3-bis(2,6-diisopropylphenyl)-1H-imidazol-2(3H)-ylidene)phosphino)-1-phenylethenolate titanium dichloride (25)

A toluene solution (2 mL) of compound **24** (42.8 mg, 0.0701 mmol, 1.0 equiv.) was added to $CpTiCl_3$ (15.4 mg, 0.0702 mmol, 1.0 equiv.) dissolved in 2 mL of toluene at room temperature. The solution was stirred for 10 min, and the solvent subsequently removed under reduced pressure to give dark green solids. The solids were washed with cold pentane (6 x 1 mL) and the supernatant was removed. The washed solids were dried under reduced pressure to give dark green solids (47.5 mg, 0.0658 mmol, 92%). ^{1}H NMR **Figure A11** (300 MHz, C_6D_6): δ 7.3–7.1 (m, 10H), 7.0 (t, $^{3}J_{HH}$ = 6.0 Hz, 1H, *p*–*CH*$_{(phenyl)}$) , 6.5 (d, $^{2}J_{PH}$ = 7.8 Hz, 1H, P–C*H*), 6.36 (s, 5H, Cp), 6.1 (s, 2H, N–*CH*C*H*–N), 2.9 (sept, $^{3}J_{HH}$ = 6.9 Hz, 4H, CH_3(C*H*)CH_3), 1.4 (d, $^{3}J_{HH}$ = 6.9 Hz, 12H, C*H*$_3$(CH)CH_3), and 1.1 (d, $^{3}J_{HH}$ = 6.9 Hz, 12H, CH_3(CH)C*H*$_3$) ppm. ^{13}C{^{1}H} NMR **Figure A12** (75 MHz, C_6D_6): δ 168.8 (d, $^{1}J_{CP}$ = 93.6 Hz, *C*=P), 167.5 (d, $^{2}J_{CP}$ = 26.4 Hz, =P–CH–*C*–O), 146.9 (*o*–*C*H$_{(Dipp)}$), 137,1 (d, $^{2}J_{CP}$ = 3.0 Hz, *ipso*–*C*$_{(phenyl)}$), 134.0 (*ipso*–*C*$_{(Dipp)}$), 130.9 (*p*–*C*H$_{(Dipp)}$), 128.4 (*m*–*C*H$_{(phenyl)}$), 125.9 (*p*–*C*H$_{(phenyl)}$), 125.0 (*m*–*C*H$_{(Dipp)}$), 123.4 (*o*–*C*H$_{(phenyl)}$), 121.0 (d, $^{3}J_{CP}$ = 2.3 Hz, N–*C*H*C*H–N), 120.3 (d, $^{2}J_{CP}$ = 4.5 Hz, Cp), 118.2 (d, $^{1}J_{CP}$ = 43.8 Hz, =P–*C*H), 29.2 (CH_3(*C*H)$CH_{3(Dipp)}$), 24.5 (*C*H_3(CH)$CH_{3(Dipp)}$), 23.5 (CH_3(CH)*C*$H_{3(Dipp)}$) ppm. ^{31}P NMR **Figure A13** (121.4 MHz, C_6D_6): δ –27.4 (d, $^{2}J_{PH}$ = 6.5 Hz) ppm. Anal. Calcd for $C_{40}H_{47}Cl_2N_2OPTi$ (%): C, 66.58; H, 6.57; N, 3.88. Found (%): C, 66.69; H, 6.63; N, 3.90. **IR (neat):** 1325 cm^{-1} ($C_{imidazole}$–P).

General Procedure for Ethylene Polymerization.

Polymerization tests were carried at 1 atm ethylene and at room temperature in a 200-mL Schlenk flask charged with a stirring bar. The flask was dried in an oven set at 160 °C overnight prior to use. The flask was charged with 20 mL toluene and three freeze-pump-thaw cycles were performed. The solution was saturated with ethylene and 5 ml of 7 wt. % MAO in a toluene solution (220 equiv.) were added subsequently. The complex (50.0 μmol) was added via syringe. The reaction mixture was vigorously stirred and subsequently quenched with 20 mL of a 50:50 solution of methanol and concentrated hydrochloric acid (see **Table 2** for reaction time). The solid was filtered, washed with water and subsequently methanol. The solids were isolated via filtration and dried in vacuo at 60 °C for several hours.

X-ray Crystallography.

Crystallographic data for compound **25** was collected at the University of Toronto on a Bruker−Nonius Kappa-CCD diffractometer using monochromated Cu Kα radiation (λ = 1.54184 Å) at 150 K and were measured using a combination of ϕ scans and ω scans with κ offsets to fill the Ewald sphere. Intensity data were processed using Denzo−SMN.[73] Absorption corrections were carried out using SORTAV.[74] The data were processed using APEX2 and SAINT.[75] Absorption corrections were carried out using SADABS.[75] Using Olex2[76], the structure was solved with the XS[77] structure solution program using Direct Methods and refined with the ShelXL[78] refinement package using Least Squares minimisation. All H atoms were included in calculated positions and allowed to refine in riding-motion approximation with U_{iso} tied to the carrier atom. The solved structure was

checked using the crystallographic program PLATON.[79] The electron density corresponding to the highly disordered solvent molecules present were flattened using the SQUEEZE[80] option in PLATON.

Computational Details.

DFT calculations were carried out using the Gaussian 16[81] for computing and Avogadro[82] version 1.2.0. for molecular visualization. The functional utilized was the hybrid B3LYP level of theory with 6-21G* as basis set. These calculations were performed on the Shared Hierarchical Academic Research Computing Network (SHARCNET: www.sharcnet.ca)

References

(1) Connor, E. F.; Younkin, T. R.; Henderson, J. I.; Waltman, A. W.; Grubbs, R. H. *Chem. Commun.* **2003**, 2272–2273.

(2) Wilke, G. *Angew. Chemie Int. Ed. Engl.* **1988**, *27* (1), 185–206.

(3) Keim, W. *Angew. Chemie Int. Ed. Engl.* **1990**, *29* (3), 235–244.

(4) Makio, H.; Kashiwa, N.; Fujita, T. *Adv. Synth. Catal.* **2002**, *344* (5), 477–493.

(5) Wang, C.; Friedrich, S.; Younkin, T. R.; Li, R. T.; Grubbs, R. H.; Bansleben, D. A.; Day, M. W. *Organometallics* **1998**, *17* (15), 3149–3151.

(6) Koltzenburg, Sebastian; Maskos, Michael; Nuyken, O. *Polymer Chemistry*, 1st ed.; Springer-Verlag Berlin Heidelberg: Berlin, 2017.

(7) Choi, K. Y.; McAuley, K. B. *Polym. React. Eng.* **2008**, 273–314.

(8) Odian, G. *Principles of Polymerization*, 4th ed.; Wiley-Intersciene, Ed.; John Wiley & sons, Inc.: New York, 2004.

(9) Makio, H.; Terao, H.; Iwashita, A.; Fujita, T. *Chem. Rev.* **2011**, *111*, 2363–2449.

(10) Hlatky, G. G. *Coord. Chem. Rev.* **1999**, *181*, 243–296.

(11) Karol, F. J. *Catal. Rev.* **1984**, *26* (3–4), 557–595.

(12) McKnight, A. L.; Waymouth, R. M. *Chem. Rev.* **2003**, *98*, 2587–2598.

(13) Eisch, J. J. *Organometallics* **2012**, *31* (17), 6504.

(14) Eisch, J. J. *J. Chem. Educ.* **1983**, *60* (12), 1009.

(15) Carraher Jr, C. E. *Introduction to Polymer Chemistry*, 2nd ed.; CRC Press., 2010.

(16) Natta, G.; Pino, P.; Corradini, P.; Danusso, F.; Moraglio, G.; Mantica, E.; Mazzanti, G. *J. Am. Chem. Soc.* **1955**, *77* (6), 1708–1710.

(17) Wilkinson, G.; Rosenblum, M.; Whiting, M. C.; Woodward, R. B. *J. Am. Chem.*

Soc. **1952**, *74* (8), 2125–2126.

(18) Wilkinson, G.; Birmingham, J. M. *J. Am. Chem. Soc.* **1954**, *76* (17), 4281–4284.

(19) Kaminsky, W. *Dalton. Trans.* **1998**, No. 9, 1413–1418.

(20) Wild, F. R. W. P.; Zsolnai, L.; Huttner, G.; Brintzinger, H. H. *J. Organomet. Chem.* **1982**, *232* (1), 233–247.

(21) Kaminsky, W.; Külper, K.; Brintzinger, H. H.; Wild, F. R. W. P. *Angew. Chemie Int. Ed. Engl.* **1985**, *24* (6), 507–508.

(22) Soga, K.; Shiono, T. *Prog. Polym. Sci.* **1997**, *22* (7), 1503–1546.

(23) Matshui, Shigekazu; Mitani, Makoto; Tohi, Yasushi; Makio, Haruyuki; Tanaka, Hidetsugu; Fujita, T. *Chem. Lett.* **1999**, *28* (12), 1263–1264.

(24) Tohi, Yasushi ; Makio, Haruyuki; Matshui, Shigekazu; Onda, Mitsuhiko; Fujita, T. *Macromolecules* **2003**, *36* (523), 523–525.

(25) Makio, H.; Terunori, F. *Acc. Chem. Res.* **2009**, *42* (10), 1532–1544.

(26) Terao, H.; Ishii, S.; Mitani, M.; Tanaka, H.; Fujita, T. *J. Am. Chem. Soc.* **2008**, *3* (130), 17636–17637.

(27) Larocque, T. G.; Dastgir, S.; Lavoie, G. G. *Organometallics* **2013**, *32* (15), 4314–4320.

(28) Keim, W.; Hoffmann, B.; Lodewick, R.; Peuckert, M.; Schmitt, G.; Fleischhauer, J.; Meier, U. *J. Mol. Catal.* **1979**, *6* (2), 79–97.

(29) Kuhn, P.; Sémeril, D.; Matt, D.; Chetcuti, M. J.; Lutz, P. *Dalt. Trans.* **2007**, *77*, 515–528.

(30) Keim, W.; Schulz, R. P. *J. Mol. Catal.* **1994**, *92* (1), 21–33.

(31) Klabunde, U.; Itten, S. D. *J. Mol. Catal.* **1987**, *41* (1–2), 123–134.

(32) Younkin, T. R.; Connor, E. F.; Henderson, J. I.; Friedrich, S. K.; Grubbs, R. H.; Bansleben, D. A. *Science (80-.).* **2000**, *287* (5452), 460–462.

(33) Doak, K. W. In *Encyclopedia of Polymer Science and Engineering*; Wiley, J. and S., Ed.; New York, 1986; pp 386–429.

(34) Johnson, L. K.; Mecking, S.; Brookhart, M. *J. Am. Chem. Soc.* **1996**, *118* (1), 267–268.

(35) Drent, E.; van Dijk, R.; van Ginkel, R.; van Oort, B.; Pugh, R. I. *Chem. Commun.* **2002**, *31*, 744–745.

(36) Nakamura, A.; Anselment, T. M. J.; Claverie, J.; Goodall, B.; Jordan, R. F.; Mecking, S.; Rieger, B.; Sen, A.; Van Leeuwen, P. W. N. M.; Nozaki, K. *Acc. Chem. Res.* **2013**, *46* (7), 1438–1449.

(37) Piche, L.; Daigle, J. C.; Poli, R.; Claverie, J. P. *Eur. J. Inorg. Chem.* **2010**, No. 29, 4595–4601.

(38) Nakamura, A.; Munakata, K.; Ito, S.; Kochi, T.; Chung, L. W.; Morokuma, K.; Nozaki, K. *J. Am. Chem. Soc.* **2011**, *133* (17), 6761–6779.

(39) Stephan, D. W. *J. Am. Chem. Soc.* **2015**, *137* (32), 10018–10032.

(40) Welch, G. C.; Juan, R. R. S.; Masuda, J. D.; Stephan, D. W. *Science (80-.).* **2006**, *1883*, 1124–1126.

(41) Stephan, D. W. *Acc. Chem. Res.* **2015**, *48* (2), 306–316.

(42) Schmidpeter, A.; Gebler, W.; Zwaschka, F.; Sheldrick, W. S. *Angew. Chemie Int. Ed. Engl.* **1980**, *19* (9), 722–723.

(43) Schmidpeter, A.; Zwaschka, F. *Angew. Chemie* **1977**, *89* (10), 747–747.

(44) Fuchs, E. P. O.; Heydt, H.; Regitz, M.; Schoeller, W. W.; Busch, T. *Tetrahedron*

Lett. **1989**, *30* (38), 5111–5114.

(45) Arduengo, A. J.; Calabrese, J. C.; Cowley, A. H.; Dias, H. V. R.; Goerlich, J. R.; Marshall, W. J.; Riegel, B. *Inorg. Chem.* **1997**, *36* (10), 2151–2158.

(46) Back, O.; Henry-Ellinger, M.; Martin, C. D.; Martin, D.; Bertrand, G. *Angew. Chemie - Int. Ed.* **2013**, *52* (10), 2939–2943.

(47) Arduengo, III, A. J.; Dias, H. V. R.; Calabrese, J. C. *Chem. Lett.* 1997, pp 143–144.

(48) Back, O.; Henry-Ellinger, M.; Martin, C. D.; Martin, D.; Bertrand, G. *Angew Chem Int. Ed. Engl.* **2013**, *52* (10), 2939–2943.

(49) Rodrigues, R. R.; Dorsey, C. L.; Arceneaux, C. A.; Hudnall, T. W. *Chem. Commun.* **2014**, *50* (2), 162–164.

(50) Aaron M. Tondreau, Zoltán Benkő, J. R. H. and H. G. *Chem. Sci.* **2014**, No. 5, 1545–1554.

(51) Cicač-Hudi, M.; Bender, J.; Schlindwein, S. H.; Bispinghoff, M.; Nieger, M.; Grützmacher, H.; Gudat, D. *Eur. J. Inorg. Chem.* **2016**, 649–658.

(52) Doddi, A.; Bockfeld, D.; Bannenberg, T.; Jones, P. G.; Tamm, M. *Angew. Chemie - Int. Ed.* **2014**, *53* (49), 13568–13572.

(53) Lothar Weber, Olaf Kaminski, Hans-Georg Stammler, B. N.; Vadim D. Romanenkob. *Z. Naturforsch. B Chem. Sci.* **1993**, *48*, 1784.

(54) Boubekeur, L.; Ricard, L.; Floch, P. Le; Mézailles, N. *Organometallics* **2005**, *24* (16), 3856–3863.

(55) Liu, L.; Ruiz, D. A.; Dahcheh, F.; Bertrand, G. *Chem. Commun.* **2015**, *51* (64), 12732–12735.

(56) Krachko, T.; Slootweg, J. C. *Eur. J. Inorg. Chem.* **2018**, *2018* (24), 2734–2754.

(57) Weber, L. *Eur. J. Inorg. Chem.* **2000**, *2000* (12), 2425–2441.

(58) Appel, R.; Geisler, K. *J. Organomet. Chem.* **1976**, *112* (1), 61–64.

(59) Pouchert, C. J. *The Aldrich Library of Infrared Spectra*, III.; Sigma Aldrich: Milwaukee, 1981.

(60) Luo, Y. *Comprenhensive Handbook of Chemical Bond Energies*, 1st ed.; Raton, B., Ed.; CRC Press.: Florida, 2007.

(61) Bott, R. K. J.; Hughes, D. L.; Schormann, M.; Bochmann, M.; Lancaster, S. J. *J. Organomet. Chem.* **2003**, *665*, 135–149.

(62) Wang, Y.; Xie, Y.; Wei, P.; King, R. B.; Schaefer, H. F.; Schleyer, P. V. R.; Robinson, G. H. *J. Am. Chem. Soc.* **2008**, *130* (2), 14970–14971.

(63) Larocque, T. G.; Lavoie, G. G. *New J. Chem.* **2014**, *38* (2), 499–502.

(64) Taguchi, H. O.; Sasaki, D.; Takeuchi, K.; Tsujimoto, S.; Matsuo, T.; Tanaka, H.; Yoshizawa, K.; Ozawa, F. *Organometallics* **2016**, *35* (10), 1526–1533.

(65) Siegbahn, P. E. M.; Jensen, V. R.; Waernmark, K.; Ystenes, M.; Aakermark, B.; Svennson, M.; Blomberg, M. R. A. *Organometallics* **2005**, *13* (1), 282–288.

(66) Pyykkö, P. *J. Phys. Chem. A* **2015**, *119* (11), 2326–2337.

(67) Peacock, Andrew; Calhoun, A. *Polymer Chemistry - Properties and Applications*; Carl Hanser Verlag GmgH & Co. KG: Munich, 2006.

(68) Peacock, Andrew; Calhoun, A. *Polymer Chemistry - Properties and Applications*; Carl Hanser Verlag GmgH & Co. KG: Munich, 2006.

(69) Singh, Ran B; Sajwan, Madhuri; Aggarwal, S. *Indian J. Criminol. Crim.* **2008**, *29* (2), 141–148.

(70) Aubauer, C.; Davidge, K.; Klapötke, T. M.; Mayer, P.; Piotrowski, H.; Schulz, A. *Z. Anorg. Allg. Chem.* **2000**, *626* (11), 2373–2378.

(71) Bradley, D. C.; Hursthouse, M. B.; Dao-hong, Z. *J. Chem. Soc. Chem. Commun. Chem. Commun.* **1991**, No. 1, 7–8.

(72) Goze, C.; Ulrich, G.; Ziessel, R. *J. Org. Chem.* **2007**, *72* (2), 313–322.

(73) Otwinowski, Zbyszek ; Minor, W. In *Methods in Enzymology*; London, 1997; Vol. 276, pp 306–326.

(74) Blessing, R. H. *Acta Crystallogr. Sect. A* **1995**, *A51*, 33–38.

(75) APEX; SAINT; SABABS; Bruker AXS, I.; Madison, Wisconsin, 2007. .

(76) Dolomanov, O. V; Bourhis, L. J.; Gildea, R. J.; Howard, J. A. K.; Puschmann, H. *Appl. Crystallogr.* **2009**, *42*, 339–341.

(77) Sheldrick, G. M. *Acta Crystallogr. Sect. A* **2014**, *A71*, 3–8.

(78) Sheldrick, G. M. *Acta Crystallogr. Sect. A* **2007**, *A64* (1), 112–122.

(79) Spek, A. L. *J. Appl. Crystallogr.* **2003**, *36* (1), 7–13.

(80) Spek, A. L. *PLATON99 A Multipurpose Crystallographic Tool*; Utretch, 1999.

(81) Frisch, M. J.; Trucks, G. W.; Schlegel, H. B.; Scuseria, G. E.; Robb, M. A.; Cheeseman, J. R.; Scalmani, G.; Barone, V.; Petersson, G. A.; Nakatsuji, H.; Li, X.; Caricato, M.; Marenich, A. V.; Bloino, J.; Janesko, B. G.; Gomperts, R.; Mennucci, B.; Hratch, D. J. *Gaussian, Inc.* Wallingford CT 2016.

(82) Curtis, D. E.; Vandermeersch, T.; Hutchison, G. R.; Lonie, D. C.; Zurek, E.; Hanwell, M. D. *J. Cheminform.* **2012**, *4* (1), 17.

Appendix

List of Spectra

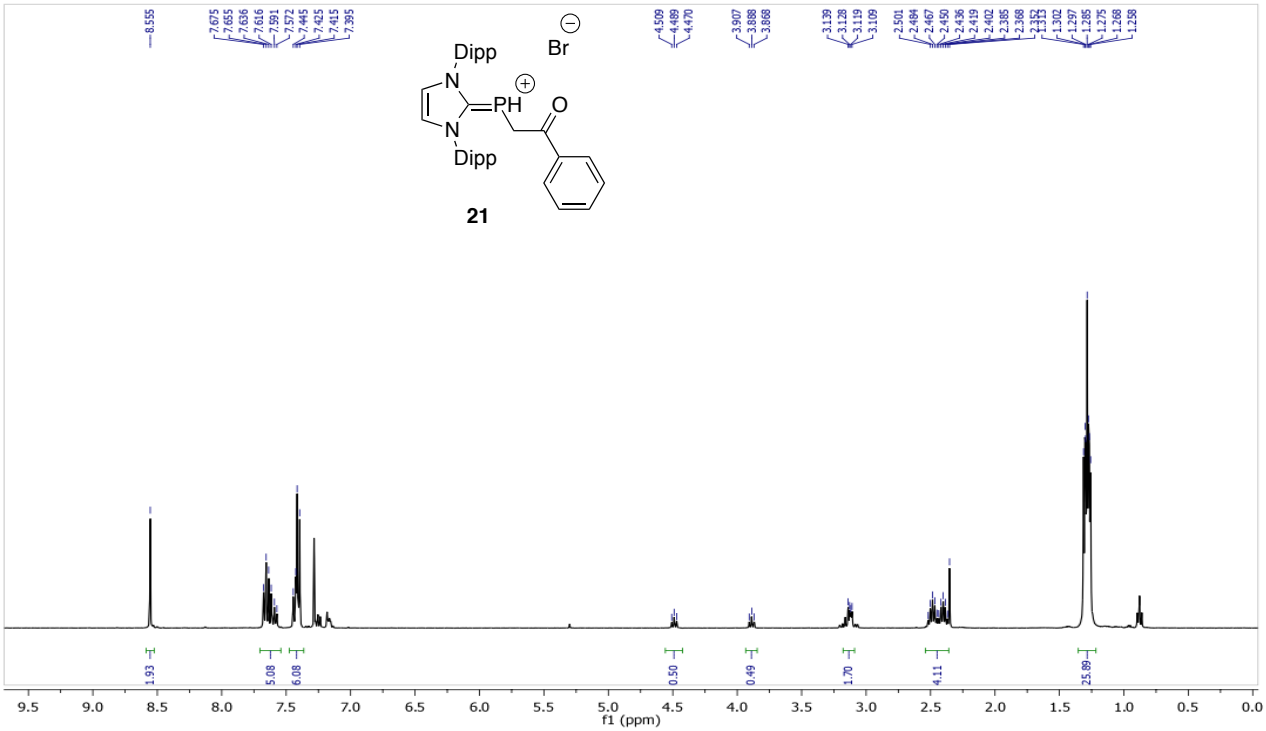

Figure A1. ^{1}H NMR Spectrum of compound **21**. (400 MHz, $CDCl_3$)

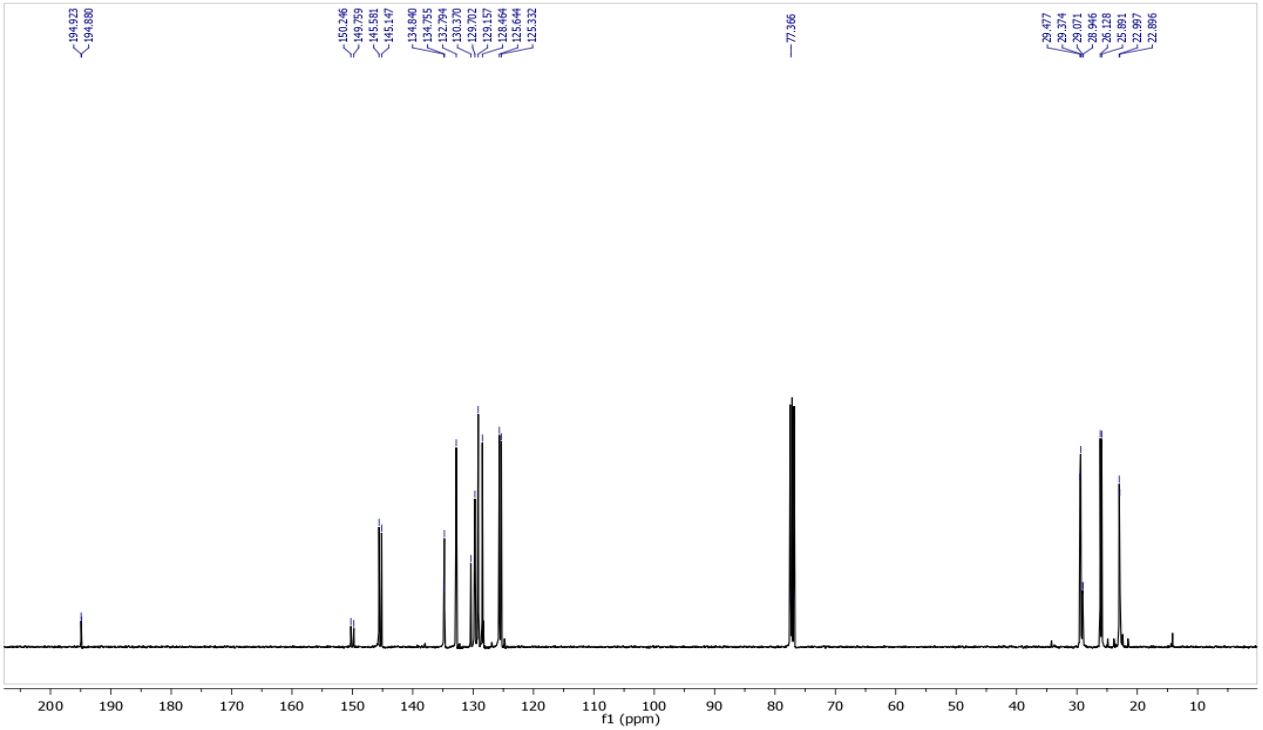

Figure A2. ^{13}C {^{1}H} NMR Spectrum of compound **21**. (100 MHz, $CDCl_3$)

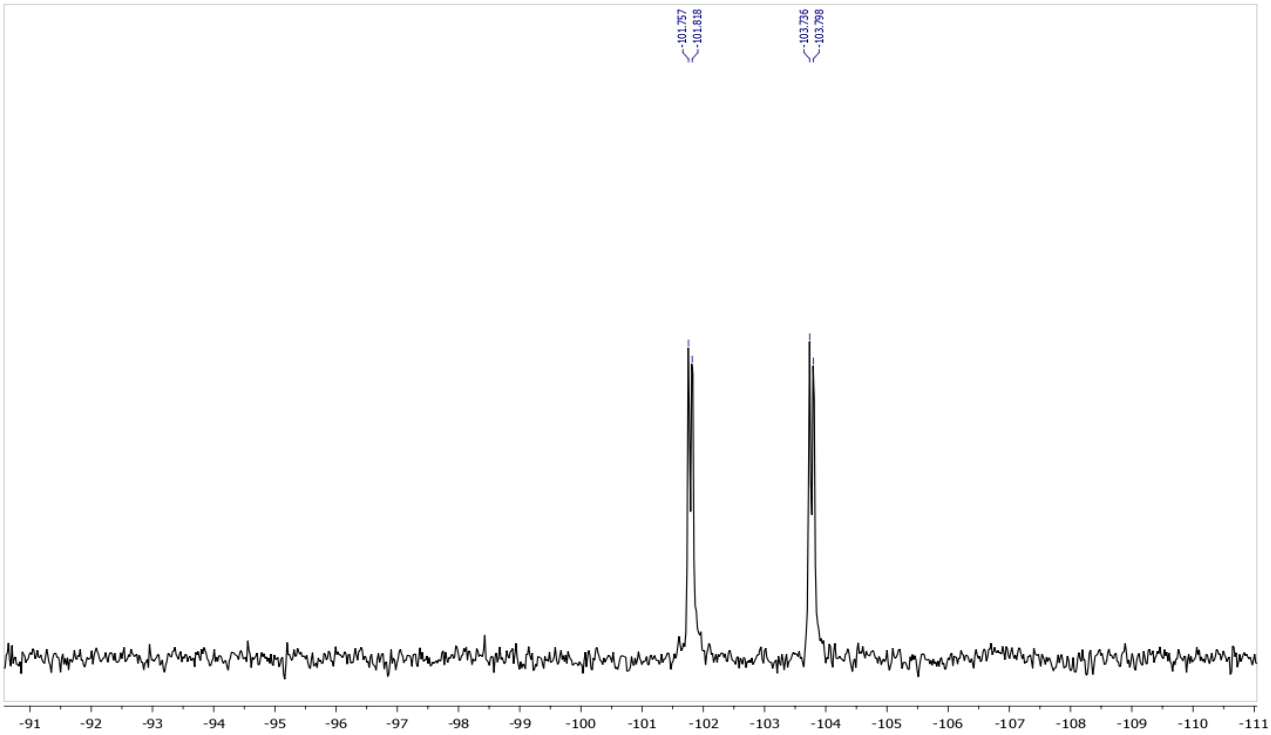

Figure A3. ^{31}P NMR Spectrum of compound **21**. (121.5 MHz, $CDCl_3$)

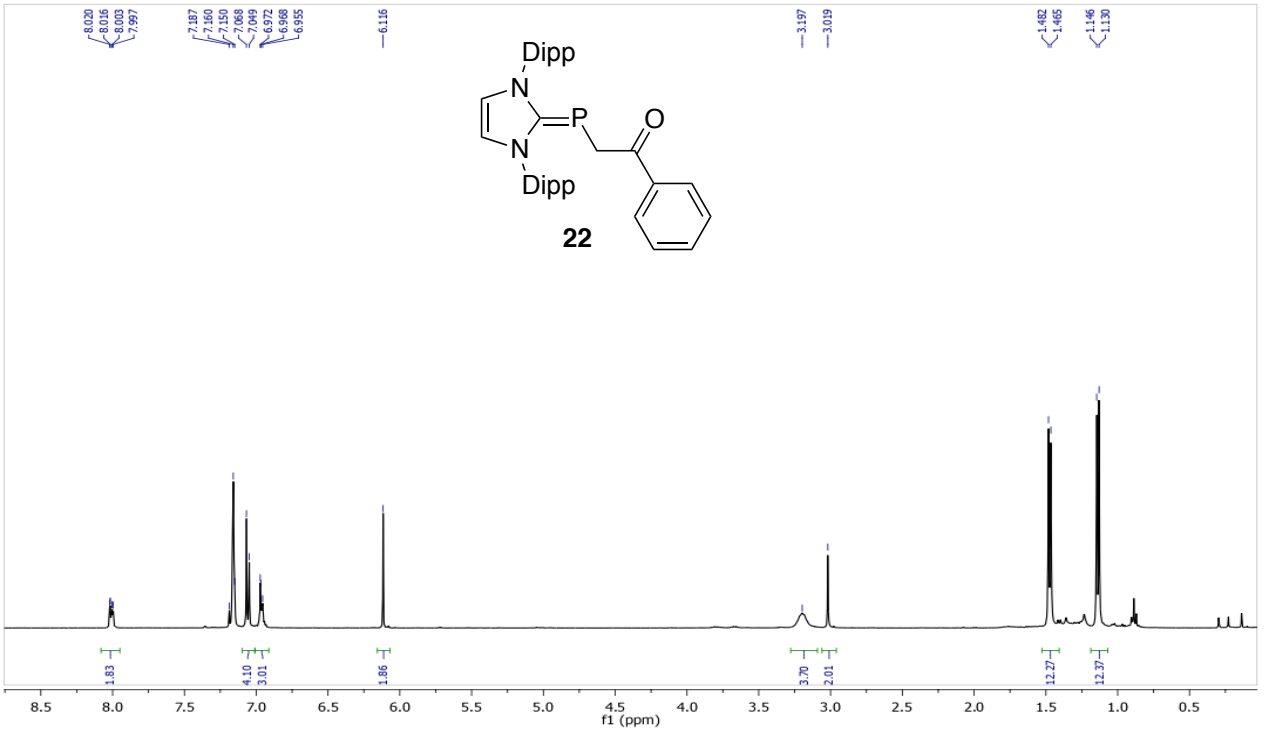

Figure A4. ^{1}H NMR Spectrum of compound **22**. (400 MHz, C_6D_6)

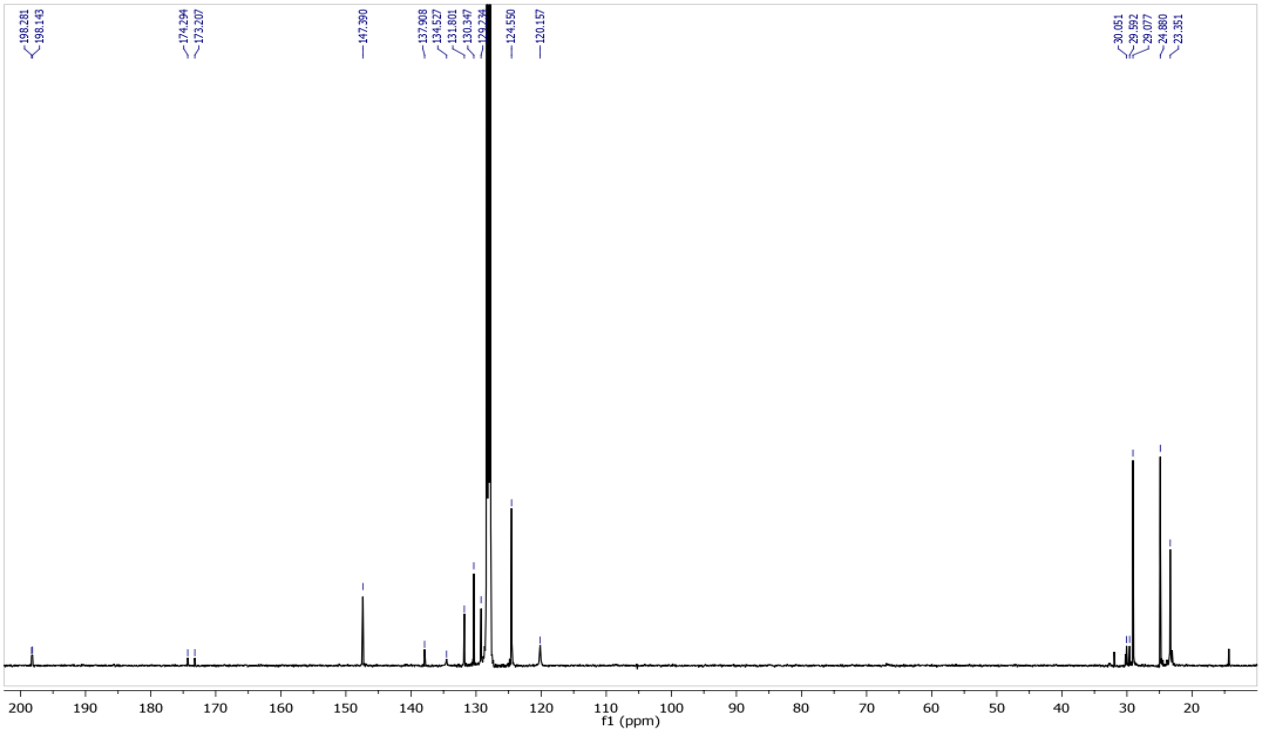

Figure A5. ^{13}C {^{1}H} NMR Spectrum of compound **22**. (100 MHz, C_6D_6)

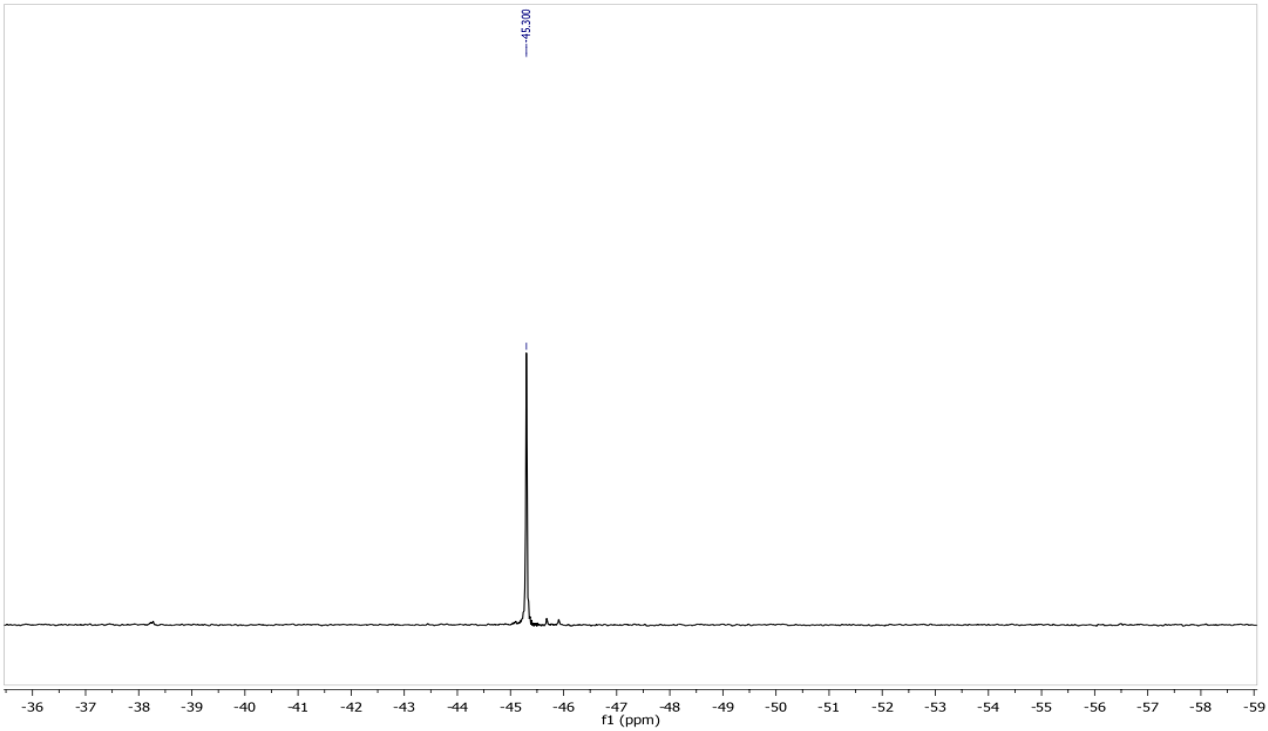

Figure A6. ^{31}P NMR Spectrum of compound **22**. (162 MHz, C_6D_6)

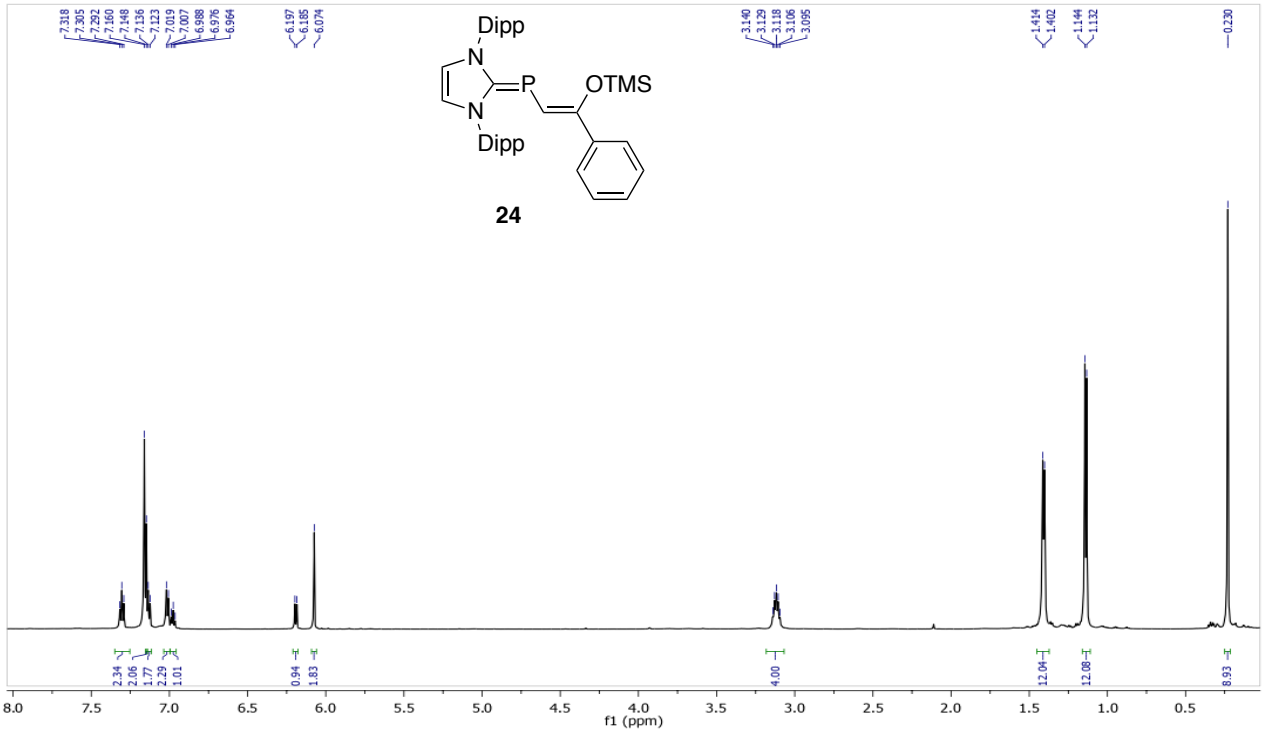

Figure A7. ^{1}H NMR Spectrum of compound **24**. (600 MHz, C_6D_6)

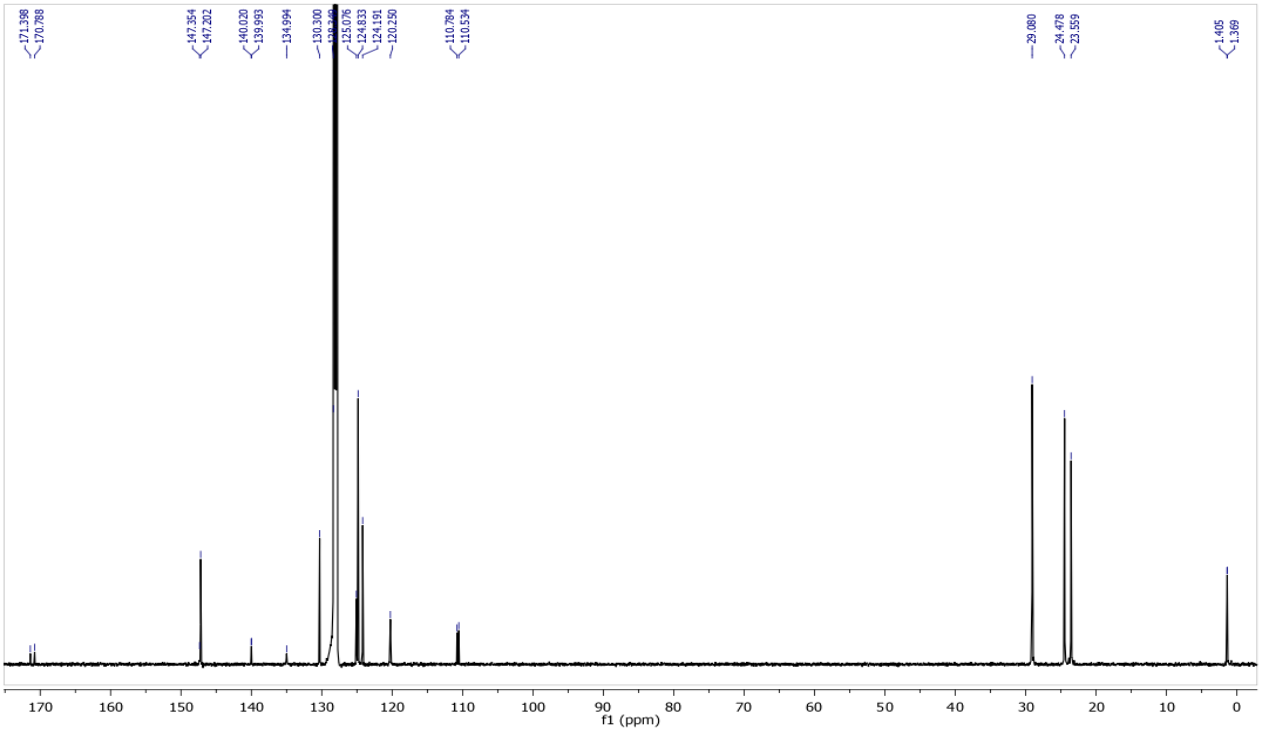

Figure A8. ^{13}C {^{1}H} NMR Spectrum of compound **24**. (150 MHz, C_6D_6)

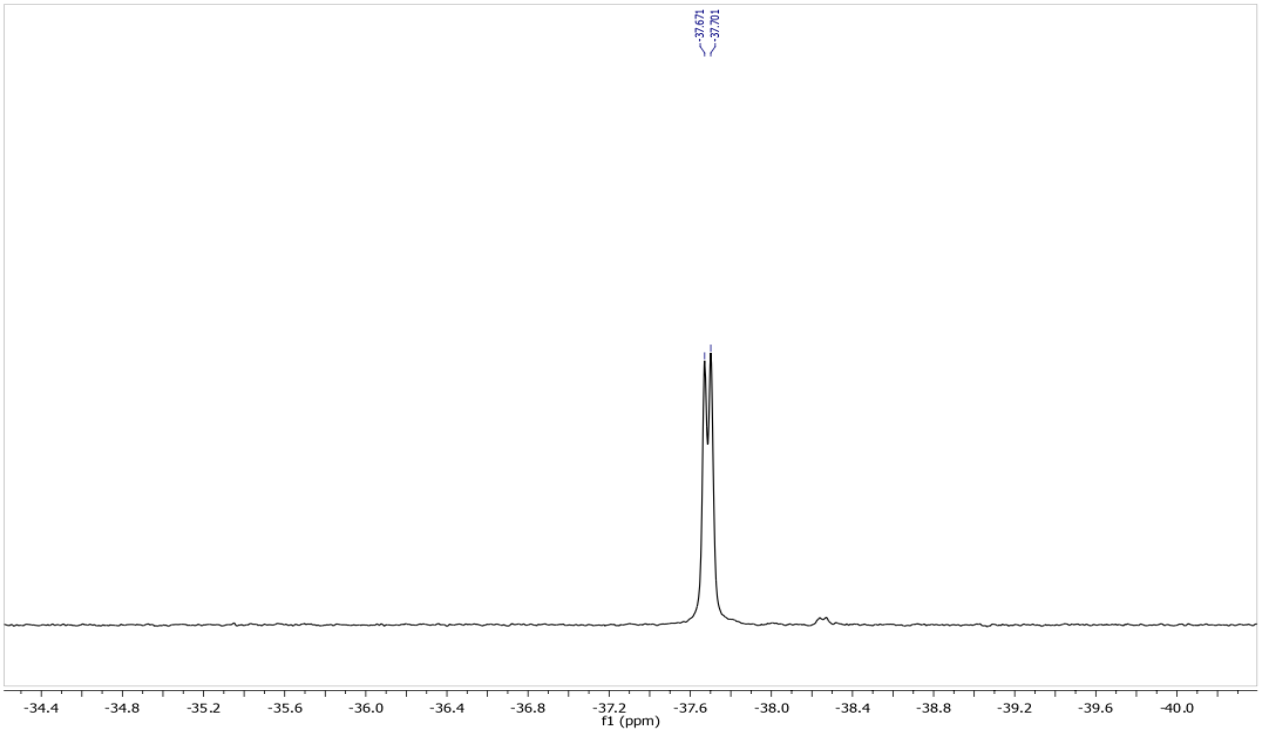

Figure A9. ^{31}P NMR Spectrum of compound **24**. (243 MHz, C_6D_6)

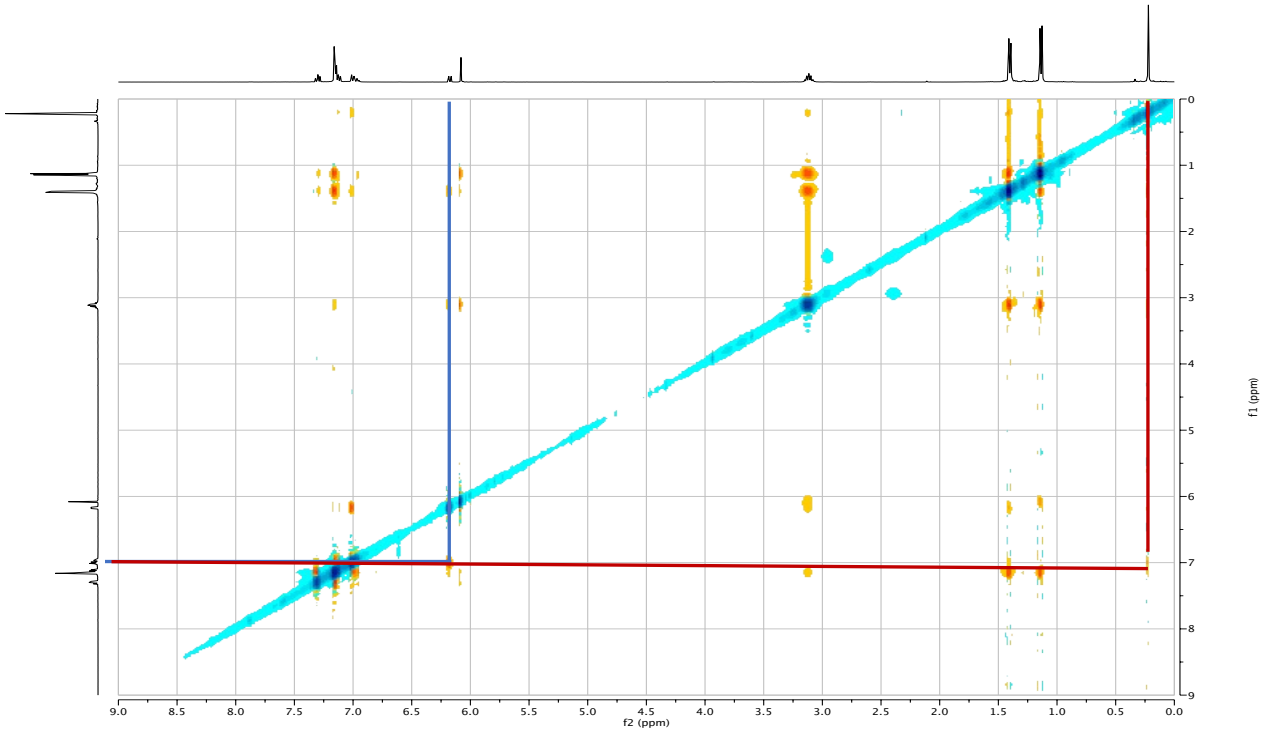

Figure A10. NOESY Spectrum for compound **24** (selected correlations are shown). (400 MHz, C_6D_6)

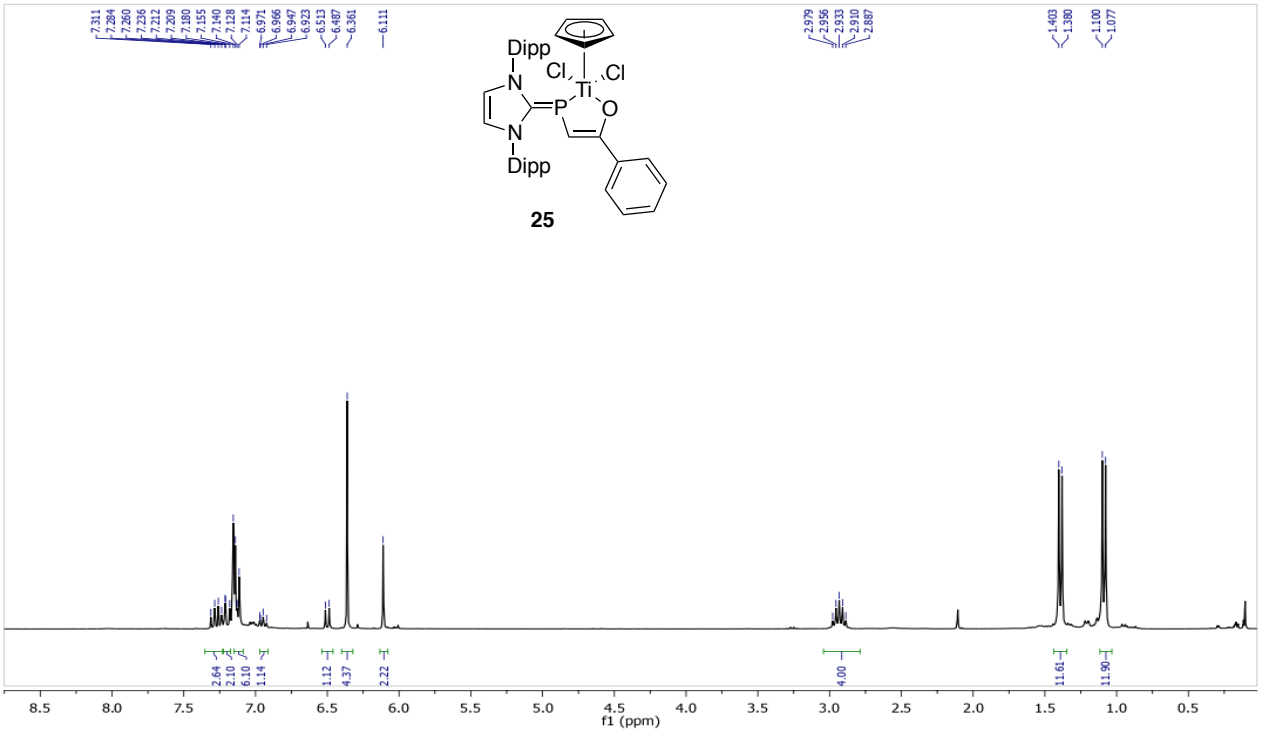

Figure A11. ^{1}H NMR Spectrum of the titanium complex **25**. (300 MHz, C_6D_6)

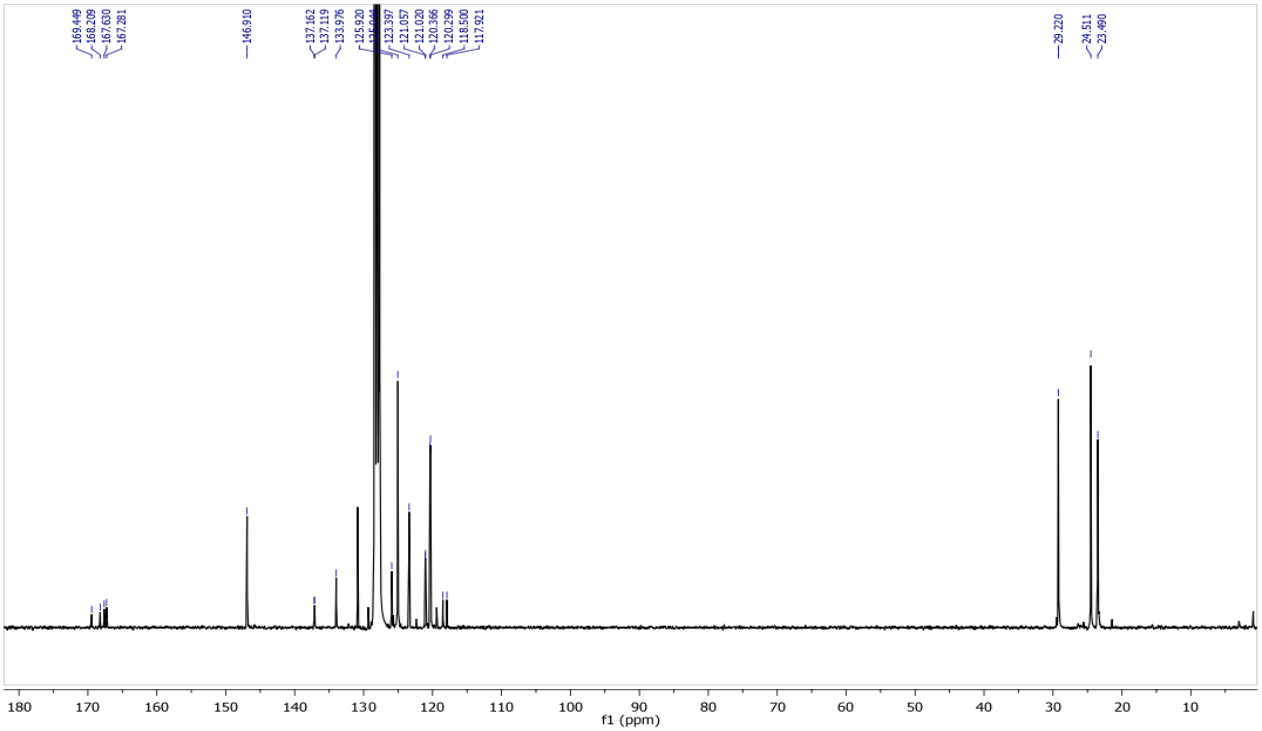

Figure A12. $^{13}C\{^{1}H\}$ NMR Spectrum of the titanium complex **29**. (75 MHz, C_6D_6)

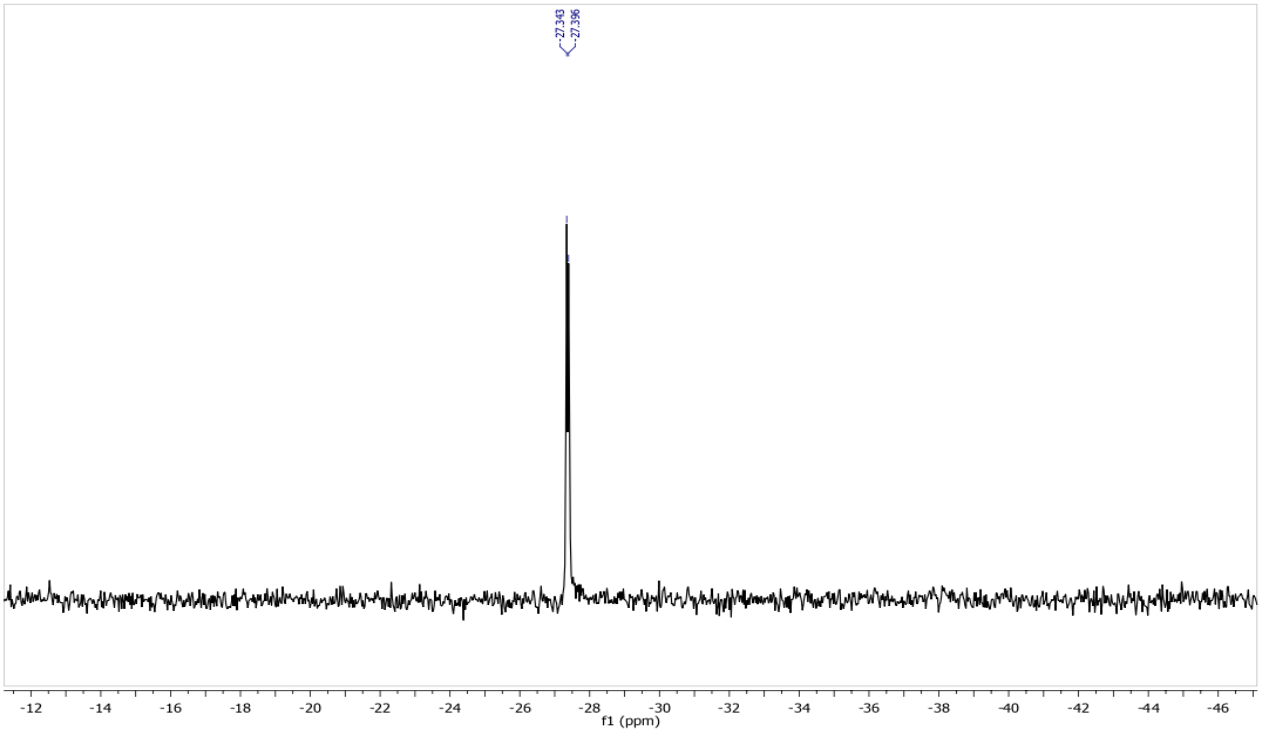

Figure A13. ^{31}P NMR Spectrum of the titanium complex **29**. (122 MHz, C_6D_6)

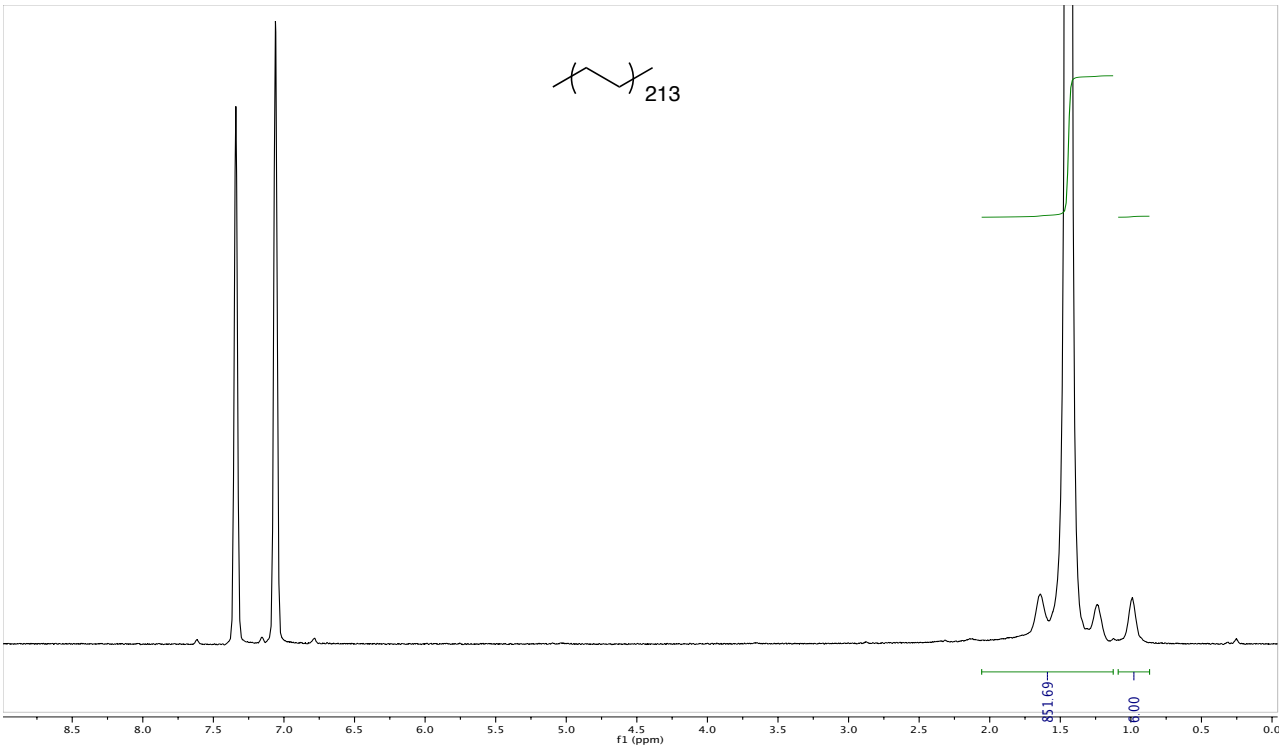

Figure A14. ^{1}H NMR Spectrum of the polymeric compound formed. (300 MHz, $C_6D_4Cl_2$, at 145 °C)

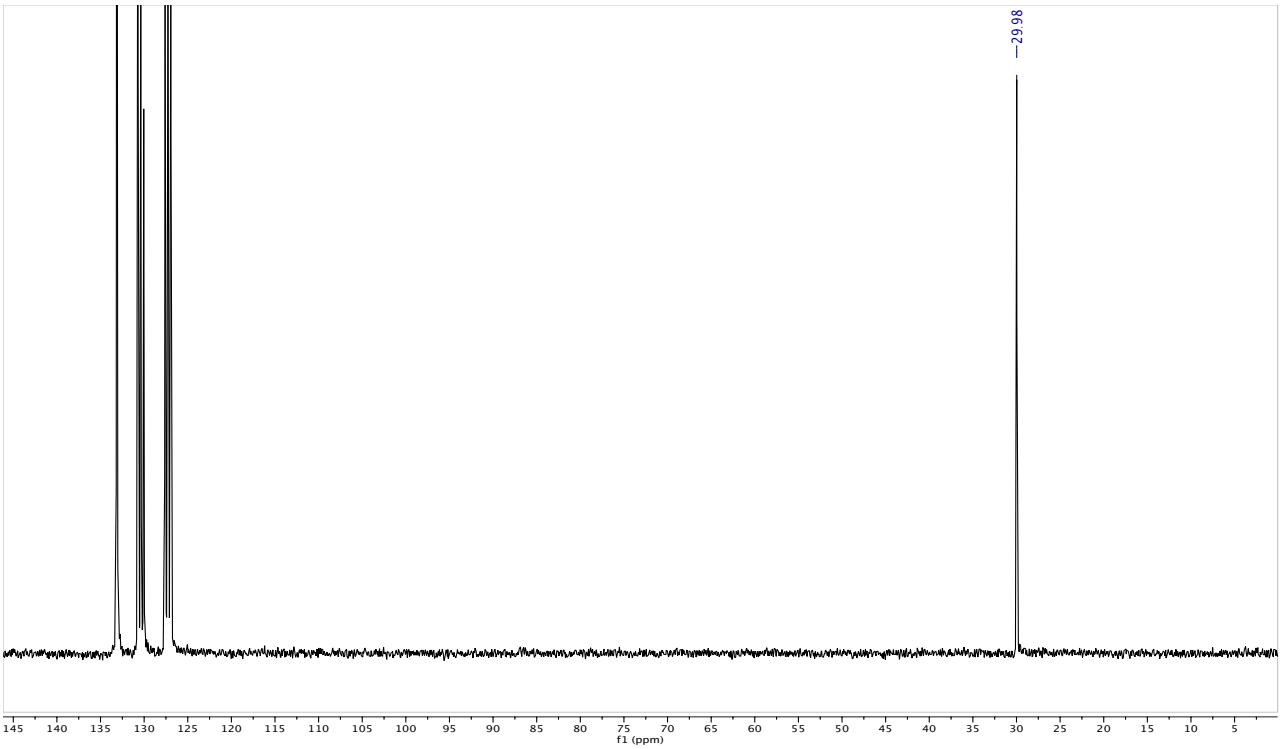

Figure A15. ^{13}C {^{1}H} NMR Spectrum of the polymeric compound formed. (300 MHz, $C_4D_4Cl_2$, at 145 °C)

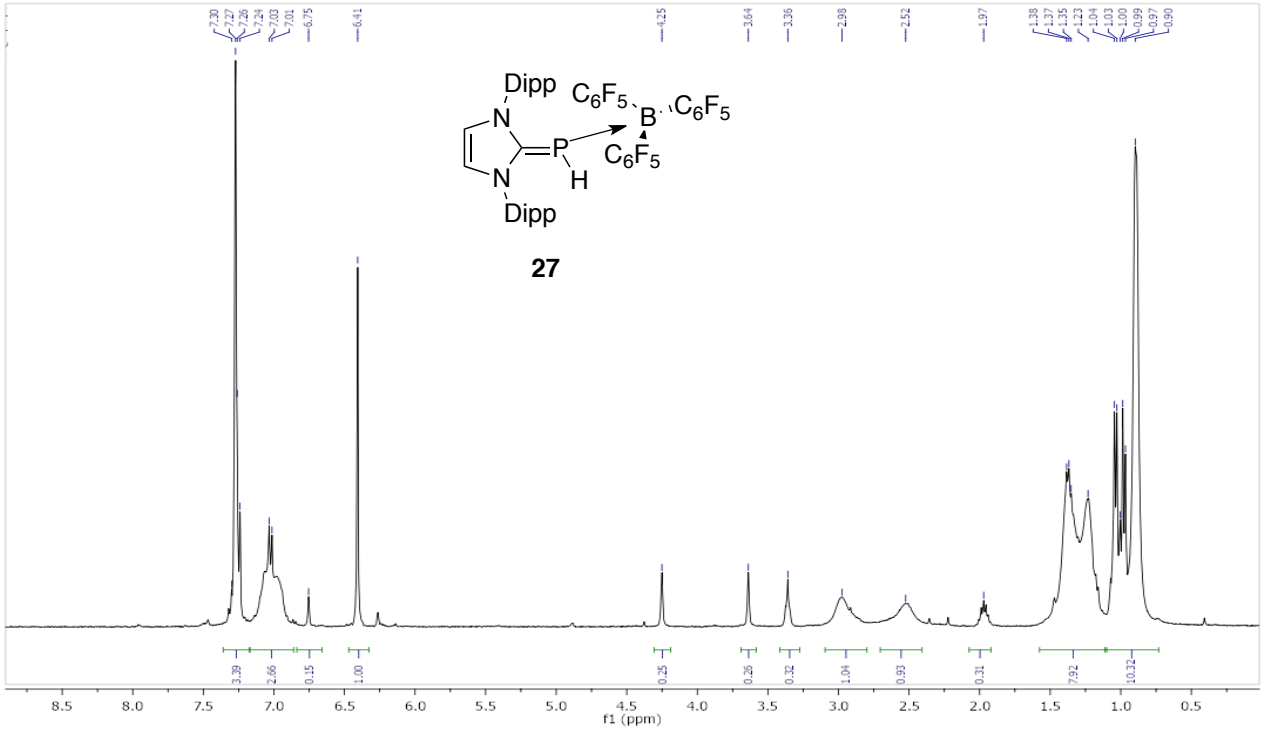

Figure A16. ^{1}H NMR Spectrum of the adduct **27** formed between compound **20** and BCF. (400 MHz, C_6D_6)

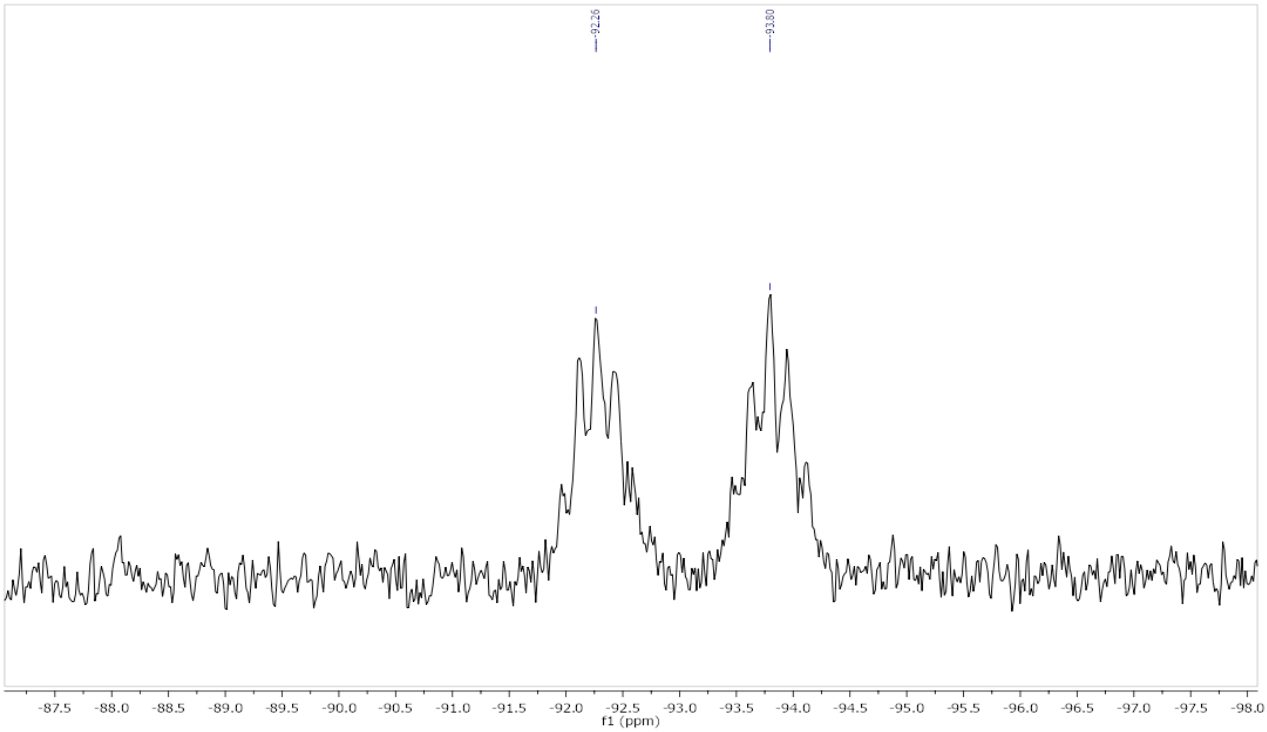

Figure A17. ^{31}P NMR Spectrum of the adduct **27** formed between compound **20** and BCF. (162 MHz, C_6D_6)

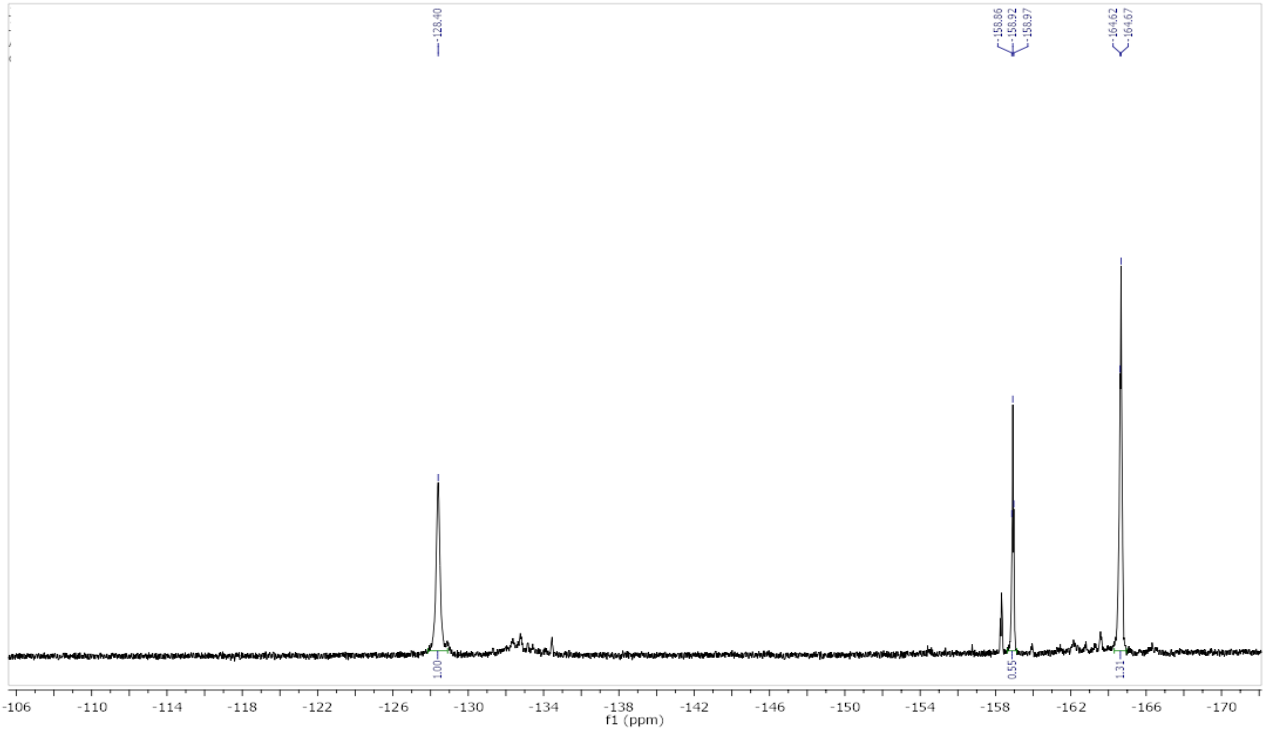

Figure A18. ^{19}F {^{1}H} NMR Spectrum of the adduct **27** formed between compound **20** and BCF. (377 MHz, C_6D_6)